To the Graduate Council:

I am submitting herewith a thesis written by Dale Leroy Johnson entitled "A Stability Analysis of AVE-IV Severe Weather Soundings." I have examined the final copy of this thesis for form and content and recommend that it be accepted in partial fulfillment of the requirements for the degree of Master of Science, with a major in Engineering Science.

Walter Frost, Major Professor

We have read this thesis
and recommend its acceptance:

Accepted for the Council:

Vice Chancellor
Graduate Studies and Research

A

# A STABILITY ANALYSIS OF AVE-IV SEVERE WEATHER SOUNDINGS

A Thesis

Presented for the

Master of Science

Degree

The University of Tennessee, Knoxville

Dale Leroy Johnson

June 1982

3060779

# ACKNOWLEDGMENTS

The author wishes to express his appreciation to the many people who have inspired and contributed to this thesis. Thanks go to The University of Tennessee Space Institute, particularly Dr. Kenneth R. Kimble and Dr. Robert E. Turner of the Thesis Committee. Special thanks to the author's major professor, advisor, and friend, Dr. Walter Frost, who helped tremendously to achieve this goal, and to Mrs. Jeannie Harper for her assistance and excellent typing of the final manuscript.

Sincere appreciation is also given to the Marshall Space Flight Center's management for allowing the author to complete this thesis. In particular, special thanks to Dr. William W. Vaughan, Dr. Robert E. Turner, and Dr. Gregory S. Wilson for their helpful discussions and encouragement throughout. Also, appreciation is expressed to Ms. Linda May for typing portions of the draft manuscript.

Finally, the author is indebted to his wife, Shirley, his daughters, Natalie and Freda, and sons, Stanley and Kevin, for their time, encouragement, and patience given throughout the course of studies in order for him to achieve this goal which otherwise would not have been accomplished.

# ABSTRACT

An investigation was made to determine whether the stability and vertical structure of an average severe storm sounding, consisting of both thermodynamic and wind vertical profiles, could be distinguished from an average lag sounding taken three to six hours prior to severe weather occurrence. The term "average" is defined here to indicate the arithmetic mean of a parameter, as a function of altitude, determined from a large number of available observations taken either close to severe weather occurrence, or else more than three hours before it occurs. The investigative computations were also done to help determine if a severe storm forecast scheme or index could possibly be used or developed.

The study presents these mean vertical profiles of thermodynamic and wind parameters as a function of severity of the weather, determined from manually digitized radar (MDR) categories observed during the National Aeronautics and Space Administration (NASA) Atmospheric Variability Experiment IV (AVE-IV) which took place on April 24-25, 1975. Profile differences and stability index differences are presented along with the development of the Johnson Lag Index (JLI) which is determined entirely upon environmental vertical parameter differences between conditions three hours prior to severe weather, and severe weather itself.

All of the stability indices tested were then used on a separate and independent data sample (AVE-SESAME-I) consisting of individual soundings taken during April 10-11, 1979. The AVE-SESAME-I data profiles are presented along with stability index computations

for each. All of the stability indices tested appeared to do a reasonable job in indicating both the severe weather, as well as the non-severe weather environment. As a pre-severe weather lag (three to six hours) index, only the JLI appears to show promise as a potential forecast index. More testing of this index, however, is needed.

# TABLE OF CONTENTS


| CHAPTER | | PAGE |
|---|---|---|
| I. | INTRODUCTION. . . . . | 1 |
| II. | DEFINITIONS . . . . . | 3 |
| | Introduction. . . . . | 3 |
| | Skew-T, Log-P Diagram . . . . . | 3 |
| | Stability Index . . . . . | 8 |
| | Stability . . . . . | 10 |
| III. | ATMOSPHERIC VARIABILITY EXPERIMENT IV | |
| | DATA DESCRIPTION. . . . . | 15 |
| | Introduction. . . . . | 15 |
| | AVE-IV Data Background. . . . . | 15 |
| | Synoptic Situation. . . . . | 19 |
| | Manually Digitized Radar Data . . . . . | 24 |
| | Rawinsonde Data Grid. . . . . | 24 |
| | AVE-IV Averaged Profiles. . . . . | 29 |
| | AVE-IV Average Lag Profiles . . . . . | 31 |
| IV. | INDICES USED IN STUDY . . . . . | 40 |
| | Introduction. . . . . | 40 |
| | Index Selection Criteria. . . . . | 40 |
| | Indices Chosen. . . . . | 41 |
| | Definition of Indices . . . . . | 41 |
| | Severe weather threat index . . . . . | 41 |
| | Vertical-totals index . . . . . | 47 |
| | Cross-totals index. . . . . | 49 |

CHAPTER PAGE

IV. (continued)

Total-totals index. . . . . 49

Theta-E methods . . . . . 50

Showalter stability index . . . . . 54

Rackcliff instability index . . . . . 57

Jefferson instability index . . . . . 59

Modified Jefferson instability index. . . . . 60

Boyden instability index. . . . . 61

K-index . . . . . 62

Bradbury potential stability index. . . . . 66

Energy index. . . . . 68

Martin index. . . . . 72

V. AVE-IV PROFILE ANALYSES . . . . . 75

Introduction. . . . . 75

AVG Profile Comparison. . . . . 76

Temperature/moisture. . . . . 76

Winds . . . . . 76

LAG Profile Comparison. . . . . 78

Temperature/moisture. . . . . 78

Winds . . . . . 78

AVG/LAG Profile Comparison. . . . . 80

Winds . . . . . 80

Temperature/moisture. . . . . 82

Theta-E AVG/LAG Comparison. . . . . 82

CHAPTER PAGE

V. (continued)

AVG/LAG Conclusions . . . . . 89

Possible Stability Index. . . . . 91

VI. AVE-IV STABILITY ANALYSES . . . . . 92

Introduction. . . . . 92

Temperature-Dependence. . . . . 92

Stability Index Results . . . . . 96

Johnson Lag Index . . . . . 99

VII. STABILITY CRITERIA APPLIED TO AVE-SESAME-I. . . . . 104

Introduction. . . . . 104

Synoptic Situation. . . . . 104

Sounding Analyses . . . . . 106

Exceptions to the Norm. . . . . 113

Lag Testing . . . . . 114

VIII. CONCLUSIONS . . . . . 116

BIBLIOGRAPHY . . . . . 118

VITA . . . . . 127

# LIST OF TABLES


| TABLE | | PAGE |
|---|---|---|
| 1. | Rawinsonde Stations Participating in AVE-IV Experiment. . . | 17 |
| 2. | Manually Digitized Radar Data Code [8]. . . . . | 26 |
| 3. | MDR Categories Used in the Present AVE-IV Analyses. . . . . | 27 |
| 4. | AVE-IV Average Profile Conditions for MDR = 0 (No Precipitation). . . . . | 32 |
| 5. | AVE-IV Average Profile Conditions for MDR > 0 (All Precipitation) . . . . . | 33 |
| 6. | AVE-IV Average Profile Conditions for MDR > 3 (All Thunderstorms) . . . . . | 34 |
| 7. | AVE-IV Average Profile Conditions for MDR > 7 (Severe Thunderstorms). . . . . | 35 |
| 8. | AVE-IV Average Lag Profile Conditions for MDR = 0 (No Precipitation). . . . . | 36 |
| 9. | AVE-IV Average Lag Profile Conditions for MDR > 0 (All Precipitation) . . . . . | 37 |
| 10. | AVE-IV Average Lag Profile Conditions for MDR > 3 (All Thunderstorms) . . . . . | 38 |
| 11. | AVE-IV Average Lag Profile Conditions for MDR > 7 (Severe Thunderstorms). . . . . | 39 |
| 12. | Stability Indices . . . . . | 42 |
| 13. | Vertical-Totals Index Thunderstorm Threshold Values for Different Areas . . . . . | 48 |
| 14. | Delta Theta-E Upper and Lower Index Critical Values . . . . | 53 |

TABLE PAGE

15. K-Index Thunderstorm Threshold Values . . . . . 64

16. K-Index Thunderstorm Probabilities. . . . . 65

17. Energy Index Values Used in Convective Forecasting. . . . . 71

18. Theta-E Differences ($^{o}$K) Between Given Pressure Levels. . . 88

19. Stability Index Range Determined by Moist and Dry Adiabatic Lapse Rates . . . . . 94

20. Stability Index Dependency as a Function of Temperature Change. . . . . 95

21. Stability Index Values for LAG and AVG MDR Profiles . . . . 97

22. JLI versus MDR Categories for LAG and AVG Conditions. . . . 102

23. Abilene, Texas, AVE-SESAME-I Sounding Stability Index Values. . . . . 111

# LIST OF FIGURES


| FIGURE | | PAGE |
|---|---|---|
| 1. | Coordinate System of the Skew-T, Log-P Diagram [3]. . . . . | 5 |
| 2. | Skew-T, Log-P Diagram, with Lifted Parcel Example [3] . . . . . | 7 |
| 3. | Skew-T, Log-P Diagram, with Heating Parcel Example [3] . . . . . | 9 |
| 4. | Atmospheric Sounding Stability Classifications. . . . . | 12 |
| 5. | Latent Instability Example. . . . . | 12 |
| 6. | Layer Potential Instability . . . . . | 14 |
| 7. | Location of Rawinsonde Stations for AVE-IV [11] . . . . . | 16 |
| 8. | Surface Map for 0000 GMT, April 24, 1975 [9]. . . . . | 20 |
| 9. | Surface Map for 0000 GMT, April 25, 1975 [9]. . . . . | 22 |
| 10. | Surface Map for 1200 GMT, April 25, 1975 [1]. . . . . | 23 |
| 11. | Manually Digitized Radar (MDR) Grid Network [8] . . . . . | 25 |
| 12. | The 18x18 Grid Used for Numerical Computations [8]. . . . . | 28 |
| 13. | Step Function Used in Computation of SWEAT Veering Term. . . . . | 46 |
| 14. | Graphical Computation of Equivalent Potential Temperature ($\theta_E$). . . . . | 51 |
| 15. | Showalter Stability Index Computation Method. . . . . | 56 |
| 16. | Rackcliff Instability Index Computation Method. . . . . | 58 |
| 17. | Bradbury Potential Stability Index Computation Method . . . | 67 |
| 18. | Relationship Between $\theta_{W850}$ and the BPI on Thunderstorm Days [59]. . . . . | 67 |

FIGURE PAGE

19. Martin Stability Index Computation Methods. . . . . 73

20. AVG Temperature and Dew-Point Profiles for A and D MDR Conditions. . . . . 77

21. AVG Wind Components for MDR A and D Conditions. . . . . 79

22. Wind Components for AVG and LAG Type D MDR Conditions . . . 81

23. Temperature and Dew-Point Temperature Profiles for AVG and LAG Conditions of MDR = D . . . . . 83

24. AVG Equivalent Potential Temperature ($\theta_E$) Vertical Profiles for Four MDR Categories. . . . . 85

25. LAG Equivalent Potential Temperature ($\theta_E$) Vertical Profiles for Four MDR Categories. . . . . 86

26. LAG and AVG Equivalent Potential Temperature ($\theta_E$) Vertical Profiles for Type A and D MDR Categories . . . . 87

27. Severe Weather Occurrences Between 1200 GMT on April 10, and 1200 GMT on April 11, 1979 in the South Central United States [68]. . . . . 107

28. Abilene, Texas, Severe Weather Soundings for April 10, 1979. . . . . 108

29. Abilene, Texas, Severe Weather Soundings for April 10-11, 1979 . . . . . 109

# LIST OF SYMBOLS

| | |
|---|---|
| $^{o}C$ | Degrees centigrade |
| $c_p$ | Specific heat of air |
| $D_e$ | Dew-point temperature at 900 meters |
| $E_S$ | Static energy |
| $E_T$ | Total energy |
| g | Acceleration of gravity |
| $^{o}K$ | Degrees Kelvin |
| L | Latent heat |
| M | Multiplication factor |
| mb | Millibar pressure |
| P | Pressure |
| q | Specific humidity |
| S | Sine equation used in SWEAT index |
| T | Temperature |
| $T_d$ | Dew-point temperature |
| $T_w$ | Wet-bulb temperature |
| U | Zonal wind component |
| V | Meridional wind component |
| W | Scalar wind speed |
| w | Mixing ratio |
| $w_s$ | Saturation mixing ratio |
| $W_e$ | Low-altitude scalar wind speed |
| WD | Wind direction |
| Z | Altitude |

| | |
|---|---|
| $\theta$ | Potential temperature |
| $\theta^*$ | Convective instability |
| $\theta_E$ | Equivalent potential temperature |
| $\theta_{GE}$ | Geo-equivalent potential temperature |
| $\theta_W$ | Wet-bulb potential temperature |
| $\alpha$ | Veering angle |
| $\Gamma_d$ | Dry adiabatic temperature lapse rate |
| $\Gamma_e$ | Environmental temperature lapse rate |
| $\Gamma_s$ | Saturated adiabatic temperature lapse rate |

# CHAPTER I

## INTRODUCTION

This study analyzes many of the standard stability index concepts used today in the prediction of convective weather, including severe thunderstorms and tornadoes. These indices are computed for the National Aeronautics and Space Administration (NASA) Atmospheric Variability Experiment (AVE) mean atmospheric soundings (vertical profiles) taken during the AVE-IV project in 1975 [1].[1] The profiles have been categorized to correspond to the differing weather conditions that occurred by using the manually digitized radar data (MDR) taken during this time period as being representative of the various weather categories that existed during AVE-IV. The AVE procedures are discussed in more detail in Chapter III. It is the purpose of this study to present and analyze the vertical weather profiles taken during AVE-IV, in terms of averaged (mean) weather profiles.

This investigation also compares several stability indices calculated from the AVE-IV mean profiles. The results and performance of the indices are discussed.

Also, it is the intent of this study to determine if averaged weather profiles taken three hours prior to severe weather occurrence

---

[1] Numbers in brackets refer to similarly numbered references in the Bibliography.

have forecast capability when based only on the AVE-IV three-hour lag data soundings.

Finally, the results obtained from this stability index/ AVE-IV study are applied to the independent AVE-SESAME-I [2] data set to see how well the conclusions based on the AVE-IV analysis apply to a set of independent, individual sounding profiles that deal with a similar weather system.

# CHAPTER II

# DEFINITIONS

## A. Introduction

This chapter presents a discussion of the Skew-T, Log-P thermodynamic diagram which was used extensively throughout the study and in the presentation of results. Secondly, a brief discussion defines the stability index. This is concluded by a section devoted to describing the different definitions of the stability of the atmosphere.

## B. Skew-T, Log-P Diagram

Throughout this investigation, stability indices, atmospheric processes, and atmospheric analyses will involve the use of a suitable meteorological thermodynamic diagram. This will better illustrate and describe atmospheric processes, as well as allow graphical computations. This section presents a brief but instructive discussion of the thermodynamic diagram used in this study.

The Skew-T, Log-P diagram is employed in this study because it is most widely used in the United States. In particular, the United States Air Force (USAF) Air Weather Service (AWS) uses this diagram exclusively. Its popularity is due to the convenience and ease of use for most atmospheric computations. The diagram will hereafter be referred to as the "Skew-T." The Skew-T contains the

same meteorological parametric lines as other thermodynamic diagrams, but their arrangement is different. Further discussion of the advantages obtained in using the Skew-T diagram is given in Reference [3].

The name of the diagram indicates how the pressure and temperature lines are presented. Constant pressure lines (isobars), expressed in millibars (mb), are plotted horizontally on a logarithmic scale. Also, constant temperature lines (isotherms), in $^{o}C$, are plotted sloping from the lower-left to the upper-right (skewed) on an approximate 45 deg angle with respect to the horizontal pressure lines. Figure 1 illustrates the isobaric and isothermal lines on a Skew-T diagram.

Also plotted on the Skew-T are slightly curved, dry adiabatic lines ($^{o}C$). They slope from lower-right to upper-left and are indicated by two small and one large alternating dashed lines. These lines indicate the rate of temperature change encountered when a parcel of unsaturated air rises or descends adiabatically (without gain or loss of heat).

Saturation adiabats (or moist adiabats, $^{o}C$) are the large-dashed, slightly curved lines also sloping from lower-right to upper-left. They begin more vertically at lower levels on the chart and become more parallel with the dry adiabatic lines at higher levels. Moist adiabatic lines represent the path along which a saturated air parcel rises. Figure 1 shows the placement of the dry and saturated adiabatic lines on the Skew-T diagram.

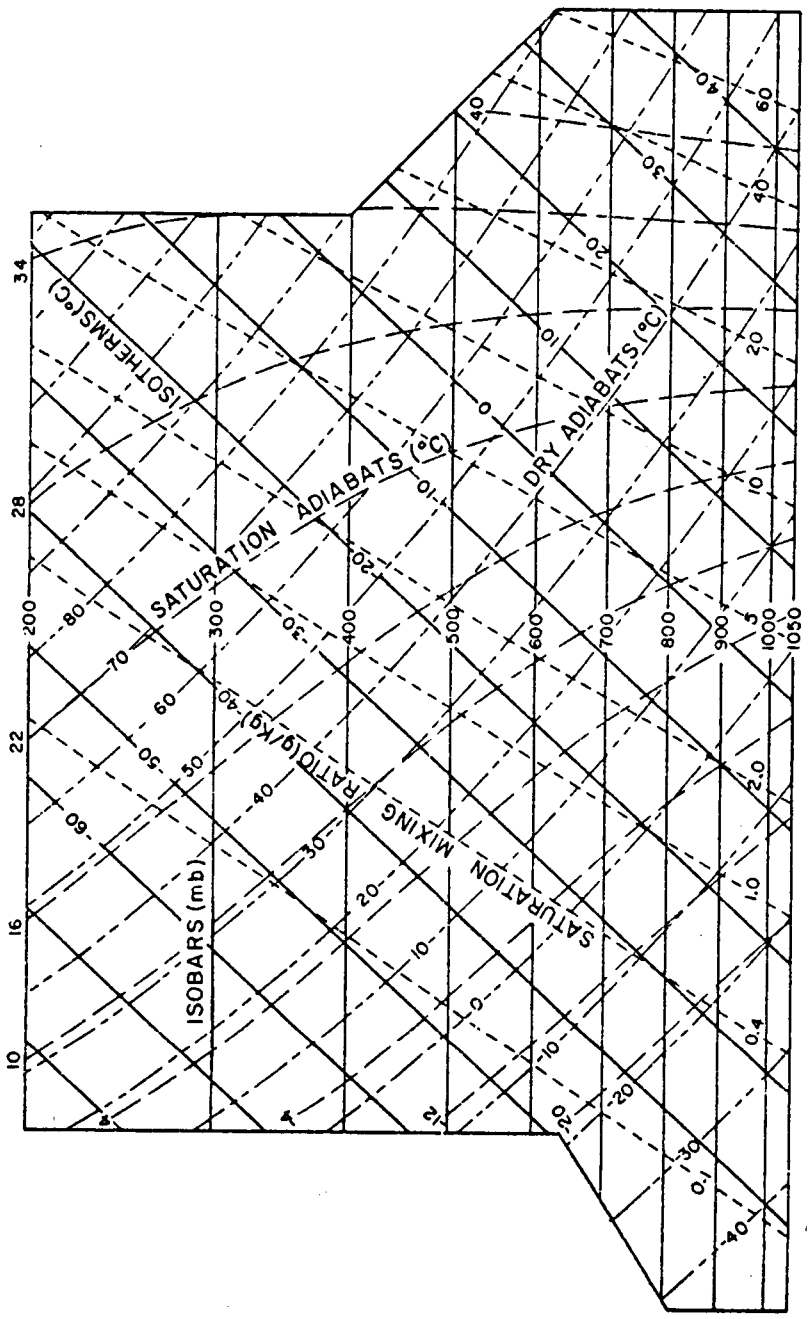


Figure 1. Coordinate system of the Skew-T, Log-P diagram [3].

Finally, saturation mixing-ratio ($w_s$) lines are shown as dashed, slightly curved lines extending from lower-left to upper-right in Figure 1. The mixing ratio of an air sample is a function of temperature and pressure. It is defined as the ratio of the mass of water vapor to the mass of dry air containing the vapor (gm/kg). At a given isobaric level, the intersection of the temperature line with the $w_s$ line gives the saturation mixing ratio value of the air at that temperature and pressure. The dew-point intersection with the $w_s$ line gives the actual mixing ratio value (w) of the air.

To illustrate the use of the Skew-T, an example sounding profile of temperature (T) and dew-point temperature ($T_d$) from the 1,000-mb level upward is plotted on the Figure 2 diagram. Dry adiabatic lifting of a surface air parcel is assumed to take place in this example. Beginning at the intersection of the $T_d$ and 1,000-mb pressure line and following the $w_s$ line upward to where it intersects the path of the dry adiabat extending upward from the surface value of T, introduces an intersection point on the Skew-T, called the lifting condensation level (LCL). At this point, saturation conditions exist. Traversing vertically from the LCL along the saturation adiabat until it intersects the environmental sounding of T defines the level of free convection (LFC) location. Above the LFC the parcel of air becomes warmer (less dense) than the environmental air around it during this period of travel. Above this level the parcel will continue to rise at the moist adiabatic rate until it becomes cooler than the environment. This, then, defines the equilibrium level (EL). As can be seen in Figure 2,

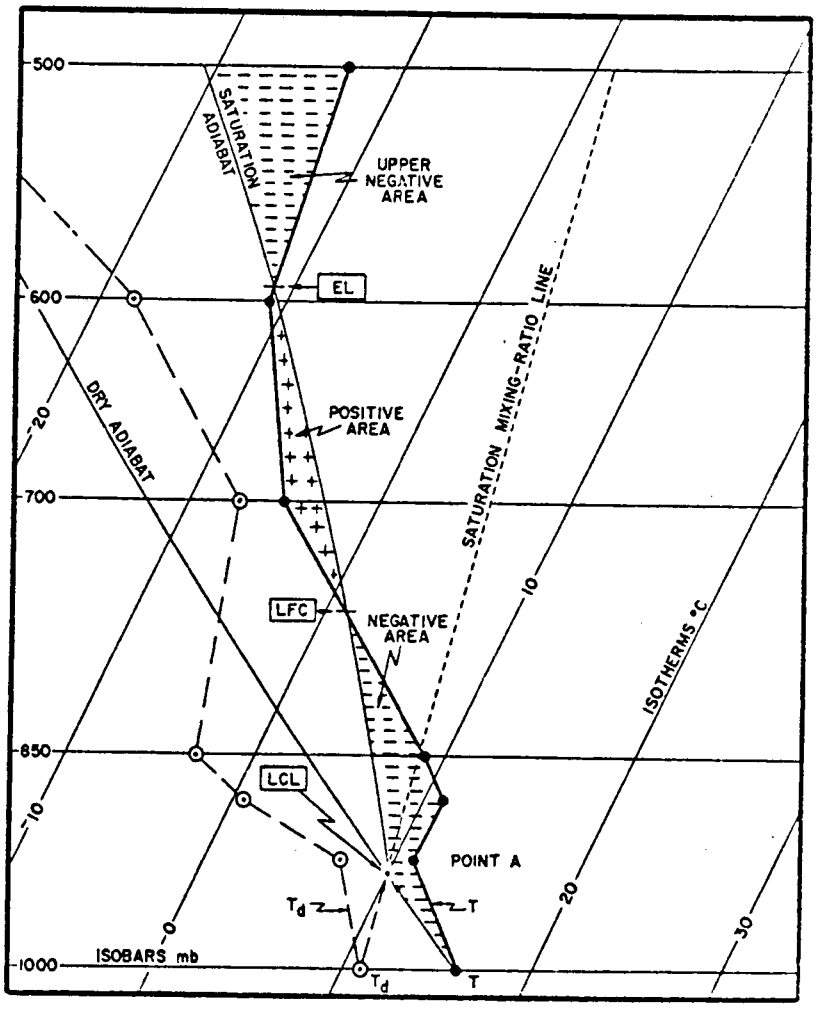


Figure 2. Skew-T, Log-P diagram, with lifted parcel example [3].

regions of negative kinetic energy which work against the vertical motion of the cooler air parcel must be overcome. Likewise, positive energy areas enhance the parcel's vertical motion.

A second example is illustrated in Figure 3. In this example it is assumed that a parcel of surface air has undergone thermal convection produced from solar-ground heating. The parcel rises dry adiabatically until reaching its convective condensation level (CCL) where it becomes saturated. The CCL is the height of the cumuliform cloud bases observed in the atmosphere. The CCL is obtained by proceeding upward from the surface $T_d$ value (1,000-mb level) along the $w_s$ line until intersection with the environmental temperature sounding occurs. The equilibrium level (EL) is defined in the same manner as indicated earlier.

## C. Stability Index

At least three main factors are determined to be necessary for the formation of convective weather: Instability of the atmosphere, sufficient moisture, and a triggering mechanism which lifts and sets the atmosphere in motion [4]. Scoggins [4] concluded that vertical motion is always required for thunderstorm development, regardless of the degree of potential instability. The instability of the atmosphere over a location can be calculated by the use of upper air data and a stability/instability index computation. With the advent of the radiosonde and its routine use in obtaining upper air data, stability indices have been developed and used by man since the mid-1940's [5].

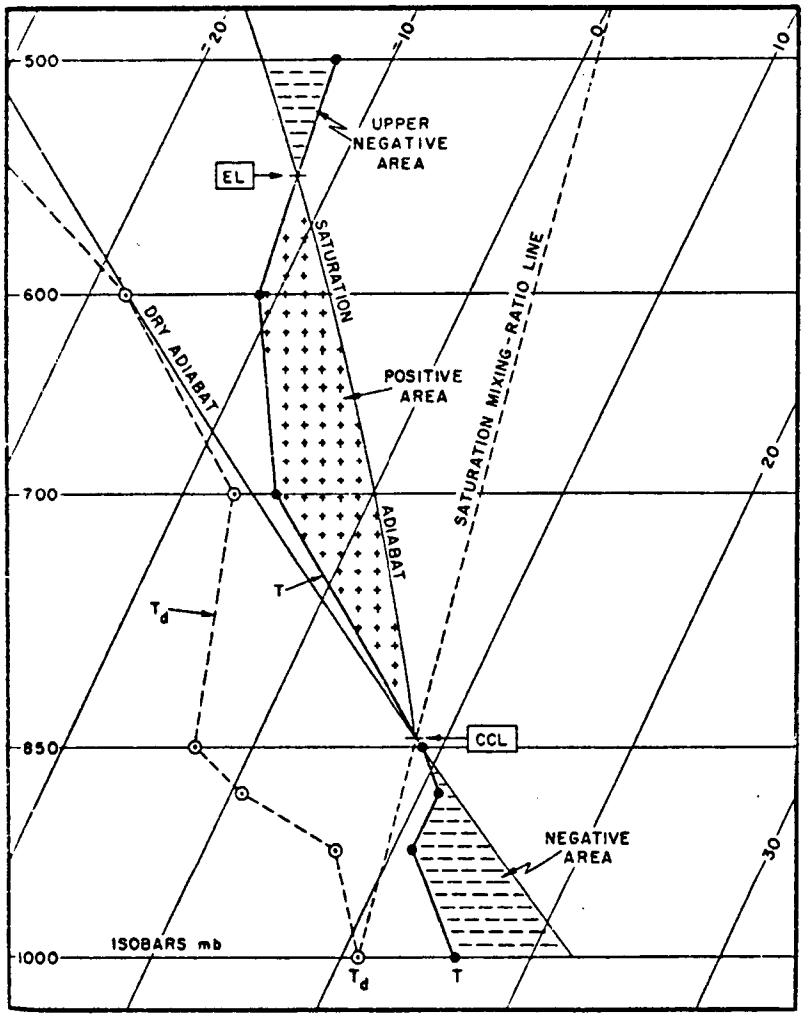


Figure 3. Skew-T, Log-P diagram, with heating parcel example [3].

Temperature, pressure, moisture, and winds can be measured throughout the upper atmosphere. These data, together with the large data processing ability of modern electronic computers, allow the researcher to use the data in testing and determining which atmospheric parameters vary, and how much, when convective weather occurs. This type of parametric study would likely evolve into the establishment of a stability index. Generally, stability indices take the form of a difference between parameters, such as temperature (T), dew-point temperature ($T_d$), potential temperature ($\theta$), mixing ratio (w), pressure (P), altitude (Z), etc., measured at two heights or pressure surfaces. The common, available pressure levels generally used in index computations are the 1,000-, 850-, 700-, and 500-mb levels.

Stability indices act only as an aid in the forecasting of convective weather, by alerting the forecaster to areas of the map or soundings which should be examined more closely by other methods.

## D. Stability

Atmospheric instability is usually defined in terms of conditional instability, latent instability, and potential instability. The definitions are not inclusive, however.

Conditional instability is defined [6] as, "the state of a column of air in the atmosphere when its lapse rate of temperature is less than the dry-adiabatic lapse rate, but greater than the saturation-adiabatic lapse rate. With reference to the vertical

displacement of an air parcel, the air will be unstable if saturated, and stable if unsaturated." This is illustrated in Figure 4.

To explain Figure 4, assume parcel theory [3]. When the environmental temperature lapse rate ($\Gamma_e$) lies to the left (PQ) of the dry adiabat ($\Gamma_d$) through point P, the atmosphere is said to have absolute instability within the vertical region between PQ. If an air parcel, originally unsaturated, ascends upward along the dry adiabat, it will be warmer (at Q') than the surrounding environment (at Q); thereby, the parcel will tend to continue to rise.

The reverse situation, indicating absolute stability with respect to saturation, is true if the environmental lapse rate is located to the right (PR) of the saturated adiabat ($\Gamma_s$) PR'. The parcel temperature (at R') would then be colder than the environment temperature (at R), allowing the parcel to sink and be stable. The region between the dry and saturated adiabats indicates the region of conditional instability. This means that the parcel is stable if not saturated, or unstable if saturated.

The parcel method mentioned here involves simply an unsaturated parcel of air which must be forced to ascend vertically along a dry adiabat ($\Gamma_d$) until saturated at the lifting condensation level. It is then forced to ascend along a saturated (or moist) adiabat ($\Gamma_s$) from this point upward through the level of free convection, and thereafter is accelerated along $\Gamma_s$ by a positive buoyancy and need not be forced. Figure 5 shows this process, with the arrows indicating the parcel's path.

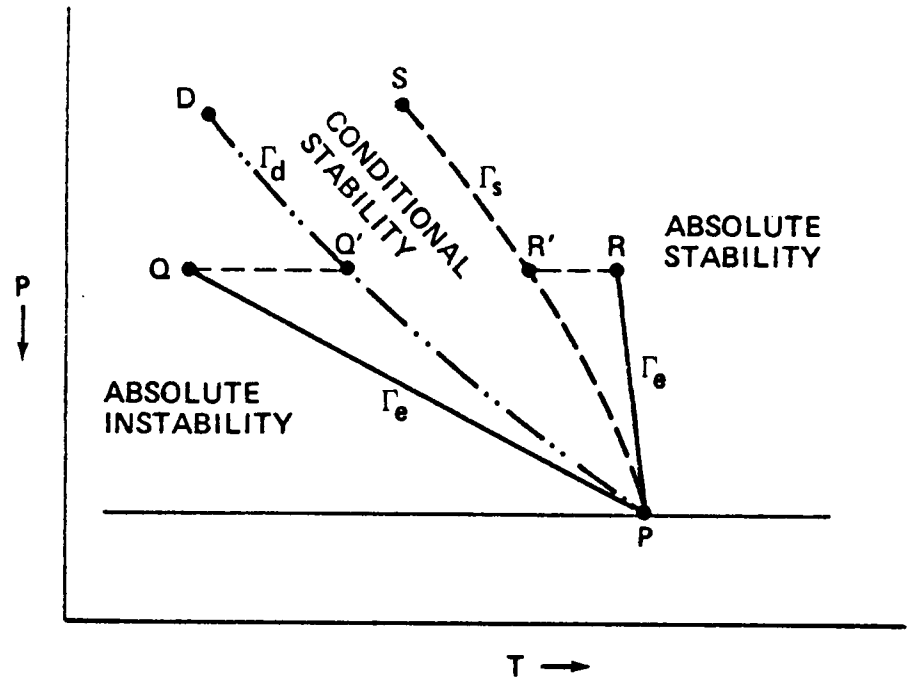


Figure 4. Atmospheric sounding stability classifications.

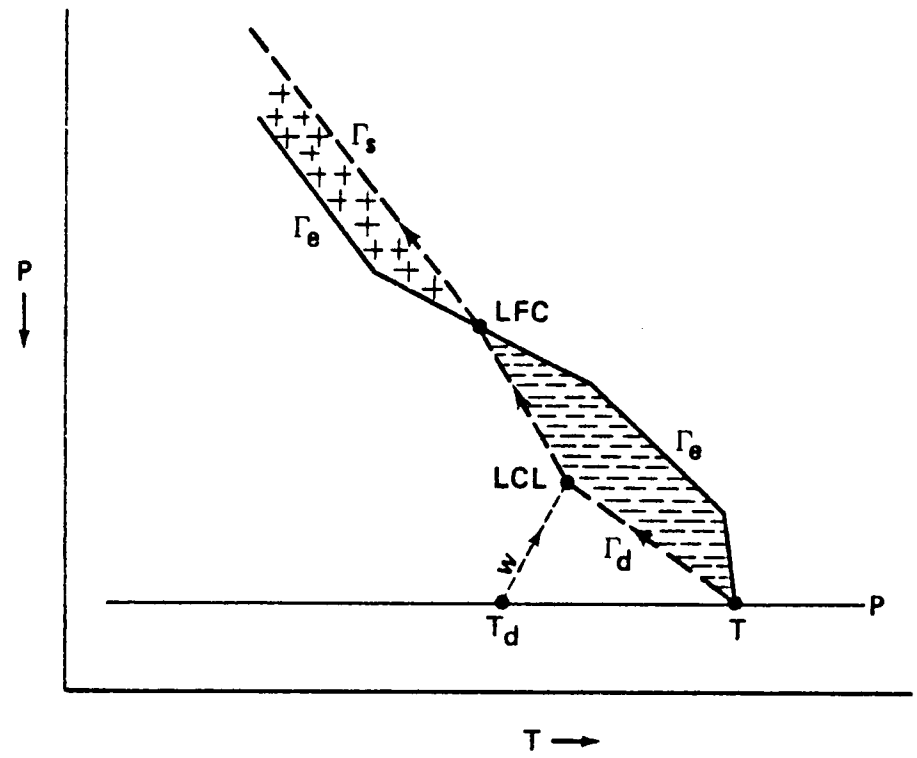


Figure 5. Latent instability example.

Latent instability is defined [6] as, "the state of that portion of a conditionally unstable air column lying above the level of free convection." The negative region (on Figure 5) shown below the LFC is the area in which the environment is warmer than the parcel. Therefore, if the parcel is initially given an impulse with sufficient kinetic energy to carry it through the negative region, then above the LFC lies the positive region which signifies the latent instability needed to accelerate the parcel, since the parcel will now be warmer than the environment.

Potential instability (or convective instability) is the last atmospheric instability category to be considered here. It is defined [6] as, "the state of an unsaturated layer or column of air in the atmosphere whose wet-bulb potential temperature ($\theta_W$), or equivalent potential temperature ($\theta_E$), decreases with altitude. If such a column is lifted bodily until completely saturated, it will become unstable" (i.e., $\Gamma_{layer} > \Gamma_s$). In this definition one is considering the stability of a whole layer of air (not a small parcel) which is lifted entirely by either frontal activity or flow over a mountain. As shown in Figure 6, the bottom of this layer (AB) may saturate, via dry/moist adiabatic processes (at A), before the top of the layer does (at B). This results in the layer lapse rate (between AB) becoming, in time, an unstable layer lapse rate (between A'B'). Potential instability (or stability) is strictly a "lifted-layer"-type of approach to stability.

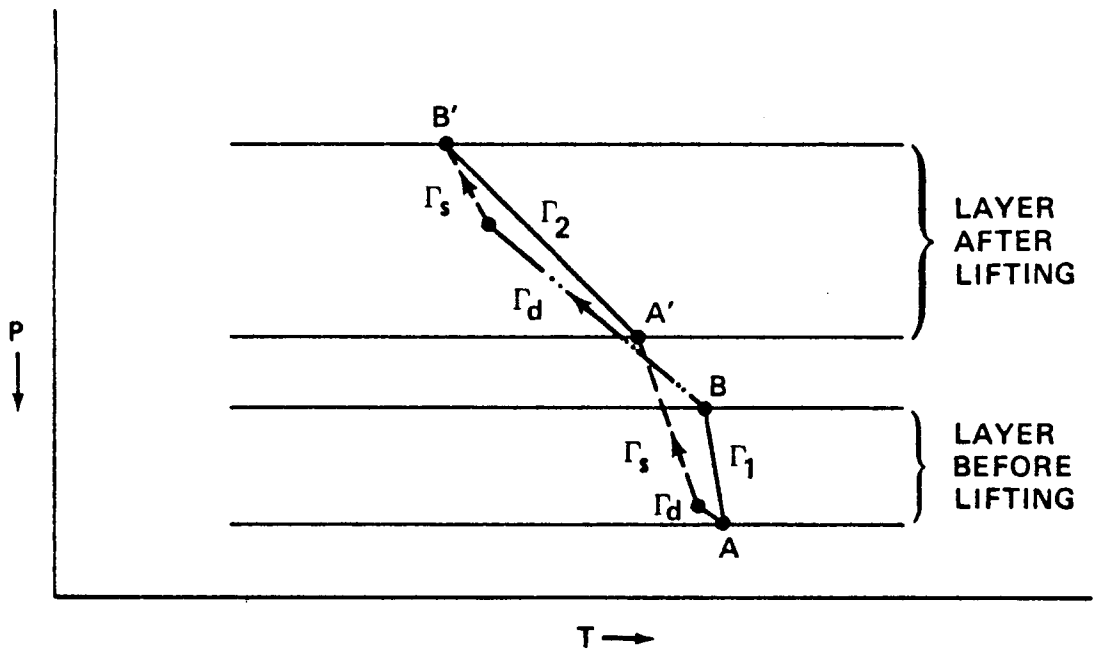


Figure 6. Layer potential instability.

# CHAPTER III

# ATMOSPHERIC VARIABILITY EXPERIMENT IV

# DATA DESCRIPTION

## A. Introduction

Presented in this chapter is the description of the Atmospheric Variability Experiment IV (AVE-IV). This includes background information for the experiment, the synoptic situation present, the data soundings obtained, the corresponding available radar data, and the data reduction technique used. Finally, averaged AVE-IV profiles pertaining to pre-storm and storm environments are presented for different severities of radar-measured weather conditions.

## B. AVE-IV Data Background

The NASA AVE-IV project [1] took place between 0000 GMT, April 24 and 1200 GMT, April 25, 1975. Forty-two AVE network rawinsonde stations participated in this 1.5-day mesoscale experiment in which atmospheric soundings, from the surface to 25 mb, were taken at each site every three hours (with some exceptions). Releases were taken nine times at most sites: April 24 at 0000, 0600, 1200, 1500, 1800, and 2100 GMT, and on April 25 at 0000, 0600, and 1200 GMT. Figure 7 shows a map of rawinsonde stations, east of the Rocky Mountains, that participated in the AVE-IV experiment. Table 1 lists each station. Because of the small temporal and spatial resolution of these sounding data, it is believed that

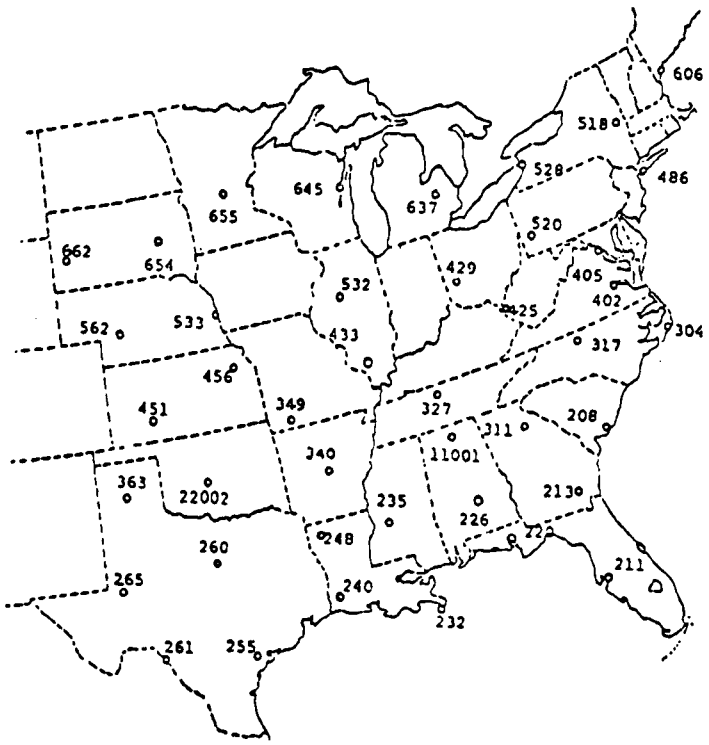


Figure 7. Location of rawinsonde stations for AVE-IV [11].

Table 1. Rawinsonde Stations Participating in AVE-IV Experiment

| Station Number | Location |
|---|---|
| 208 (CHS) | Charleston, South Carolina |
| 211 (TPA) | Tampa, Florida |
| 213 (AYS) | Waycross, Georgia |
| 220 (VPS) | Apalachicola, Florida |
| 226 (CEN) | Centerville, Alabama |
| 232 (BVE) | Boothville, Louisiana |
| 235 (JAN) | Jackson, Mississippi |
| 240 (LCH) | Lake Charles, Louisiana |
| 248 (SHV) | Shreveport, Louisiana |
| 255 (VCT) | Victoria, Texas |
| 260 (SEP) | Stephenville, Texas |
| 261 (DRT) | Del Rio, Texas |
| 265 (MAF) | Midland, Texas |
| 304 (HAT) | Hatteras, North Carolina |
| 311 (AHN) | Athens, Georgia |
| 317 (GSO) | Greensboro, North Carolina |
| 327 (BNA) | Nashville, Tennessee |
| 340 (LIT) | Little Rock, Arkansas |
| 349 (UMN) | Monette, Missouri |
| 363 (AMA) | Amarillo, Texas |
| 402 (WAL) | Wallops Island, Virginia |
| 405 (IAD) | Sterling, Virginia (Dulles Airport) |
| 425 (HTS) | Huntington, West Virginia |
| 429 (DAY) | Dayton, Ohio |
| 433 (SLO) | Salem, Illinois |
| 451 (DDC) | Dodge City, Kansas |

Table 1. (continued)

| Station Number | Location |
|---|---|
| 456 (TOP) | Topeka, Kansas |
| 486 (JFK) | Fort Totten, New York (Kennedy Airport) |
| 518 (ALB) | Albany, New York |
| 520 (PIT) | Pittsburg, Pennsylvania |
| 528 (BUF) | Buffalo, New York |
| 532 (PIA) | Peoria, Illinois |
| 553 (OMA) | Omaha, Nebraska |
| 562 (LBF) | North Platte, Nebraska |
| 606 (PWM) | Portland, Maine |
| 637 (FNT) | Flint, Michigan |
| 645 (GRB) | Green Bay, Wisconsin |
| 654 (HUR) | Huron, South Dakota |
| 655 (STC) | St. Cloud, Minnesota |
| 662 (RAP) | Rapid City, South Dakota |
| 11001 (MFS) | Marshall Space Flight Center, Alabama |
| 22002 (FSI) | Fort Sill, Oklahoma |

smaller meteorological scale (mesoscale) can be studied in terms of the variability of atmospheric parameters, than have been studied in the past, in application to stability analyses. Normally, across the United States, rawinsonde releases take place with a 12-hour separation and over a significantly wider spatial network of stations. The data reduction and processing procedures, together with further project information and the data itself (with 25-mb spacing), are presented in Reference [1].

## C. Synoptic Situation

The surface synoptic weather map for the beginning of the AVE-IV experiment (0000 GMT, April 24, 1975) is presented in Figure 8. The general weather situation throughout the AVE-IV experiment consisted of a cold polar air mass moving slowly across the northern United States with warm, moist air from the Gulf of Mexico flowing over the southern and eastern states. This movement was due to circulation around a high-pressure cell located off the coast of the Carolinas. At the start of the experiment, these two differing air masses were separated by a pseudo-stationary front extending from a low-pressure cell over lower Michigan into a secondary low located over Kansas. From there, the front trailed into west Texas, as shown in Figure 8. Throughout the AVE-IV period, the primary low moved into the Gulf of St. Lawrence, while the secondary low had moved into Kentucky by the end of the experiment.

The upper atmospheric flow pattern remained basically zonal throughout the experiment, with the exception of two short wave

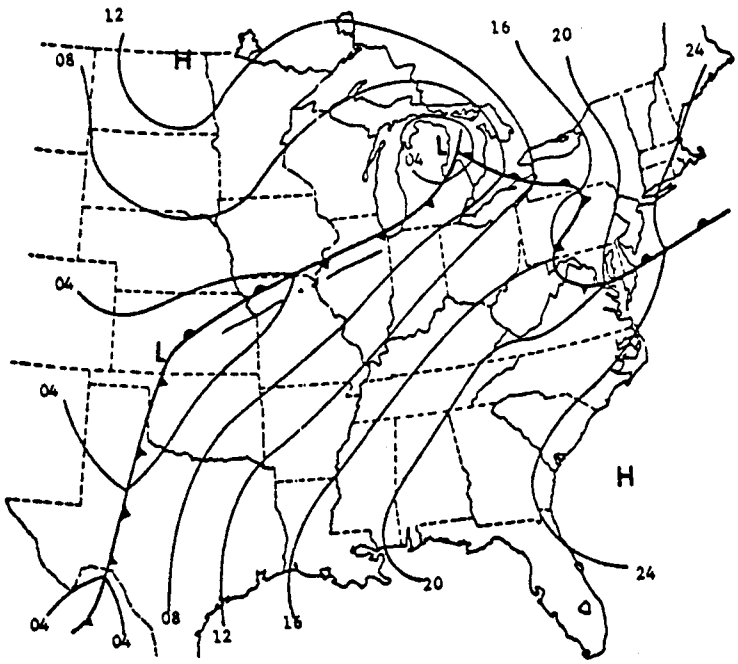


Figure 8. Surface map for 0000 GMT, April 24, 1975 [9].

passages which moved through the network. This wave activity resulted in the formation of two squall lines which produced severe weather.

The first short wave disturbance was already located in the Midwest at the beginning of AVE-IV and produced the squall line, from Kansas through Illinois, as shown in Figure 8 (at 0000 GMT, April 24, 1975). The squall line then moved easterly, ahead of the front, and produced maximum thunderstorm activity between 0300 and 0600 GMT. All thunderstorm, hail, and tornadic activity produced by this system had ended by 0000 GMT on April 25, 1975.

The second short wave passage produced the squall line situated through Oklahoma at 0000 GMT, April 25, 1975, as shown in Figure 9. Most of the tornadic and severe weather throughout AVE-IV resulted from this second squall line as it moved eastward. This second squall line formed initially sometime after 2100 GMT on April 24, stretching from Missouri into Texas. Storms and convective development continued until 0600 GMT, April 25, 1975, when maximum squall development occurred, producing large hail, strong winds, and tornadoes. This activity included the Neosho, Missouri, tornado at 0040 GMT, April 25. The line was moving eastward and was still strong by the end of the experiment, although the thunderstorm activity had lessened. The final surface weather map of AVE-IV for 1200 GMT, April 25, 1975, is shown in Figure 10.

The AVE-IV data collection and analyses have been carried out by several investigators. Complete AVE-IV information and analyses can be found in References [1] and [7 through 22].

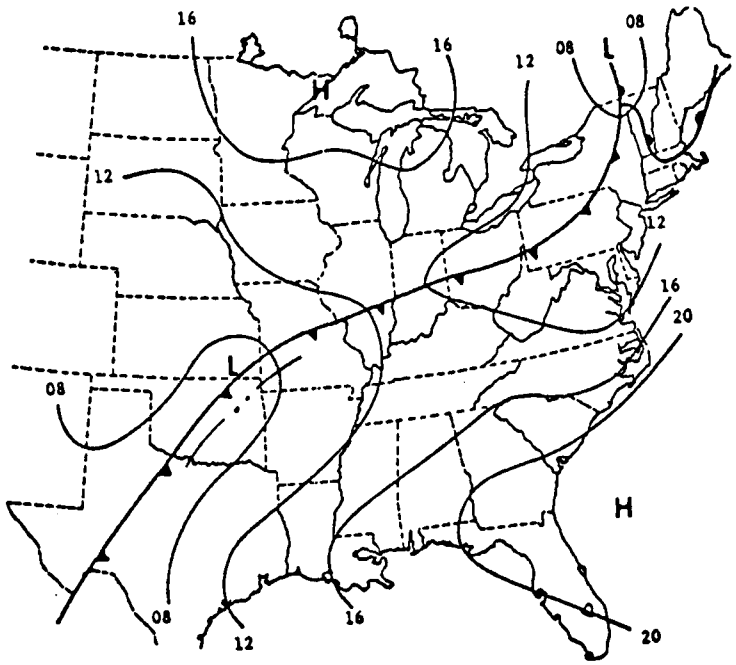


Figure 9. Surface map for 0000 GMT, April 25, 1975 [9].

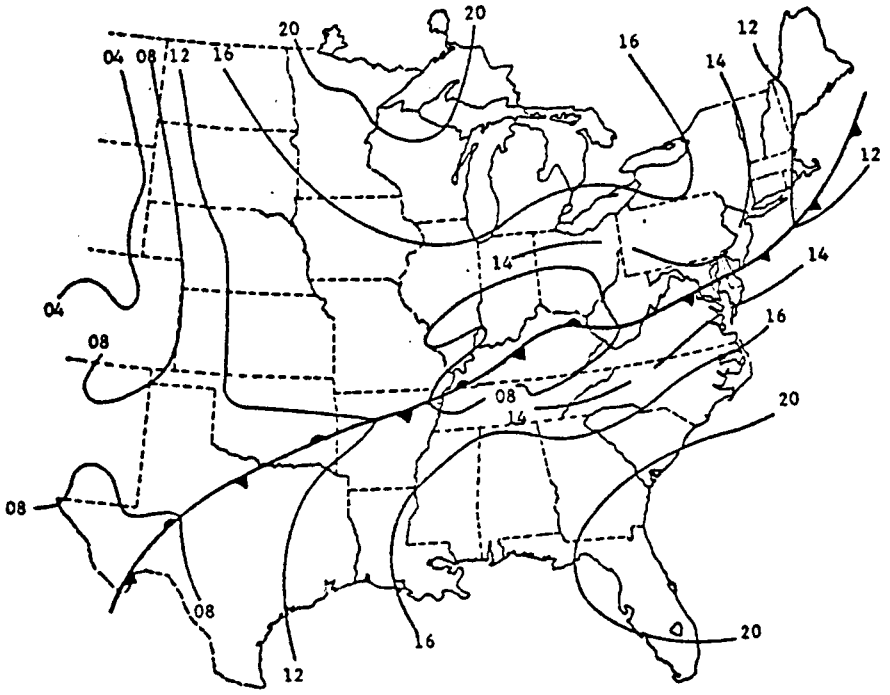


Figure 10. Surface map for 1200 GMT, April 25, 1975 [1].

## D. Manually Digitized Radar Data

In order to correlate the stability analyses with the radar measurements of precipitation which developed during AVE-IV, the manually digitized radar (MDR) data, from the National Oceanic and Atmospheric Administration (NOAA) Techniques Development Laboratory, were used. These data had been obtained and correlated previously for other AVE-IV investigations before use in the present study. The MDR grid network of squares (83 km on a side) is shown in Figure 11. Areal coverage and echo intensity of rainfall within each square, for every hour, determined the MDR code (from 0 to 9) assigned to each square. The code used is described by Foster and Reap [23] and is given in Table 2. Radar data for each square were then compiled, with the maximum hourly radar intensity value over a three-hour period being used. The MDR time period was centered on each of the nine AVE-IV rawinsonde observation times in order to compare the two sets directly. However, for this study, instead of using all nine categories of MDR precipitation codes, only four composite categories of MDR precipitation intensity/coverage classifications were used. These MDR definitions were taken from Reap [24] and Wilson [17] and are presented in Table 3.

## E. Rawinsonde Data Grid

The AVE-IV 25-mb spaced rawinsonde profile data were interpolated for each of the nine time periods using an 18x18 grid, with 160-km spacing between grid points, as shown in Figure 12.

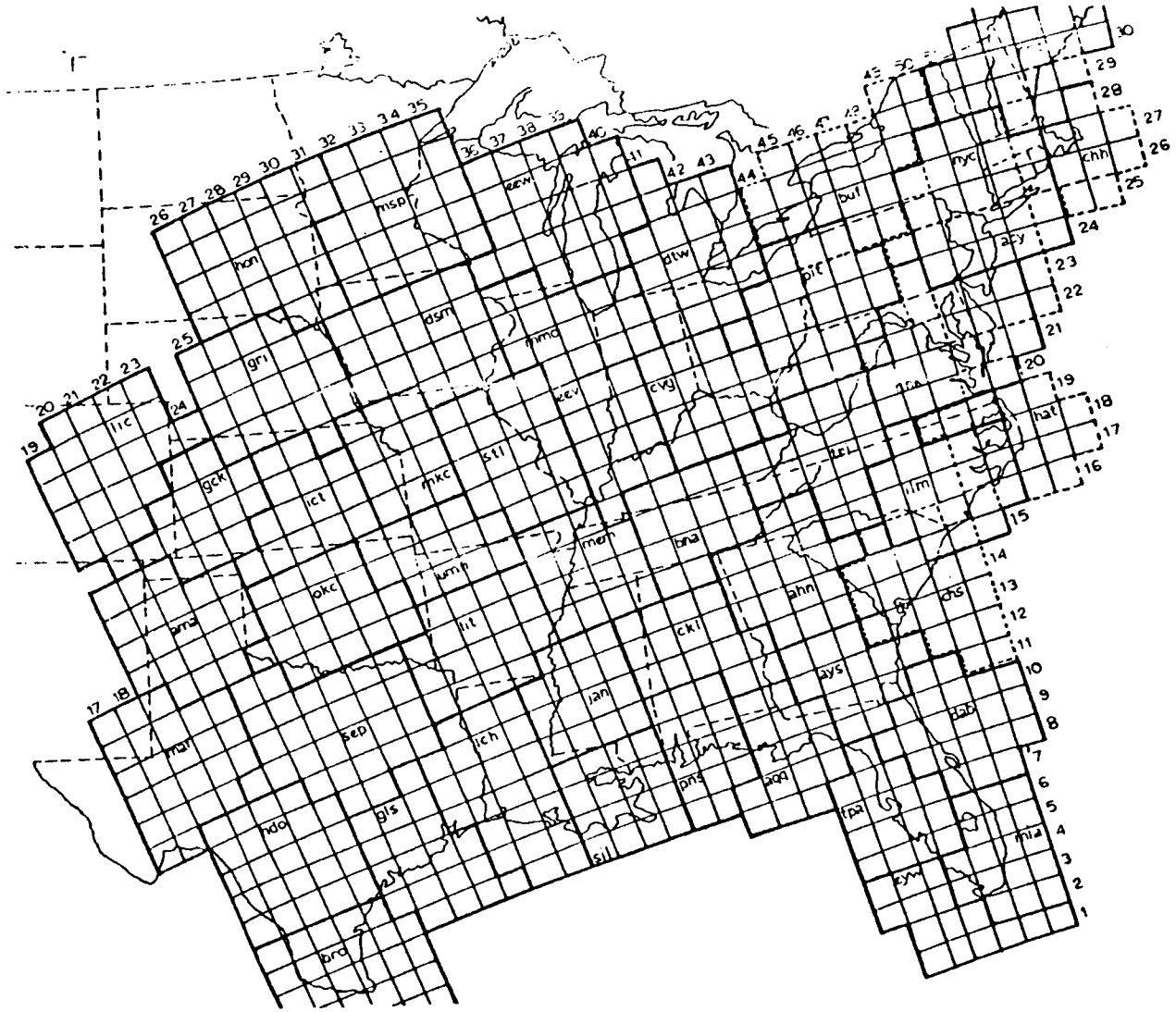


Figure 11. Manually digitized radar (MDR) grid network [8].

Table 2. Manually Digitized Radar Data Code [8]

| Code No. | Intensity, Maximum Observed VIP[a] Values | Coverage, Percent of VIP Coverage In Box | Maximum Rainfall Rate (in $h^{-1}$) | Intensity Category |
|---|---|---|---|---|
| 0 | No Echoes | | | |
| 1 | 1 | Any VIP1 | <0.1 | Weak |
| 2 | 2 | ≤50% of VIP2 | 0.1 to 0.5 | Moderate |
| 3 | 2 | >50% of VIP2 | 0.5 to 1.0 | Moderate |
| 4 | 3 | ≤50% of VIP3 | 1.0 to 2.0 | Strong |
| 5 | 3 | >50% of VIP3 | 1.0 to 2.0 | Strong |
| 6 | 4 | ≤50% of VIP3 and 4 | 1.0 to 2.0 | Very Strong |
| 7 | 4 | >50% of VIP3 and 4 | 1.0 to 2.0 | Very Strong |
| 8 | 5 or 6 | ≤50% of VIP3, 4, 5, and 6 | >2.0 | Intense or Extreme |
| 9 | 5 or 6 | >50% of VIP3, 4, 5, and 6 | >2.0 | Intense or Extreme |

[a]Video Integrator Processor (intensity of returned radar signal, gated).

Table 3. MDR Categories Used in the Present AVE-IV Analyses

| Category | MDR Value | Convective Activity |
|---|---|---|
| A | 0 | No precipitation |
| B | > 0 | All precipitation |
| C | > 3 | All thunderstorm activity |
| D | > 7 | All severe thunderstorm activity |

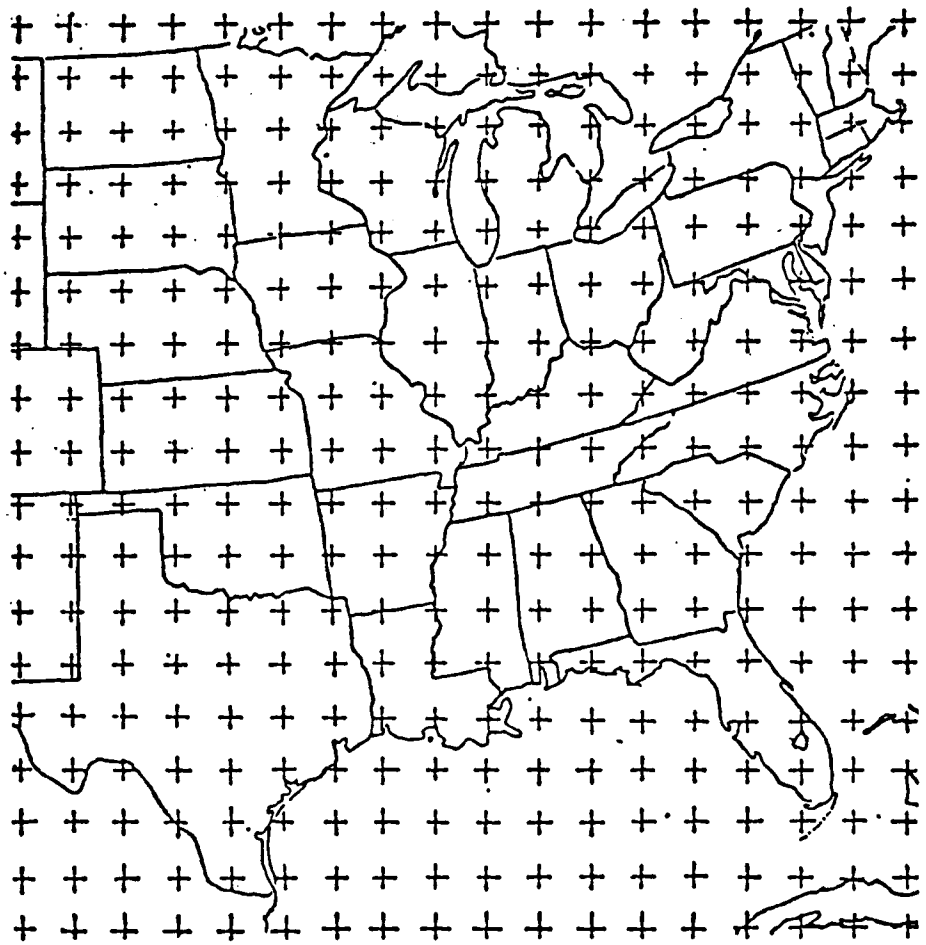

Figure 12. The 18x18 grid used for numerical computations [8].

This produced a workable field of measured data at all grid points. According to Barr et al. [25], this grid spacing produces the maximum resolution possible given a sample of randomly spaced rawinsonde stations. More detail concerning numerical computation criteria in using the AVE grid is given in the 1976 report of Wilson and Scoggins [26].

## F. AVE-IV Averaged Profiles

A number of stability analyses have been carried out for storm and severe storm environments where stability indices were calculated. Most analyses involved the computation of only one or maybe two indices. However, there have been only a few studies in which a number of stability indices have been computed with identical data and compared. Some of these studies are reported in References [26 through 31]. Most of these studies involved comparisons of the different station indices computed throughout convective development of a moving storm system. Also, four reports on stability analyses during the AVE-IV project have been published [7, 9, 11, 18].

However, as indicated in the Introduction, a different type of atmospheric stability analysis will be examined here; that is, one involving arithmetically averaged soundings which relate to different AVE-IV weather criteria, ranging from no weather to severe weather. It was suggested that if mean atmospheric profiles representing a certain convective atmospheric environment were compared with soundings representing, say, "a more severe environment," then an examination of all parameter profile averages might indicate a

structural trend within these profiles that would be related directly to the degree of convection just prior to or during occurrence of severe weather. A forecast tool might result from these trends if examined. This average profile study may uncover something unique when applied to a convective situation, not observable from an individual station's vertical sounding. It is suggested that atmospheric stability through a stability index procedure is one way to do an analysis on averaged profile soundings. This averaged-profile method is not new. Wilson and Scoggins [20] in 1978 presented a quick-look at AVE-IV average sounding analyses involving temperature, dew point, and vector wind, along with a few calculated parameters. The present study extends the work of Wilson and Scoggins [20] in terms of a detailed study of just the thermodynamic stability of the AVE-IV atmosphere.

The AVE-IV profile data, related to a grid, can now be linked to the MDR grid data. This computational linking had previously been done by objective techniques [21] for use in other AVE-IV studies. This resulted in producing the six averaged (mean) vertical profiles of temperature, dew-point temperature, mixing ratio, zonal (east-west) and meridional (north-south) wind speed, and pressure level height for the 17 pressure levels of data from 900 to 100 mb, with 50-mb spacing for the nine AVE-IV time periods. The procedure to obtain these average profiles versus weather category is described by example in the following paragraph.

As an example, consider the most severe thunderstorm cases (MDR>7). The following procedure was used to create average

soundings for the six measured parameters described in the preceding paragraph. All values of the parameters at grid points within ~80 km of a three-hour composite MDR value >7 were averaged for the total AVE-IV time period. This procedure was also carried out for the other three MDR categories defined in Table 3, page 27. The resulting four tables of averaged (mean) profiles are presented in Tables 4 through 7.

## G. AVE-IV Average Lag Profiles

As a final task using the AVE-IV data, average lag profiles were computed. Lag here is defined as the time difference between the sounding and the occurrence of severe weather, three hours later. Examination of lag profiles promises a certain forecast capability through determination of the average environment three hours prior to severe weather occurrence.

The three-hour composite MDR data had previously been categorized according to the four weather types given in Table 3. To create the average lag profile, all soundings three hours[1] prior to the occurrence of each MDR convective category were extracted from the data set for each parameter. These were then averaged to obtain the average lag profile for the four MDR cases. The results are presented in Tables 8 through 11.

---

[1] If three-hour sounding separation was not available, the sounding taken six hours prior was used.

Table 4. AVE-IV Average Profile Conditions for MDR = 0 (No Precipitation)

| Press. mb | Ht. m | Temp. $^{o}C$ | Dew Pt. $^{o}C$ | U Wind m/s | V Wind m/s | Mix. Ratio gm/kg | Wind Sp. m/s | Wind Dir. Deg. |
|---|---|---|---|---|---|---|---|---|
| 900 | 1,010 | 13.8 | 8.0 | 2.0 | 4.3 | 8.0 | 4.7 | 205 |
| 850 | 1,490 | 12.4 | 2.9 | 4.0 | 4.0 | 6.3 | 5.7 | 225 |
| 800 | 2,000 | 10.1 | -2.6 | 5.7 | 3.4 | 4.7 | 6.6 | 239 |
| 750 | 2,530 | 7.6 | -10.5 | 7.4 | 2.8 | 3.1 | 7.9 | 249 |
| 700 | 3,100 | 4.4 | -15.5 | 8.9 | 2.5 | 2.2 | 9.2 | 254 |
| 650 | 3,700 | 0.5 | -17.9 | 10.4 | 2.4 | 1.9 | 10.7 | 257 |
| 600 | 4,330 | -4.1 | -22.6 | 11.9 | 2.1 | 1.5 | 12.1 | 260 |
| 550 | 5,010 | -9.0 | -26.8 | 13.6 | 2.0 | 1.2 | 13.8 | 262 |
| 500 | 5,740 | -14.2 | -31.8 | 15.4 | 2.5 | 0.8 | 15.6 | 261 |
| 450 | 6,530 | -19.8 | -39.3 | 17.4 | 3.0 | 0.5 | 17.7 | 260 |
| 400 | 7,400 | -26.4 | -44.4 | 19.7 | 3.3 | 0.3 | 20.0 | 260 |
| 350 | 8,350 | -33.7 | -50.4 | 22.8 | 3.9 | 0.2 | 23.1 | 260 |
| 300 | 9,410 | -42.0 | --- | 26.2 | 4.9 | --- | 26.7 | 259 |
| 250 | 10,600 | -51.1 | --- | 30.1 | 5.7 | --- | 30.6 | 259 |
| 200 | 12,000 | -59.5 | --- | 32.2 | 5.1 | --- | 32.6 | 261 |
| 150 | 13,800 | -59.5 | --- | 28.2 | 5.0 | --- | 28.6 | 260 |
| 100 | 16,400 | -62.2 | --- | 19.1 | 4.7 | --- | 19.7 | 256 |

Note: Number of soundings = 1,053.

Table 5. AVE-IV Average Profile Conditions for MDR > 0 (All Precipitation)

| Press. mb | Ht. m | Temp. °C | Dew Pt. °C | U Wind m/s | V Wind m/s | Mix. Ratio gm/kg | Wind Sp. m/s | Wind Dir. Deg. |
|---|---|---|---|---|---|---|---|---|
| 900 | 998 | 13.7 | 9.8 | 5.1 | 7.6 | 8.8 | 9.2 | 214 |
| 850 | 1,480 | 11.3 | 6.4 | 8.1 | 7.2 | 7.6 | 10.8 | 228 |
| 800 | 1,980 | 8.8 | 3.1 | 10.2 | 6.4 | 6.4 | 12.0 | 238 |
| 750 | 2,520 | 5.9 | -2.4 | 11.6 | 6.0 | 5.0 | 13.1 | 243 |
| 700 | 3,080 | 2.6 | -8.0 | 12.8 | 6.2 | 3.6 | 14.2 | 244 |
| 650 | 3,670 | -1.1 | -11.8 | 14.4 | 6.6 | 2.9 | 15.8 | 245 |
| 600 | 4,310 | -5.3 | -17.0 | 16.1 | 6.8 | 2.2 | 17.5 | 247 |
| 550 | 4,990 | -9.9 | -22.2 | 18.0 | 6.7 | 1.7 | 19.2 | 250 |
| 500 | 5,710 | -14.7 | -28.1 | 19.7 | 6.9 | 1.2 | 20.9 | 251 |
| 450 | 6,500 | -20.2 | -34.9 | 20.9 | 7.4 | 0.7 | 22.2 | 251 |
| 400 | 7,370 | -26.5 | -40.9 | 22.6 | 8.0 | 0.4 | 24.0 | 251 |
| 350 | 8,320 | -33.8 | -47.2 | 24.9 | 8.5 | 0.2 | 26.3 | 251 |
| 300 | 9,380 | -42.1 | --- | 27.5 | 9.6 | --- | 29.1 | 251 |
| 250 | 10,600 | -51.5 | --- | 30.5 | 10.5 | --- | 32.3 | 251 |
| 200 | 12,000 | -60.6 | --- | 32.5 | 9.2 | --- | 33.8 | 254 |
| 150 | 13,800 | -59.5 | --- | 28.9 | 6.7 | --- | 29.7 | 257 |
| 100 | 16,300 | -60.2 | --- | 20.2 | 4.5 | --- | 20.7 | 257 |

Note: Number of soundings = 567.

Table 6. AVE-IV Average Profile Conditions for MDR > 3 (All Thunderstorms)

| Press. mb | Ht. m | Temp. °C | Dew Pt. °C | U Wind m/s | V Wind m/s | Mix. Ratio gm/kg | Wind Sp. m/s | Wind Dir. Deg. |
|---|---|---|---|---|---|---|---|---|
| 900 | 987 | 15.9 | 11.2 | 5.4 | 6.7 | 9.6 | 8.6 | 219 |
| 850 | 1,470 | 13.3 | 7.7 | 8.6 | 6.6 | 8.2 | 10.8 | 233 |
| 800 | 1,980 | 10.5 | 4.4 | 10.8 | 6.0 | 7.1 | 12.4 | 241 |
| 750 | 2,520 | 7.3 | -0.1 | 12.3 | 5.7 | 5.7 | 13.6 | 245 |
| 700 | 3,080 | 3.9 | -7.5 | 14.0 | 6.2 | 3.8 | 15.3 | 246 |
| 650 | 3,680 | -0.1 | -12.1 | 15.8 | 7.4 | 2.9 | 17.5 | 245 |
| 600 | 4,310 | -4.5 | -17.1 | 17.9 | 8.1 | 2.1 | 19.7 | 246 |
| 550 | 4,990 | -9.4 | -22.5 | 19.9 | 8.5 | 1.6 | 21.6 | 247 |
| 500 | 5,720 | -14.3 | -29.1 | 21.4 | 8.8 | 1.1 | 23.1 | 248 |
| 450 | 6,510 | -19.7 | -35.5 | 22.5 | 9.3 | 0.7 | 24.4 | 248 |
| 400 | 7,380 | -26.1 | -40.6 | 24.0 | 10.0 | 0.4 | 26.0 | 247 |
| 350 | 8,330 | -33.5 | -46.6 | 25.8 | 10.4 | 0.3 | 27.8 | 248 |
| 300 | 9,390 | -41.7 | --- | 27.8 | 11.4 | --- | 30.1 | 248 |
| 250 | 10,600 | -51.1 | --- | 30.0 | 12.0 | --- | 32.3 | 248 |
| 200 | 12,000 | -60.5 | --- | 32.1 | 10.9 | --- | 33.9 | 251 |
| 150 | 13,800 | -60.0 | --- | 29.3 | 8.6 | --- | 30.5 | 254 |
| 100 | 16,300 | -60.7 | --- | 20.7 | 6.7 | --- | 21.8 | 252 |

Note: Number of soundings = 189.

Table 7. AVE-IV Average Profile Conditions for MDR > 7 (Severe Thunderstorms)

| Press. mb | Ht. m | Temp. °C | Dew Pt. °C | U Wind m/s | V Wind m/s | Mix. Ratio gm/kg | Wind Sp. m/s | Wind Dir. Deg. |
|---|---|---|---|---|---|---|---|---|
| 900 | 978 | 18.8 | 11.6 | 4.3 | 6.2 | 9.9 | 7.6 | 215 |
| 850 | 1,470 | 15.6 | 8.2 | 7.5 | 6.4 | 8.5 | 9.9 | 230 |
| 800 | 1,980 | 12.5 | 5.0 | 8.9 | 5.6 | 7.3 | 10.5 | 238 |
| 750 | 2,520 | 8.6 | 0.7 | 10.2 | 4.6 | 5.9 | 11.2 | 246 |
| 700 | 3,090 | 4.8 | -7.8 | 12.1 | 5.4 | 3.6 | 13.3 | 246 |
| 650 | 3,680 | 0.5 | -11.8 | 14.4 | 7.0 | 2.8 | 16.0 | 244 |
| 600 | 4,320 | -4.4 | -17.2 | 17.4 | 8.0 | 2.0 | 19.2 | 245 |
| 550 | 5,000 | -9.4 | -23.5 | 19.5 | 8.9 | 1.4 | 21.4 | 245 |
| 500 | 5,730 | -13.9 | -29.9 | 20.5 | 9.5 | 1.0 | 22.6 | 245 |
| 450 | 6,520 | -19.4 | -35.9 | 22.3 | 10.0 | 0.6 | 24.4 | 246 |
| 400 | 7,390 | -25.9 | -40.4 | 24.3 | 10.8 | 0.4 | 26.6 | 246 |
| 350 | 8,340 | -33.4 | -45.9 | 26.7 | 10.9 | 0.3 | 28.8 | 248 |
| 300 | 9,410 | -41.5 | --- | 29.4 | 11.8 | --- | 31.7 | 248 |
| 250 | 10,600 | -51.0 | --- | 32.8 | 12.6 | --- | 35.1 | 249 |
| 200 | 12,000 | -60.2 | --- | 35.3 | 12.0 | --- | 37.3 | 251 |
| 150 | 13,800 | -60.7 | --- | 31.1 | 10.1 | --- | 32.7 | 252 |
| 100 | 16,300 | -61.0 | --- | 21.8 | 7.8 | --- | 23.2 | 250 |

Note: Number of soundings = 66.

Table 8. AVE-IV Average Lag Profile Conditions for MDR = 0 (No Precipitation)

| Press. mb | Ht. m | Temp. °C | Dew Pt. °C | U Wind m/s | V Wind m/s | Mix. Ratio gm/kg | Wind Sp. m/s | Wind Dir. Deg. |
|---|---|---|---|---|---|---|---|---|
| 900 | 1,010 | 14.3 | 8.2 | 2.1 | 4.4 | 8.1 | 4.9 | 206 |
| 850 | 1,490 | 12.5 | 3.6 | 4.2 | 4.1 | 6.5 | 5.9 | 226 |
| 800 | 2,000 | 10.1 | -1.7 | 6.0 | 3.5 | 5.0 | 7.0 | 240 |
| 750 | 2,530 | 7.5 | -9.0 | 7.7 | 2.9 | 3.4 | 8.2 | 249 |
| 700 | 3,100 | 4.3 | -14.4 | 9.2 | 2.7 | 2.3 | 9.6 | 254 |
| 650 | 3,700 | 0.4 | -16.7 | 10.7 | 2.7 | 2.0 | 11.0 | 256 |
| 600 | 4,330 | -4.1 | -21.3 | 12.4 | 2.4 | 1.6 | 12.6 | 259 |
| 550 | 5,010 | -9.0 | -25.3 | 14.1 | 2.2 | 1.3 | 14.3 | 261 |
| 500 | 5,740 | -14.1 | -30.4 | 15.9 | 2.6 | 0.9 | 16.1 | 261 |
| 450 | 6,540 | -19.7 | -37.7 | 17.7 | 3.2 | 0.5 | 18.0 | 260 |
| 400 | 7,400 | -26.2 | -43.3 | 19.9 | 3.7 | 0.3 | 20.2 | 259 |
| 350 | 8,350 | -33.5 | -49.5 | 22.7 | 4.5 | 0.2 | 23.1 | 259 |
| 300 | 9,410 | -41.9 | --- | 26.0 | 5.6 | --- | 26.6 | 258 |
| 250 | 10,600 | -51.1 | --- | 29.7 | 6.6 | --- | 30.4 | 257 |
| 200 | 12,000 | -59.4 | --- | 32.0 | 6.1 | --- | 32.6 | 259 |
| 150 | 13,800 | -59.3 | --- | 28.3 | 5.5 | --- | 28.8 | 259 |
| 100 | 16,400 | -62.2 | --- | 19.4 | 4.7 | --- | 20.0 | 256 |

Note: Number of soundings = 956.

Table 9. AVE-IV Average Lag Profile Conditions for MDR > 0 (All Precipitation)

| Press. mb | Ht. m | Temp. °C | Dew Pt. °C | U Wind m/s | V Wind m/s | Mix. Ratio gm/kg | Wind Sp. m/s | Wind Dir. Deg. |
|---|---|---|---|---|---|---|---|---|
| 900 | 999 | 13.5 | 9.9 | 5.3 | 8.5 | 8.8 | 10.0 | 212 |
| 850 | 1,480 | 11.3 | 6.1 | 8.3 | 7.9 | 7.6 | 11.5 | 226 |
| 800 | 1,980 | 8.8 | 2.7 | 10.4 | 6.9 | 6.3 | 12.5 | 236 |
| 750 | 2,520 | 6.1 | -3.0 | 11.7 | 6.4 | 4.9 | 13.3 | 241 |
| 700 | 3,080 | 2.7 | -8.4 | 13.1 | 6.4 | 3.6 | 14.6 | 244 |
| 650 | 3,670 | -1.0 | -12.5 | 14.8 | 6.7 | 2.8 | 16.3 | 246 |
| 600 | 4,310 | -5.2 | -18.1 | 16.4 | 6.9 | 2.1 | 17.8 | 247 |
| 550 | 4,990 | -10.0 | -22.5 | 18.2 | 6.8 | 1.6 | 19.4 | 250 |
| 500 | 5,710 | -14.8 | -28.2 | 20.1 | 7.0 | 1.1 | 21.3 | 251 |
| 450 | 6,500 | -20.2 | -35.5 | 21.4 | 7.6 | 0.7 | 22.7 | 250 |
| 400 | 7,370 | -26.6 | -41.3 | 22.9 | 7.8 | 0.4 | 24.2 | 251 |
| 350 | 8,320 | -33.9 | -48.0 | 25.4 | 8.1 | 0.2 | 26.7 | 252 |
| 300 | 9,380 | -42.3 | --- | 28.0 | 9.0 | --- | 29.4 | 252 |
| 250 | 10,600 | -51.8 | --- | 31.1 | 9.6 | --- | 32.6 | 253 |
| 200 | 12,000 | -60.6 | --- | 32.7 | 8.4 | --- | 33.8 | 256 |
| 150 | 13,800 | -59.4 | --- | 29.4 | 6.9 | --- | 30.2 | 257 |
| 100 | 16,300 | -60.0 | --- | 20.4 | 4.7 | --- | 20.9 | 257 |

Note: Number of soundings = 484.

Table 10. AVE-IV Average Lag Profile Conditions for MDR > 3 (All Thunderstorms)

| Press. mb | Ht. m | Temp. °C | Dew Pt. °C | U Wind m/s | V Wind m/s | Mix. Ratio gm/kg | Wind Sp. m/s | Wind Dir. Deg. |
|---|---|---|---|---|---|---|---|---|
| 900 | 994 | 15.9 | 11.5 | 5.7 | 9.2 | 9.7 | 10.8 | 212 |
| 850 | 1,480 | 13.3 | 8.0 | 8.9 | 8.5 | 8.4 | 12.3 | 226 |
| 800 | 1,990 | 10.5 | 4.6 | 11.3 | 7.3 | 7.1 | 13.5 | 237 |
| 750 | 2,520 | 7.7 | -1.1 | 12.9 | 6.8 | 5.4 | 14.6 | 242 |
| 700 | 3,090 | 4.3 | -8.8 | 14.5 | 7.1 | 3.5 | 16.1 | 244 |
| 650 | 3,690 | 0.5 | -14.6 | 16.6 | 7.9 | 2.6 | 18.4 | 245 |
| 600 | 4,330 | -4.0 | -19.6 | 18.4 | 8.6 | 1.8 | 20.3 | 245 |
| 550 | 5,010 | -9.0 | -23.9 | 20.3 | 8.6 | 1.4 | 22.1 | 247 |
| 500 | 5,740 | -14.0 | -30.1 | 22.4 | 8.8 | 0.9 | 24.1 | 249 |
| 450 | 6,530 | -19.5 | -37.6 | 23.4 | 9.4 | 0.5 | 25.2 | 248 |
| 400 | 7,390 | -26.0 | -42.8 | 24.5 | 9.4 | 0.3 | 26.2 | 249 |
| 350 | 8,350 | -33.3 | -49.4 | 26.5 | 9.3 | 0.2 | 28.1 | 251 |
| 300 | 9,410 | -41.8 | --- | 28.0 | 10.3 | --- | 29.8 | 250 |
| 250 | 10,600 | -51.1 | --- | 30.3 | 10.4 | --- | 32.0 | 251 |
| 200 | 12,000 | -60.2 | --- | 32.4 | 9.7 | --- | 33.8 | 253 |
| 150 | 13,800 | -59.9 | --- | 30.3 | 8.8 | --- | 31.6 | 254 |
| 100 | 16,400 | -60.9 | --- | 20.9 | 6.2 | --- | 21.8 | 253 |

Number of soundings = 164.

Table 11. AVE-IV Average Lag Profile Conditions for MDR > 7 (Severe Thunderstorms)

| Press. mb | Ht. m | Temp. °C | Dew Pt. °C | U Wind m/s | V Wind m/s | Mix. Ratio gm/kg | Wind Sp. m/s | Wind Dir. Deg. |
|---|---|---|---|---|---|---|---|---|
| 900 | 992 | 18.5 | 13.1 | 4.6 | 8.9 | 10.7 | 10.0 | 207 |
| 850 | 1,480 | 15.8 | 8.9 | 7.8 | 8.2 | 8.9 | 11.3 | 224 |
| 800 | 1,990 | 12.7 | 4.7 | 10.1 | 6.3 | 7.2 | 11.9 | 238 |
| 750 | 2,530 | 9.4 | -0.6 | 11.3 | 5.4 | 5.4 | 12.5 | 244 |
| 700 | 3,100 | 5.9 | -7.7 | 12.9 | 6.2 | 3.5 | 14.3 | 244 |
| 650 | 3,700 | 1.8 | -12.6 | 15.1 | 7.7 | 2.5 | 17.0 | 243 |
| 600 | 4,340 | -3.3 | -18.4 | 17.5 | 9.1 | 1.8 | 19.7 | 243 |
| 550 | 5,030 | -8.6 | -22.8 | 20.0 | 9.3 | 1.3 | 22.1 | 245 |
| 500 | 5,760 | -13.6 | -28.0 | 23.1 | 9.7 | 1.0 | 25.1 | 247 |
| 450 | 6,550 | -19.1 | -36.8 | 25.1 | 10.0 | 0.5 | 27.0 | 248 |
| 400 | 7,420 | -25.7 | -41.2 | 26.8 | 10.0 | 0.4 | 28.6 | 250 |
| 350 | 8,370 | -33.1 | -46.1 | 29.5 | 9.8 | 0.2 | 31.1 | 252 |
| 300 | 9,430 | -41.6 | --- | 32.4 | 10.0 | --- | 33.9 | 253 |
| 250 | 10,600 | -50.7 | --- | 35.3 | 10.1 | --- | 36.7 | 254 |
| 200 | 12,100 | -59.9 | --- | 37.0 | 10.9 | --- | 38.6 | 254 |
| 150 | 13,900 | -60.7 | --- | 32.6 | 10.2 | --- | 34.2 | 253 |
| 100 | 16,400 | -61.4 | --- | 22.5 | 6.9 | --- | 23.5 | 253 |

Note: Number of soundings = 51.

# CHAPTER IV

# INDICES USED IN STUDY

## A. Introduction

This chapter presents the criteria used in the selection of stability indices that were chosen for analyses in the present study. The indices are then presented, with a detailed description given for each.

## B. Index Selection Criteria

The stability indices used in this study were selected to utilize the available AVE-IV data described in Chapter III. Indices were chosen based on ease of computation. Computations involving differences, additions, multiplications, and divisions among the available atmospheric parameters at or between vertical pressure levels were, in general, selected.

Mean profile data for AVE-IV does not extend below the 900-mb level and therefore, all atmospheric stability indices which use the surface or data levels up to 900 mb were eliminated from this study. Indices which require complex computation with the available data were also eliminated (i.e., indices which require forecasted temperature or moisture parameters at the surface or aloft). Finally, since the computer was used in computing index values for this study, most indices involving a thermodynamic diagram computation were not used.

## C. Indices Chosen

Fourteen atmospheric stability indices were chosen for testing with the AVE-IV mean profile data. They are listed in Table 12 and are described in detail in Section D.

## D. Definition of Indices

This section defines and gives historical information concerning each stability index used in the study. In order for the reader to follow various thermodynamic procedures involved in atmospheric processes used in the index computation, a simplified Skew-T diagram (as described in Chapter II) is given whenever possible to help describe and visualize the steps taken during the index computation.

### Severe Weather Threat Index

The Severe Weather Threat (SWEAT) index was developed by the United States Air Force Global Weather Central (AFGWC) and presented in 1970 [32, 33, 34] for use in forecasting potentially critical convective weather (i.e., severe thunderstorms and tornadoes). It is a computer-prepared index based on weighted, empirical parameters at the 850- and 500-mb levels. The Air Force has revised the SWEAT index twice thus far, and all revisions to date will be presented in this section.

The initial SWEAT index ($SWEAT_1$) from Reference [32] was derived subjectively from a study of 328 severe storm vertical soundings and is written as:

Table 12. Stability Indices

| Index Name | Symbol |
|---|---|
| SWEAT Index | SWEAT |
| Vertical Totals Index | VTI |
| Cross Totals Index | CTI |
| Total Totals Index | TTI |
| Theta E | $\theta_E^*$ |
| Showalter Index | SI |
| Rackcliff Index | RI |
| Jefferson Index | JI |
| Modified Jefferson Index | MJI |
| Boyden Index | BI |
| Bradbury Potential Stability Index | BPI |
| K-Index | KI |
| Energy Index | EI |
| Modified Martin Index | MI |

$$SWEAT_1 = 12\ T_{d850} + 20(TTI - 49) + 2W_{850} + W_{500}\ , \qquad (1)$$

where,

$T_{d850}$ = dew-point temperature ($^{o}C$) at the 850-mb level (positive $T_{d850}$ values only are used; if $T_{d850} < 0$, then set $T_{d850} = 0$) ,

TTI = total-totals index ($^{o}C$)

$TTI = (T + T_d)_{850} - 2\ T_{500}$

(if $TTI < 49$, set $TTI = 49$; the second term then drops out of Eq. (1)) ,

$W_{850}$ = 850-mb wind speed (knots) ,

$W_{500}$ = 500-mb wind speed (knots) .

The SWEAT index is always positive. No individual term may ever be negative. Based on empirical data, the SWEAT index threshold value for tornado cases is ~350, while for severe thunderstorms it is ~250. Miller [35] refers to this initial SWEAT index as the "Soft SWEAT" index.

The SWEAT index was further modified [32] to include the 500-mb/850-mb level wind directional shear term. This shear term is also based upon directional wind shears observed during severe weather cases and changes the SWEAT index ($SWEAT_2$) equation to read:

$$SWEAT_2 = 12\ T_{d850} + 20(TTI - 49) + 2W_{850} + W_{500} + 125(S+0.2)\ , \qquad (2)$$

where,

$$S = \sin(WD_{500} - WD_{850}) ,$$

and

$$WD = \text{wind direction (degrees)} .$$

If the 850-mb wind is not within the range 130 and 250 deg, or if the 500-mb wind is not between 210 and 310 deg, or if the expression $WD_{500} - WD_{850} < 0$, set $S = -0.2$ to drop the shear term. The addition of the shear term to the SWEAT index raises the severe thunderstorm threshold to ~300, and that for tornadoes to ~400 to 425.

The SWEAT index is not a tool for forecasting ordinary thunderstorms. It is designed to indicate the potential of severe thunderstorms (with gusts at least 50 kts and/or hail at least 0.75 in. diameter) or tornadoes.

Lastly, in the SWEAT equation, Miller [35] replaced the 850-mb level with the 900-meter level (except in the TTI and shear calculations) and changed the wind directional shear procedure. The revised SWEAT equation ($SWEAT_3$) thus reads:

$$SWEAT_3 = 12D_e + 20(TTI - 49) + 2W_e + W_{500} + 125\, f(\alpha) , \qquad (3)$$

where,

$D_e$ = low level dew point ($^oC$) at the 900-meter level,[1]

$W_e$ = low level wind speed (kts) at the 900-meter level,[2]

$f(\alpha)$ = a step function[3] of the veering[4] angle $W_e$ to $W_{500}$ .

The term $f(\alpha)$ is set to 0 if both $W_e$ and $W_{500}$ are not $\geq$15 kts. The 850- and 500-mb level wind directions must also fall within earlier stated ranges (see Figure 13). All other terms are defined exactly as before. The use of 900-meter level parameters in the calculation of the SWEAT index is referred to as "BLM SWEAT" since it is the equation used in the AFGWC Fine Mesh and Boundary Layer Models (BLM) forecast model.

The soft SWEAT index plots can be computer-calculated within 1.5 hours of the 00 GMT or 12 GMT sounding time. The BLM SWEAT calculations take up to four hours of computer time. Both SWEAT index methods are currently being used and 12-, 24-, and 36-hour SWEAT index prognostic maps are generally output.

Recently, Miller and his associates [35, 36] have noticed that many times severe weather has formed within overlapping areas

---

[1] Use 850-mb dew point in soft SWEAT.

[2] Use 850-mb wind speed in soft SWEAT.

[3] Use of the sine function was discontinued for soft or BLM SWEAT because it was not representative from 30 to 120 deg.

[4] Veering is defined as a change in wind direction versus altitude, in a clockwise sense.

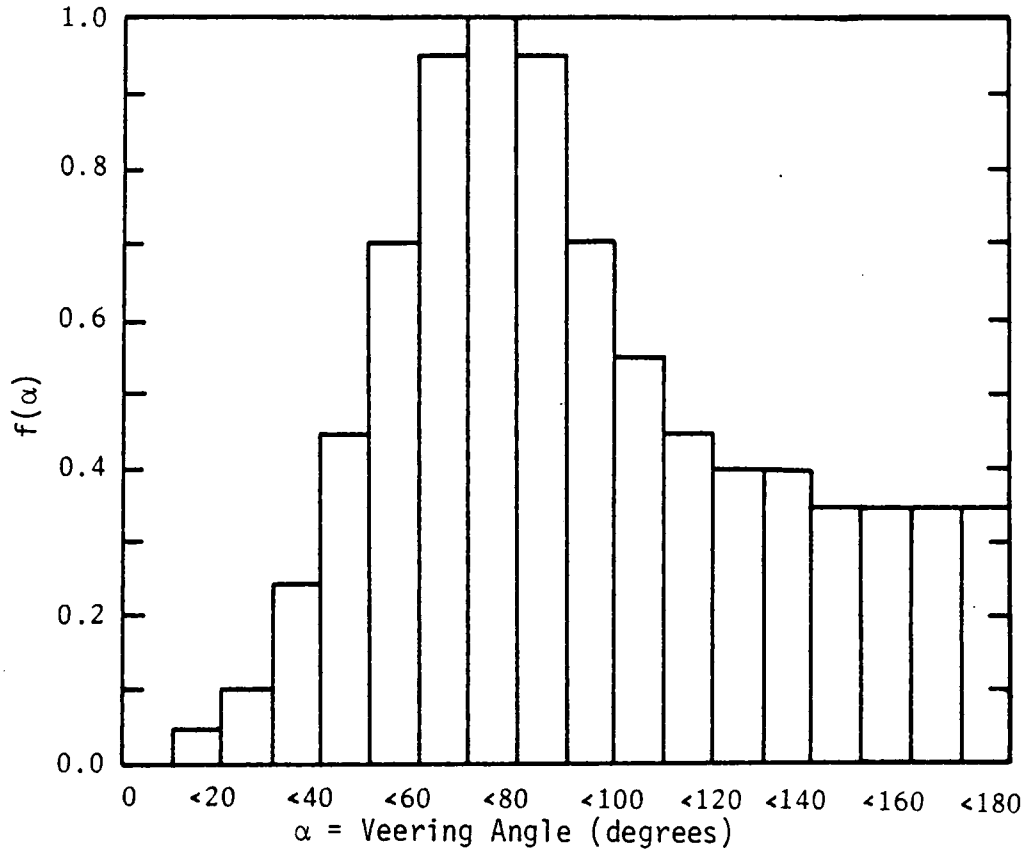


Figure 13. Step function used in computation of SWEAT veering term.

of high SWEAT and high SPOT (Surface Potential index [37]) values. Therefore, these two statistically derived indices can be used together as an aid to accurately identify short-term (three to six hours), small-scale potential severe storm areas. The false alarm rate within the SWEAT/SPOT forecast overlap area is much smaller than that of either index used separately.

The second SWEAT equation (Eq. (2)) has been programmed and is used in the present study as the SWEAT index.

Vertical-Totals Index

In 1967, Miller [38] introduced the term "vertical totals" in relation to potential thunderstorm development. The vertical-totals index (VTI) represents the stability of the atmosphere (temperature lapse rate) between 850 and 500 mb with no moisture parameters involved. It is defined as the 500-mb temperature subtracted from the 850-mb temperature; that is,

$$VTI = T_{850} - T_{500} \ (^{o}C) \ , \qquad (4)$$

Vertical-totals values give a measure of instability. Generally, values ≥26 represent thunderstorm development without regard to moisture. Specific areas and their approximate critical VTI thunderstorm threshold values are listed in Table 13.

Although the VTI can be used alone, it is also valuable when added to the cross-totals moisture index (CTI). Combination of VTI and CTI results in a total-totals index (TTI) is described later.

Table 13. Vertical-Totals Index Thunderstorm Threshold Values for Different Areas

| Area | Critical VTI |
|---|---|
| Gulf Coast | ≥26 |
| British Isles | ≥22 |
| Western Europe | ≥28 |
| West of the Rockies | ≥29 |
| Pacific Coastal Areas | ≥30 |
| Great Lakes | ≥30 |

Cross-Totals Index

Also in 1967, Miller [38] introduced the cross-totals index (CTI) as the 500-mb temperature subtracted from the 850-mb dew-point temperature; that is,

$$CTI = T_{d850} - T_{500} \ (^{o}C) \ . \tag{5}$$

Thus, a low-level moisture parameter is introduced into the index calculation. The CTI has been used to indicate thunderstorm potential, with the cross-totals thunderstorm threshold usually about 18. However, along the Gulf Coast a CTI of 16 (with VTI $\geq$23) generally produces a thunderstorm. The cross-totals index is also an initial index used in the calculation of the total-totals stability index explained in the next section.

Total-Totals Index

In 1967, Miller [38] introduced the concept of the total-totals index (TTI) as being a measure of atmospheric instability between the 850- and 500-mb level. The TTI is defined as the arithmetic sum of the vertical-totals index and the cross-totals index; that is,

$$TTI = VTI + CTI \ (^{o}C) \ , \tag{6}$$

or

$$TTI = (T_{850} + T_{d850}) - 2 \ T_{500} \ (^{o}C) \ . \tag{7}$$

The VTI thunderstorm threshold of 26 and the CTI of 18 produces a minimum threshold of 44 for the total-totals index. Total-totals index values $\geq$50 generally indicate the potential of numerous

and severe thunderstorm/tornadic activity if an adequate low-level moisture supply and a trigger mechanism are both present. The TTI proved to be more accurate in forecasting of thunderstorms, in all places and seasons, than did either the VTI or CTI alone.

Theta-E Methods

The use of equivalent potential temperature ($\theta_E$) can be used in synoptic meteorological practice as a measure of atmospheric stability [39]. The quantity $\theta_E$ is quasi-invariant (conservative) with respect to both dry and moist adiabatic processes, and is invariant (does not change) with respect to evaporation of falling rain [40, 41, 42]. Equivalent potential temperature is a single parameter which takes into account both temperature and moisture content. Theta-E cannot be measured directly since it is simply a concept. It is defined as follows: A parcel of air at temperature $T_o$, dew-point temperature $T_{do}$, and any pressure level $P_o$ rises vertically by a dry-adiabatic process until saturated (at LCL) and then follows the moist-adiabat until all moisture precipitates out. At this point, the moist-adiabat is parallel with the dry-adiabat on the Skew-T diagram. If the air parcel is now compressed dry-adiabatically down to a pressure of 1,000 mb, it will have a temperature defined as the equivalent potential temperature expressed in degrees absolute. Figure 14 illustrates this process.

Theta-E is also a measure of potential stability in that it gives a measure of the effect lifting will have on a column of air [39]. Theta-E can be computed at two vertical levels on a

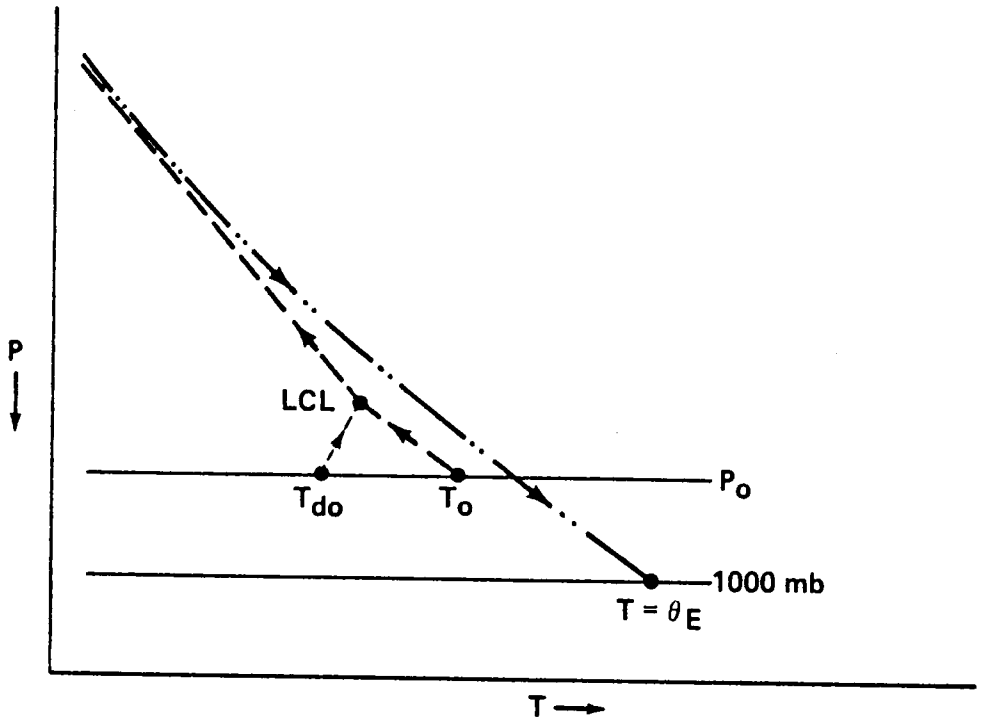


Figure 14. Graphical computation of equivalent potential temperature ($\theta_E$).

sounding, and if it decreases with height between the two levels (i.e., $\Delta\theta_E/\Delta Z$ or $\Delta\theta_E/\Delta P < 0$), this layer is absolutely unstable if lifted to the saturation level [26, 31]. On the other hand, the layer remains stable if lifted to the saturation level when $\theta_E$ increases with height. Reference [43] reports that computed 700-mb Theta-E charts were being transmitted via the facsimile network to aid in the forecasting of thunderstorm activity as early as 1950. The 700-mb Theta-E critical value of ~327°K together with the 6 g/kg mixing ratio line was generally used to outline areas likely to experience heat-type thunderstorms. Values of $\theta_E$ ~321°K and w~4 g/kg indicated the potential of a lifting-type thunderstorm.

Delta Theta-E ($\Delta\theta_E$) values have also been used in thunderstorm forecasting [44], which expressed the change in $\theta_E$ versus pressure-altitude ($\Delta\theta_E/\Delta P$), as indicated earlier. The difference in Theta-E between 850 and 700 mb forms a lower index, and that between 700 and 500 mb an upper index; that is,

$$\Delta\theta_{EL} = \theta_{E850} - \theta_{E700} , \tag{8}$$

$$\Delta\theta_{EU} = \theta_{E700} - \theta_{E500} . \tag{9}$$

Critical values for each index are presented in Table 14, with positive differences indicating instability.

Recently, Alaka et al. [31] have used and tested a simple $\theta_E$ difference equation of the form:

$$\theta^* = \theta_{E700} - \frac{\theta_{ESfc} + \theta_{E850}}{2} , \tag{10}$$

Table 14. Delta Theta-E Upper and Lower Index Critical Values

| $\Delta\theta_E$ | Index | Stability |
|---|---|---|
| > ±0 | Lower | Unstable |
| > -5 | Upper | |
| < ±0 but ≥ -2 | Lower | Questionably Unstable |
| > -5 | Upper | |
| < -2 | Lower | Stable |
| < -5 | Upper | |

where $\theta^*$ defines convective instability, if $\theta^* < 0$ at altitudes between 700 mb and close to the ground (surface and 850 mb). This difference is similar to the lower index of the Delta Theta-E method mentioned previously. The $\theta_E$ index selected for this study is that of Alaka, with Eq. (10) being modified by replacing $\theta_{ESfc}$ with $\theta_{E900}$, since the 900-mb level is the lowest level of averaged data available. This index will be referred to as $\theta_E^*$. Also, all equivalent potential temperature ($\theta_E$) computations made in this study are derived from the approximate form ($\theta_{GE}$) from Eq. (21), as explained later on in the Energy Index section of this chapter.

Showalter Stability Index

The Showalter Stability Index (SI) was developed by A. K. Showalter of the United States Weather Bureau in 1946 and documented more widely in 1953 [5]. It is a thermodynamic static index which can provide a quick, simple estimate of possible thunderstorms based on the potential (convective) instability concept. This index was designed for initial use in the southwestern United States, but has been used extensively all around the world. It was believed that areas of instability are not generally altered significantly at 850 mb and above. Therefore, a stability-index map based on this level and above can be derived and the stability movement prognosticated for 12 and up to 24 hours.

The SI is computed as follows: Dew-point temperature ($T_d$) and temperature (T) values (in $^oC$) are obtained at the 850-mb level (the assumed top of the moisture layer), together with the temperature value (in $^oC$) at 500 mb. Showalter indicated that mountain

sites can use T and $T_d$ values from the 700-mb level instead of the 850-mb level in their SI computations. The 850-mb parcel is now lifted dry-adiabatically to the saturation level (LCL) and then lifted moist-adiabatically to 500 mb. The lifted 500-mb temperature is then subtracted from the observed 500-mb temperature; that is,

$$SI = T_{\substack{OBS \\ 500}} - T_{\substack{LIFTED \\ 500}} \text{ (in } ^{o}C) \text{ .} \qquad (11)$$

The procedure is depicted graphically in Figure 15. Showalter Stability Index values of +3 deg or less generally indicate probable showers and some thunderstorms in the area; SI values from +1 to -2 deg indicate increasing probability of thunderstorms; SI values from -3 to -5 deg (or less) indicate possible severe thunderstorms; SI values from -6 deg or less indicate suspect conditions for tornadoes.

The Showalter index has been used extensively over the years in different capacities. It has been directly correlated with hail [45, 46] and with storm radar echoes [47 through 49]. It has been used in the forecasting of general showers resulting from surface heating as well as from lifting [3]. This index has also been used in heating calculations because, besides being a function of the $\theta_E$ or $\theta_W$ lapse rates, it is also partly a function of the ordinary temperature lapse rate and is, therefore, indicative of stability for use in surface-parcel heating applications. This index is a measure of convective stability when the index value is greater than +6, and convective instability when

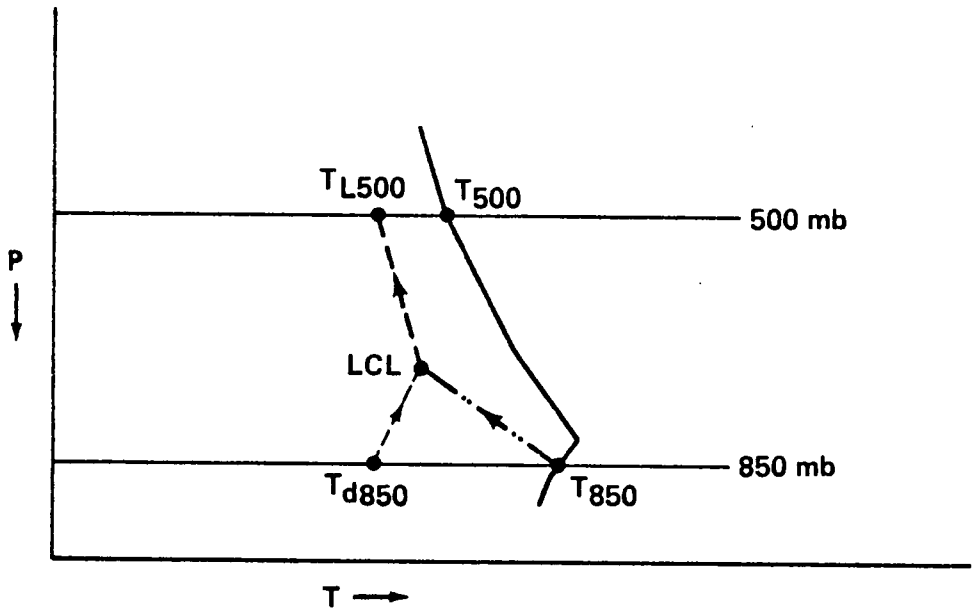


Figure 15. Showalter stability index computation method.

values are less than zero. Also, the index is a first approximation in estimating latent instability, because negative index values do indicate that a positive area (energy) does exist above the LFC.

The Showalter index is limited for use in mountain areas, and will not work well if the air is extremely dry, or if critical instability exists higher than the 850-mb level. This is because the index uses only the one lower point at 850 mb as being representative of low-level moisture and temperature.

Rackcliff Instability Index

In 1962, Rackcliff [50] introduced a simple latent instability index, patterned after the lifted-index [51], for use in regional forecasting of air-mass-type summer thunderstorms in the British Isles and Western Europe.

While the lifted-index uses a forecasted maximum afternoon temperature in its calculation, Rackcliff used a computed temperature in the calculation of his index. The 900-mb wet-bulb potential temperature ($\theta_{W900}$) was the low-level temperature parameter selected by Rackcliff. It is obtained by taking the 900-mb wet-bulb temperature and descending moist-adiabatically to the 1,000-mb level, as shown in Figure 16. The $\theta_{W900}$ value is believed to be representative of the air at low levels and is also only slightly affected at night by outgoing terrestrial radiation. The environmental temperature at 500 mb ($T_{500}$) is again used as the indicator of middle-tropospheric temperature. The Rackcliff index (RI) is then defined as the algebraic difference of the 500-mb temperature from the 900-mb wet-bulb potential temperature; that is,

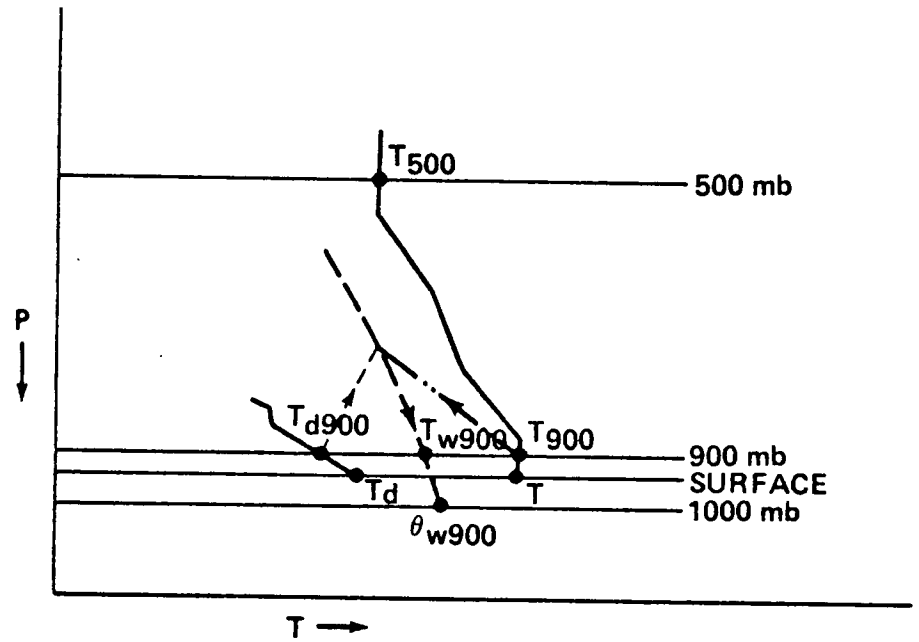


Figure 16. Rackcliff instability index computation method.

$$RI = \theta_{W900} - T_{500} \ (^{o}C) \ , \qquad (12)$$

where positive values represent latent instability. Rackcliff determined the following thunderstorm/no thunderstorm criteria:

1. RI < 25 (stable condition).
2. RI > 25 (showers possible).
3. RI > 30 (thunderstorms possible).
4. RI > 35 (heavy thunderstorms possible).

The value of 30 is a thunderstorm threshold value used in forecasting nonfrontal thunderstorm activity in the British Isles.

Jefferson Instability Index

A modification of Rackcliff's index was made by Jefferson [52] in 1963 so that the instability index could be used in summertime air-mass thunderstorm forecasting at the London Airport. Jefferson determined that Rackcliff's index makes no allowance for the fact that instability in a layer depends not only on the temperature difference across the layer, but also on its mean temperature. Since the value of $\theta_W$ varies between 10 and 20$^{o}$C over northwest Europe in summertime thunderstorm situations, this would give a variable Rackcliff index value between 36 and 29. Therefore, Jefferson amended Rackcliff's formula with an empirical study and obtained an instability index value independent of temperature, but with the same threshold value of 30 for thunderstorms. This was true for a wide range of temperatures. This modified index can now be used in wider areas and for all seasons. The Jefferson instability index (JI) is expressed as:

$$JI = 1.6\ \theta_{W900} - T_{500} - 11\ , \qquad (13)$$

where $\theta_{W900}$ is the 900-mb wet-bulb potential temperature ($^{o}C$) and $T_{500}$ is the observed 500-mb temperature ($^{o}C$). Positive index values represent instability.

Modified Jefferson Instability Index

In 1963, Jefferson [53] published a second modification to the Rackcliff index, or simply, a modified Jefferson index (MJI). While using the Jefferson index at the London Airport, it was determined empirically that the index was forecasting thunderstorms (i.e., JI values exceeded 30) in the Mediterranean area, but many times no thunderstorms formed. This was found to be caused by very dry air existing above 900 and 500 mb over the Mediterranean area. Since the base of thunderclouds over the Mediterranean is generally quite high (~700 mb), the idea of introducing a 700-mb moisture parameter seemed logical, as long as the index continued to work for north-central Europe. This modified Jefferson index (MJI) is written as:

$$MJI = 1.6\ \theta_{W900} - T_{500} - 1/2\ \Delta T_{d700} - 8\ (^{o}C)\ , \qquad (14)$$

where,

$\theta_{W900}$ = 900-mb wet-bulb potential temperature ($^{o}C$) ,

$T_{500}$ = 500-mb observed temperature ($^{o}C$) ,

$\Delta T_{d700}$ = 700-mb dew-point depression ($T_{700} - T_{d700}$) ($^{o}C$) .

The factor 1/2 $\Delta T_{d700}$ was introduced to avoid overweighting by the $\Delta T_{d700}$ parameter.

Boyden Instability Index

Just prior to the 1963 publication of the modified Jefferson index, Boyden [54] also introduced an instability index to be used in the forecasting of thunderstorms and heavy rain over southeast England during the months of May to September. Boyden assumed that the development of heavy showers and thunderstorms over land on a summer afternoon depends on the mean temperature lapse rate only up to 700 mb. For neutral static stability conditions (i.e., dry-bulb temperatures along a moist adiabat), Boyden determined that the 1,000- to 700-mb thickness (in decameters) minus the 700-mb temperature ($^{o}C$) was an approximate constant (~294) for all summer-time atmospheric conditions measured over Crawley, England. Instability is then measured by the amount this difference exceeds the constant. Therefore, instability exists if the 700-mb temperature is a low (cold) value as compared to the 1,000- to 700-mb thickness value. Boyden's index (BI) is expressed as:

$$BI = \Delta Z_{(1,000 \text{ to } 700)} - T_{700} - 200 , \qquad (15)$$

where,

$\Delta Z$ = 1,000- to 700-mb thickness (decameters) ,

$T_{700}$ = 700-mb temperature ($^{o}C$) .

The units conflict in the BI expression. Only the numerical value should be used. The value 200 is used to remove the large unwanted

number generated by this index. It allows the BI to take on a value around 90.

The BI is strictly a measure of the mean stability in the entire layer below 700 mb. The Boyden index is not intended to forecast slight or moderate showers. The diurnal variation of BI was found to be low, allowing a 12-hour forecasting of the index to be made. It was determined that Boyden index isopleths (drawn in intervals of two units) move with the 700-mb wind.

For both frontal and non-frontal summer days, it was found that there was, indeed, a marked increase in thunderstorm/heavy rain occurrence when BI reached values of 94 and higher. Since humidity was found to be very loosely related to the development of thunderstorms, it was not included with the Boyden index. The main advantage claimed for the Boyden index is its usefulness at mobile sites during frontal or non-frontal weather.

For the present study, the Boyden index was modified, since 1,000-mb heights are not obtainable from the averaged soundings. Therefore, the 900-mb height was used in place of the 1,000-mb height.

K-Index

The K-index (KI) was developed by Whiting and documented by George (both of Eastern Air Lines) in 1960 [55]. This simply derived stability index is used in the forecasting of inland air mass thunderstorms with weak winds and without apparent frontal or cyclonic influence. It is prepared from the 1200 GMT soundings and is generally issued on an areal map (with KI intervals every five units).

The Whiting-George K-index measures air mass thunderstorm potential by direct indication of the vertical temperature lapse rate ($T_{850} - T_{500}$), lower atmospheric moisture ($T_{d850}$), and very indirect indications of the vertical extent of the moist layer (700-mb dew-point spread). The K-index is expressed as:

$$KI = (T_{850} - T_{500}) + T_{d850} - (T_{700} - T_{d700}) \ (^{o}C) \ , \qquad (16)$$

where K-values versus thunderstorm occurrence frequencies generally fall within the categories given in Table 15.

The K-index map used concurrently with a subjective analysis of convergence and relative vorticity has been proven by George to be a valuable air mass thunderstorm forecasting tool. Areas of confluence, determined by constructing 850- plus 700-mb height areal charts, are used to represent convergent flow conditions between these two levels. Confluence areas below 700 mb, with winds <20 knots, generally require an adjustment to the next higher category of K-values. If the winds are >20 knots, adjust upward two categories. Positive vorticity also increases the chance of thunder-storm development.

Bryan [56] and Hambridge [57] have tested the K-index versus thunderstorm activity over the mid-South and Western United States, respectively; they found a high correlation. Hambridge suggested the assignment of thunderstorm probabilities versus K-value given in Table 16.

In 1971 [58], the K-index chart was added to the lifted index panel of the composite moisture index chart. This chart is

Table 15. K-Index Thunderstorm Threshold Values

| K-Index Value | Thunderstorm Frequency |
|---|---|
| $K < 20$ | None |
| $20 < K < 25$ | Isolated |
| $25 < K < 30$ | Widely Scattered |
| $30 < K < 35$ | Scattered |
| $35 < K$ | Numerous |

Table 16. K-Index Thunderstorm Probabilities

| K-Index Value | Thunderstorm Probability |
|---|---|
| < 15 | 0% |
| 15 to 20 | < 20% |
| 21 to 25 | 20 to 40% |
| 26 to 30 | 40 to 60% |
| 31 to 35 | 60 to 80% |
| 36 to 40 | 80 to 90% |
| > 40 | Near 100% |

distributed via the NWS NAFAX (National Weather Service National Facsimile Network) system to all meteorologists across the United States.

Bradbury Potential Stability Index

In 1977, Bradbury published an article [59] dealing with the use of wet-bulb potential temperature ($\theta_W$) charts in weather analysis and forecasting. One conclusion he reached was that many summer thunderstorms broke out over Europe when low-level southerly winds advected air with $\theta_{W850} \geq 16^{o}C$. Bradbury then developed a potential stability index (BPI), since the $\theta_{W850}$ values alone failed to identify occasions of thunderstorm development in a relatively cool air mass. This index, similar in structure to Rackcliff's and Jefferson's index, is defined by subtracting the value of $\theta_W$ at 850 mb from the value at 500 mb. A negative value of this difference indicates that the air between the two levels is potentially unstable. In equation form, the BPI is expressed as:

$$BPI = \theta_{W500} - \theta_{W850} \ (^{o}C) \ . \qquad (17)$$

One can obtain the BPI from a thermodynamic diagram procedure as illustrated in Figure 17.

Bradbury also found that the BPI varied as a function of $\theta_{W850}$, when used in the forecasting of thunderstorms during the year. This is illustrated in Figure 18, where 5%, 50%, and Limit represent the cumulative percentage frequency of BPI versus $\theta_{W850}$ for 544 thunderstorm day soundings from 1973 to 1976. The graph

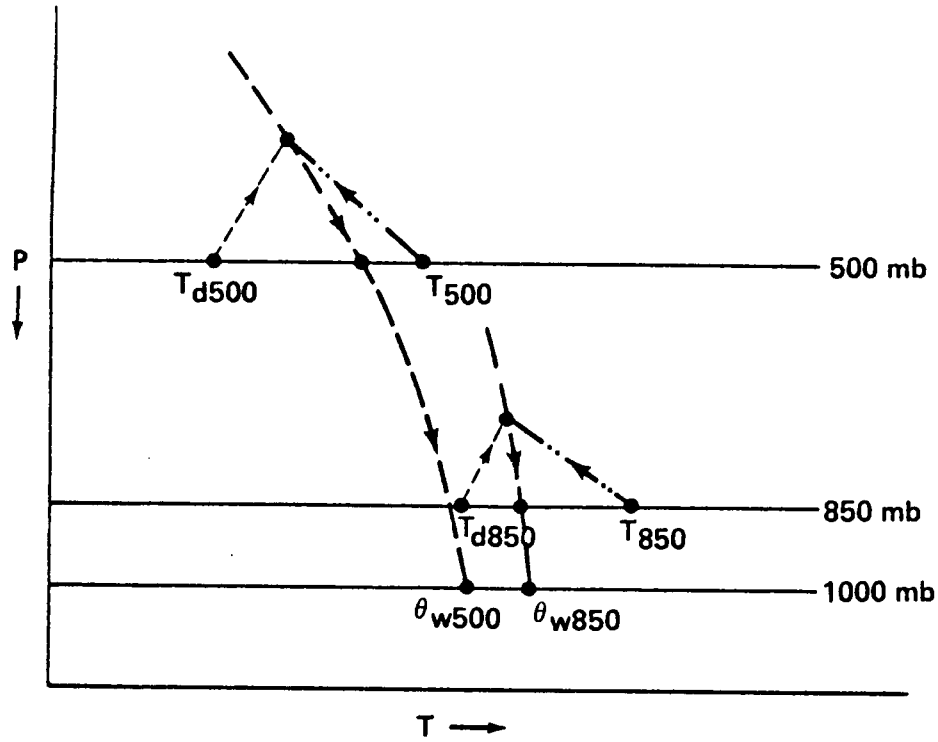


Figure 17. Bradbury potential stability index computation method.

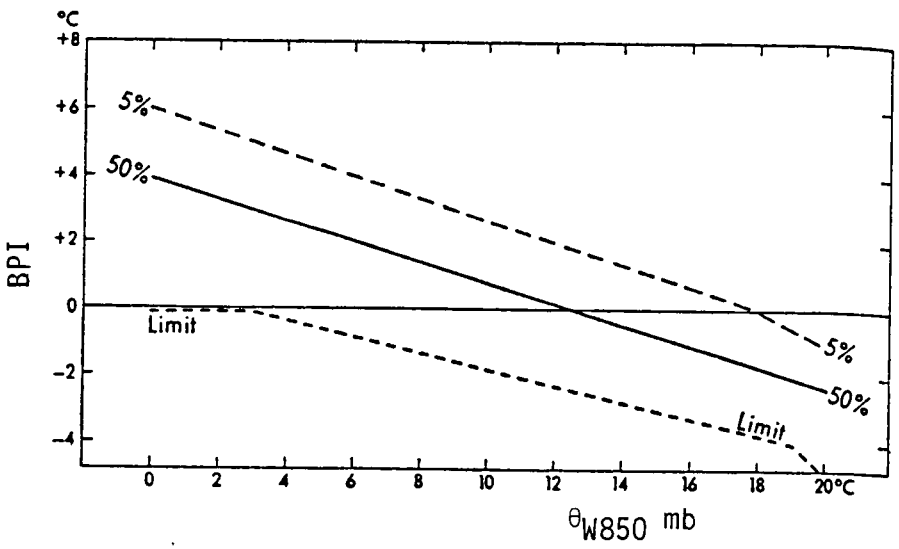


Figure 18. Relationship between $\theta_{W850}$ and the BPI on thunderstorm days [59].

merely indicates a range of conditions that existed when thunderstorms occurred. Thunderstorms would be unlikely outside the range given. One should not use the BPI as a strict thunderstorm forecasting rule, but rather, as a guide along with routine surface and upper-air charts.

Energy Index

A unique and reliable substitute for the widely used thermodynamic indices, used in the forecasting of convective storms, is the total energy index (EI). It was introduced by Darkow [60] in 1967 and deals with the total energy ($E_T$) of a unit mass of air. The specific enthalpy ($c_pT$), potential energy ($gZ$), latent energy ($Lq$), and kinetic energy ($W^2/2$) of the unit mass of air is combined as:

$$E_T = c_pT + gZ + Lq + W^2/2 \ (\text{cal gm}^{-1}) , \qquad (18)$$

where,

$c_p$ = specific heat of air (0.24 cal $\text{gm}^{-1}\ {}^{o}\text{K}^{-1}$) ,

$T$ = temperature ($^{o}$K) ,

$g$ = acceleration of gravity (980 cm $\text{sec}^{-2}$) ,

$Z$ = altitude (km) ,

$L$ = latent heat (cal $\text{gm}^{-1}$) ,

$q$ = specific humidity (gm $\text{kg}^{-1}$) ,

$W$ = scalar velocity (cm $\text{sec}^{-1}$) .

Since the kinetic energy term is two orders of magnitude smaller than the other three terms, it can be neglected, resulting in the energy formula being called static energy ($E_S$); that is,

$$E_S \approx E_T \approx c_p T + gZ + L_o w \ , \tag{19}$$

where,

$$L \approx L_o = 600 \text{ cal gm}^{-1} \ ,$$

$$q \approx w \ = \text{mixing ratio (gm kg}^{-1}) \ ;$$

therefore,

$$E_T \approx 0.24\ T + 2.34\ Z + 0.6\ w \text{ (cal gm}^{-1}) \ . \tag{20}$$

Static or total energy is conserved with respect to both types of adiabatic processes and is related to the pseudo-equivalent potential temperature ($\theta_E$) and wet-bulb potential temperature ($\theta_W$). This fact can be seen by dividing $E_T$ by $c_p$, which produces a geo-equivalent potential temperature ($\theta_{GE}$), which is a conservative (invariant) property in regard to adiabatic processes. The term $\theta_{GE}$ differs just slightly in definition from $\theta_E$ and is expressed as:

$$\theta_{GE} = \frac{E_T}{c_p} = T + 9.8\ Z + 2.5\ w \ (^{o}K) \ . \tag{21}$$

Total energy or geo-equivalent potential temperature can both be computed easily for use in the forecasting of convective activity. This total energy concept can be used in both ascent and descent air parcel theory convective calculations, and the amount of potential convective instability of the air column is indicated by

the decrease of total energy with increasing altitude. This defines the Darkow total energy index (EI). It is expressed as the algebraic difference between the atmospheric total energy at the 500- and 850-mb levels; that is,

$$EI = E_{T500} - E_{T850} \ (\text{cal gm}^{-1}) \ . \tag{22}$$

Empirical testing of the index produced the ranges given in Table 17 for forecasting severe weather. The total energy index horizontal map pattern turns out to be very similar in structure to the Showalter index pattern. This is due in part because low-level total energy is usually greater than mid-tropospheric values.

The total energy index combines temperature, moisture, and height fields. Darkow [60] indicates that this gives it a possible advantage over the Showalter and lifted indices since it is the only one to take into account the possible contribution of descending, potentially cold, mid-tropospheric air on the total energy release of convective storms. Most indices involve only the process of ascending warm air.

Darkow took an additional step by suggesting that a modified energy index can be developed which takes into account the mean mixing ratio of the lowest 100-mb layer (or of the first kilometer altitude) above the ground. This may be more representative of lower level moisture than using just the 850-mb value of mixing ratio.

A number of atmospheric studies have used the Darkow energy index and total energy concept. Some of these studies are presented

Table 17. Energy Index Values Used in Convective Forecasting

| EI | Forecast[a] |
|---|---|
| 0.0 to -1.0 | Non-severe thunderstorms possible. |
| -1.0 to -2.0 | Isolated severe thunderstorms possible. |
| < -2.0 | Severe thunderstorms and tornado activity possible. |

[a]If a trigger mechanism is available to release potential instability, otherwise, convective activity may not take place.

in References [61 through 64]. Eagleman [61] used Darkow's index separately and also combined with a wind shear index to aid in forecasting tornadoes. Darkow has also applied the static energy concept to surface analysis in detecting areas of high static energy related to thunderstorm and severe storm occurrences [65, 66].

Martin Index

Wright-Patterson Air Force Base, Ohio, published a stability index constructed by D. O. Martin [67] said to be more sensitive to low-level moisture than the Showalter index, since it uses the maximum value of low-level moisture.

The procedure in computing the Martin index (MI) (see Figure 19) is as follows: From the 500-mb temprature (A), descend moist-adiabatically to the intersection (B) of this line and the mixing ratio line that passes through the point (C) of maximum mixing ratio. From this intersection, move dry-adiabatically to the 850-mb level (D). The MI is defined as the difference between the observed sounding temperature and calculated temperature at 850 mb; that is,

$$MI = T_{\substack{850 \\ Calc.}} - T_{\substack{850 \\ Obs.}} \quad (^{o}C) \; . \tag{23}$$

The only exception to this procedure occurs whenever a marked low-level turbulence or subsidence inversion (non-surface, non-radiation) is established below 850 mb. Then the point (D) is obtained at the pressure level where the inversion base is located. The normal and the exception cases are illustrated in Figure 19.

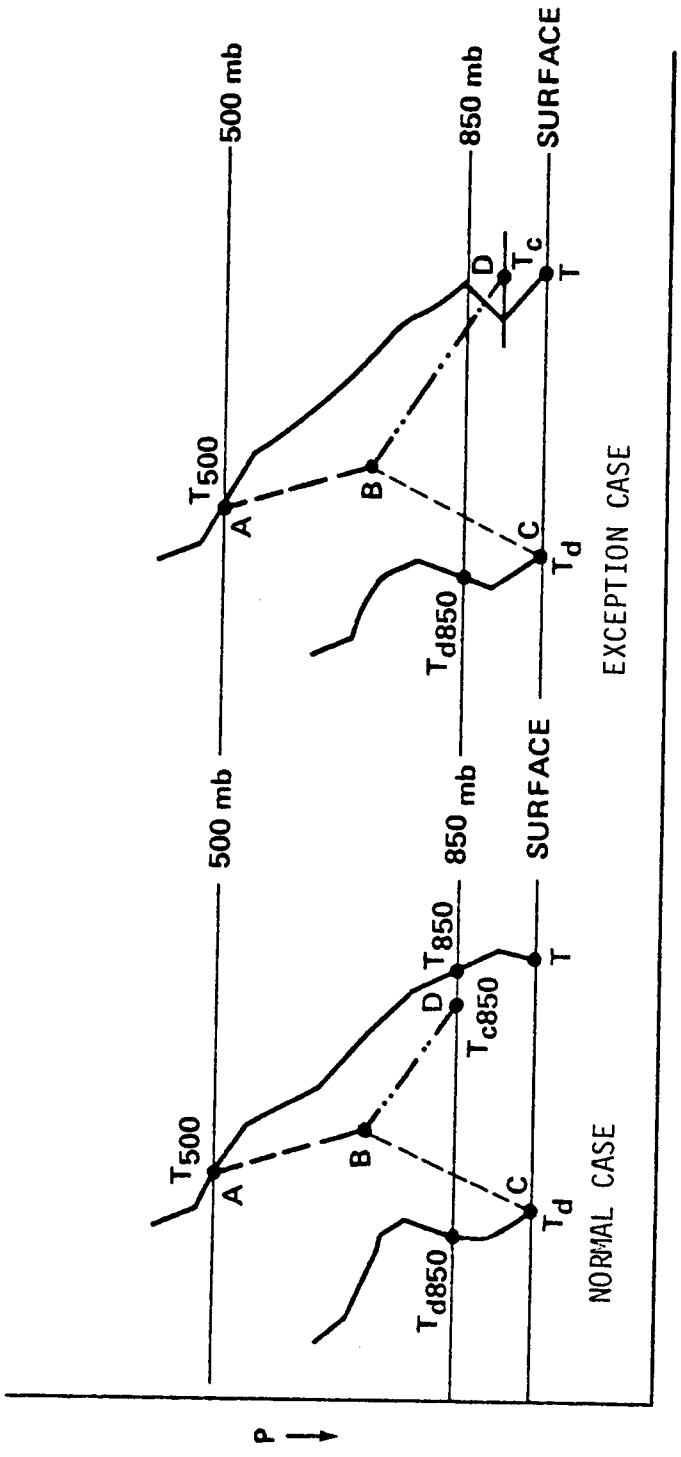


Figure 19. Martin stability index computation methods.

Since this study involves the 900-mb level as being the closest level to the surface, the index will be referred to as the modified Martin index (MI).

# CHAPTER V

# AVE-IV PROFILE ANALYSES

## A. Introduction

Before stability indices can be constructed, used, or evaluated, the atmospheric parametric profiles themselves need to be examined and understood. Therefore, this section presents a discussion of the AVE-IV average and lag soundings as they are compared with the four MDR precipitation categories, and as they are compared with each other. Tabular values of these profile parameters have been presented in Chapter III, Tables 4 through 11, pages 32 through 39.

For clarity, and to avoid confusion, the average profiles which pertain to precipitation conditions occurring at the time of the sounding observation will hereafter be referred to as AVG. Also, the averaged lag profiles, which represent the environmental observations three hours prior to a precipitation category occurrence, will hereafter be referred to as LAG profiles.

Throughout this section, more attention will be given to the parametric average profile differences which exist between precipitation categories A and D (defined in Table 3, page 27). Categories B and C parameter differences have been compared but are not always presented here because they either do not represent any drastic environmental change, or since they do have inherent category D information, they could present a bias. In most all cases these two intermediate precipitation categories merely link

categories A and D. The average profiles of LAG and AVG temperature, potential temperature, and winds are presented and compared for the storm categories A and D. Differences are noted for possible inclusion in a forecast-type of storm index.

## B. AVG Profile Comparison

### Temperature/Moisture

The vertical temperature profile differences noted between A (non-precipitation) and D (severe storm) conditions for the AVE-IV average (AVG) profiles are shown in Figure 20. Although the two temperature profiles are almost identical above 700 mb, the D profile temperatures increase $5^{o}C$ warmer than the A conditions between the 700- and 900-mb levels.

The dew-point temperature profile for D conditions is 2 to 10 deg warmer (more moist) than for A conditions at all altitudes, as shown in Figure 20. Most of the difference (6 to $10^{o}C$) occurs between the 600- and 800-mb levels.

### Winds

As one would expect, for all altitudes, winds are higher when going from precipitation categories A to D using the AVG wind profile information. Wilson and Scoggins [20] also confirmed this. This increase pertains to both meridional and zonal wind components. The category D meridional wind component exhibited the most difference (~8 m $sec^{-1}$) over category A conditions. Zonal (and scalar) wind differences between A and D categories generally range

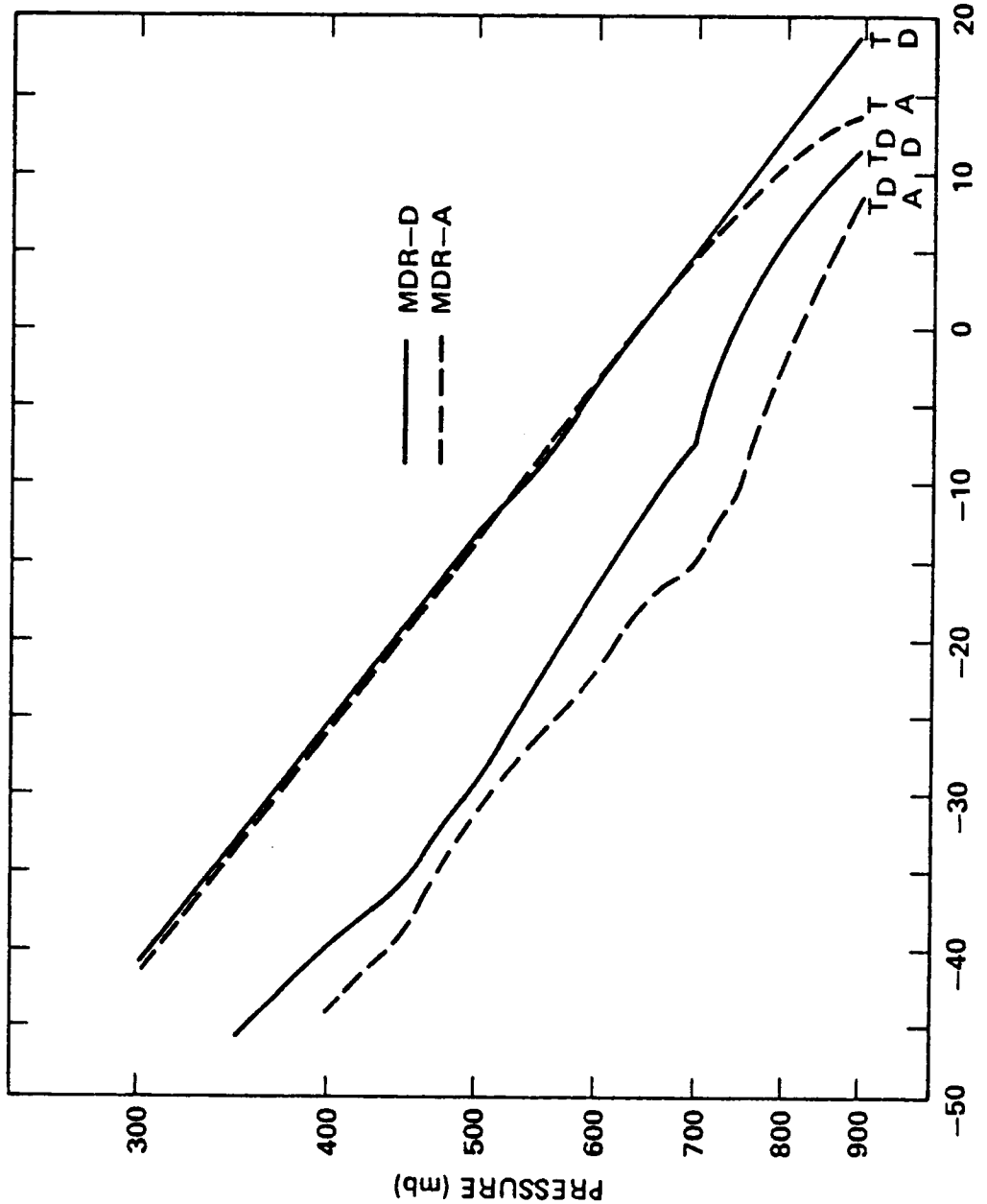


Figure 20. AVG temperature and dew-point profiles for A and D MDR conditions.

between 2 and 6 m $sec^{-1}$ (see Figure 21). All wind components calculated are positive (i.e., zonal winds being westerly and meridional winds southerly) for all AVG and LAG conditions presented. Zonal westerly winds dominate in magnitude.

## C. LAG Profile Comparison

To determine if a forecast scheme can be realized based on AVE-IV data, this stability study will involve the analysis of LAG profiles and how their average conditions differ from the AVG profiles representing storm activity.

### Temperature/Moisture

LAG thermodynamic profile conditions for the four precipitation categories are very similar in appearance to the four respective AVG profiles. Temperatures of category D are warmer by a similar magnitude than category A, as was the case for the AVG profiles. This effect extends higher, however, from 900 to 650 mb. The category D dew-point profile also remains warmer by a similar moisture differential spread, as was the case with the AVG dew-point data.

### Winds

LAG winds again invoked a pattern similar to that of AVG winds, with both D wind components exhibiting stronger flow than A wind component conditions. Category D LAG wind directions between 7 and 13 km altitude are slightly westerly, so as to resemble category B LAG wind directions over this altitude range. This is

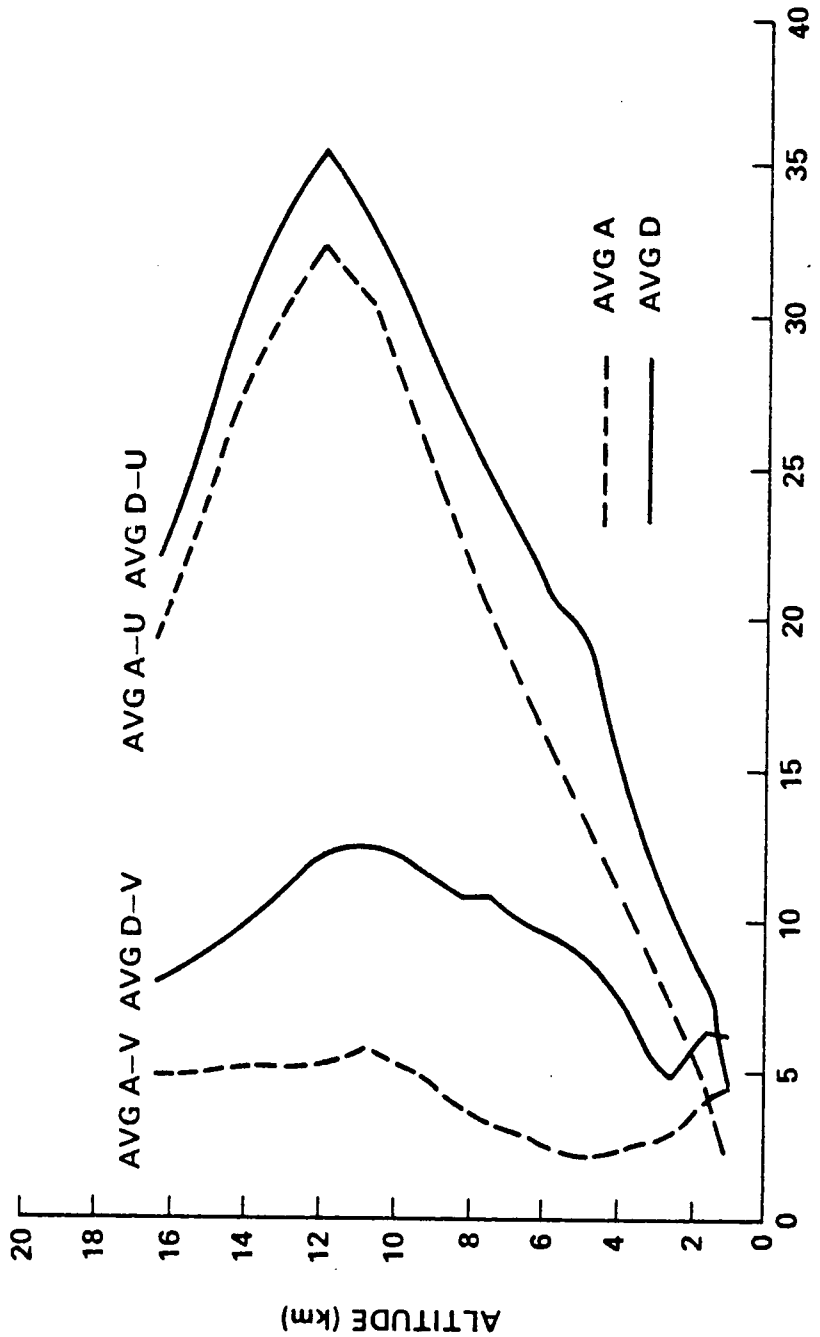


Figure 21. AVG wind components for MDR A and D conditions.

completely unlike the AVG D, AVE-IV storm wind directions, which are farthest away from the west of all four precipitation categories. This directional change will be discussed further in Section D.

## D. AVG/LAG Profile Comparison

Winds

Differences between the AVE-IV average LAG (three to six hours prior to storm occurrence) and AVG (time of storm occurrence) wind profiles are, again, generally small. However, the largest differences do occur between the category D (severe storm) wind profiles of each. Therefore, only category D comparisons will be discussed here.

From Tables 7 and 11, pages 35 and 39, respectively, scalar wind speeds and U-component (zonal) speeds are ~2 m $sec^{-1}$ stronger for the LAG average than for the AVG average, between 6- and 12-km altitude. Wind magnitude differences were less than this value above 12-km altitude (see Figure 22).

Magnitudes of the V-component wind (meridional) give slightly stronger (~2 m $sec^{-1}$) southerly winds at AVG time than LAG time, between 8- and 12-km altitude. This stronger AVG V-component effect coupled with the weaker AVG U-component results in the AVG wind direction between 8- and 12-km altitude being ~5 deg more from the south (248 deg) than the LAG average (253 deg). Meaning, on the average, winds during the LAG period are 1 to 2 m $sec^{-1}$ stronger and from a more westerly direction than conditions existing during severe storm occurrence.

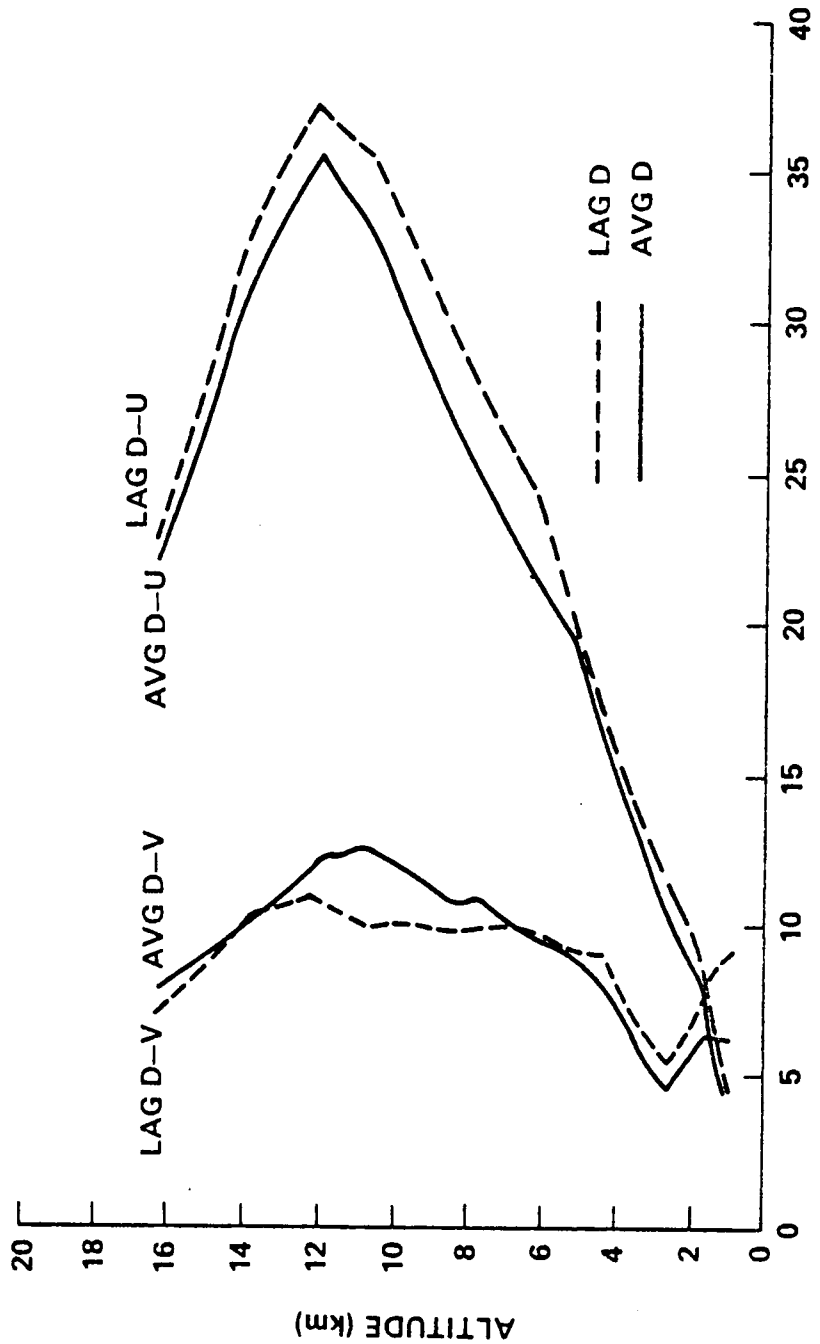


Figure 22. Wind components for AVG and LAG type D MDR conditions.

Temperature/Moisture

The thermodynamic structure between AVG and LAG category D profiles, in terms of temperature and dew point, is shown in Figure 23. Average conditions for each respective parameter are, indeed, very similar. The unusual feature is the ~1.5°C temperature difference that exists around 650 mb, with equal or lesser differences indicated between the 800- and 500-mb levels, and with LAG temperatures being slightly warmer. Also, the layer between 500 and 650 mb is more unstable three hours prior to storm activity. The temperature lapse rate of the LAG sounding between these two levels is 15.4°C/150 mb; whereas, only 14.4°C/150 mb (difference = 1.0°C) existed during AVG storm time. This slightly more unstable layer is noticed at a lower altitude between 800 and 650 mb at storm time. It then has a temperature gradient of 12.0°C/150 mb as compared to 10.9°C/150 mb (difference = 1.1°C) for this layer on the prior LAG profile.

Three hours prior to storm activity, the dew-point temperature at 900 mb is ~1°C higher than at the time of storm activity. By the 850-mb level, this difference vanishes and neither AVG nor LAG dew-point temperatures dominate above this level.

## E. Theta-E AVG/LAG Comparison

Before the stability index results are presented and discussed, it is desirable to select an index or procedure involving equivalent potential temperature ($\theta_E$) as an instability measure (see

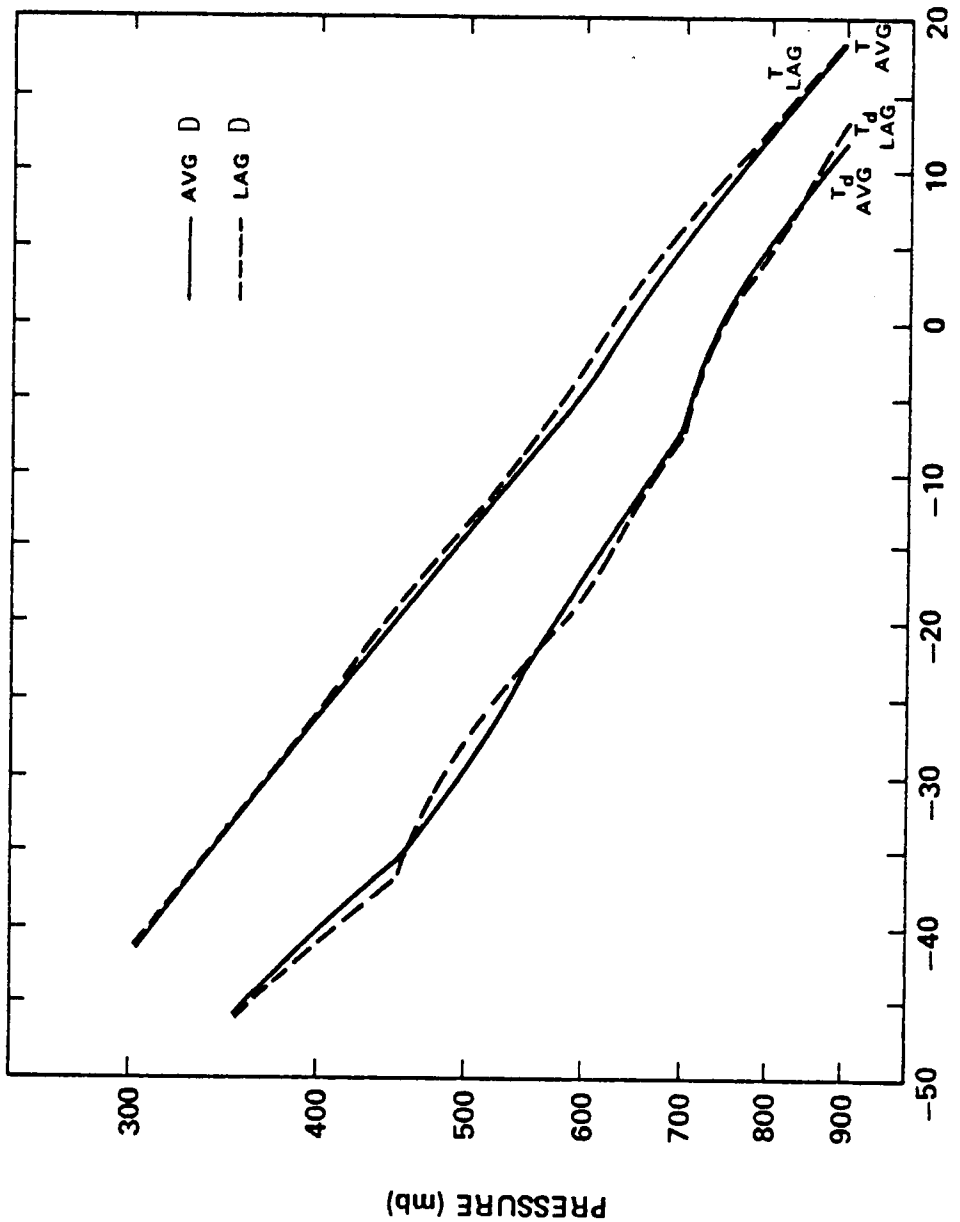


Figure 23. Temperature and dew-point temperature profiles for AVG and LAG conditions of MDR = D.

Chapter IV discussion of $\theta_E$). This is an important decision to make because of the many number of ways in which $\theta_E$ can represent atmospheric instability.

AVG $\theta_E$ profiles are presented for the four MDR conditions in Figure 24. Similar LAG $\theta_E$ profiles are given in Figure 25. The two figures present similar results and show higher values of $\theta_E$ for more severe weather activity. The comparison between LAG and AVG profiles of $\theta_E$ are given in Figure 26 for categories A and D MDR conditions. The LAG profiles exhibit slightly greater $\theta_E$ (or total energy) than do the AVG profiles. The altitude of minimum $\theta_E$ occurs at ~700 mb for the two profiles with no MDR activity (category A), while it occurs higher (~600 mb) for both the MDR>7 (category D) profiles. One item of significance is the more stable $\theta_E$ gradient observed between 850 and 800 mb on the AVG-D profile than the LAG profile indicates. The AVG-D $\theta_E$ profile also indicates a slightly more unstable region between 750 and 700 mb, as compared to LAG-D conditions.

Results from the convective stability equation of Alaka et al. [31] and the $\theta_E$ differences between 800 to 850-, 800 to 900-, and 700 to 750-mb levels, as suggested by observing the $\theta_E$ LAG and AVG vertical profiles, are presented in Table 18. It should be noted that Alaka's equation (Eq. (10)) is similar in structure to the Delta Theta-E equation (Eq. (8)), as discussed earlier in Chapter IV.

While the $\theta^*$ equation of Alaka (Eq. (10)) is representative of the entire lower atmospheric instability when applied to

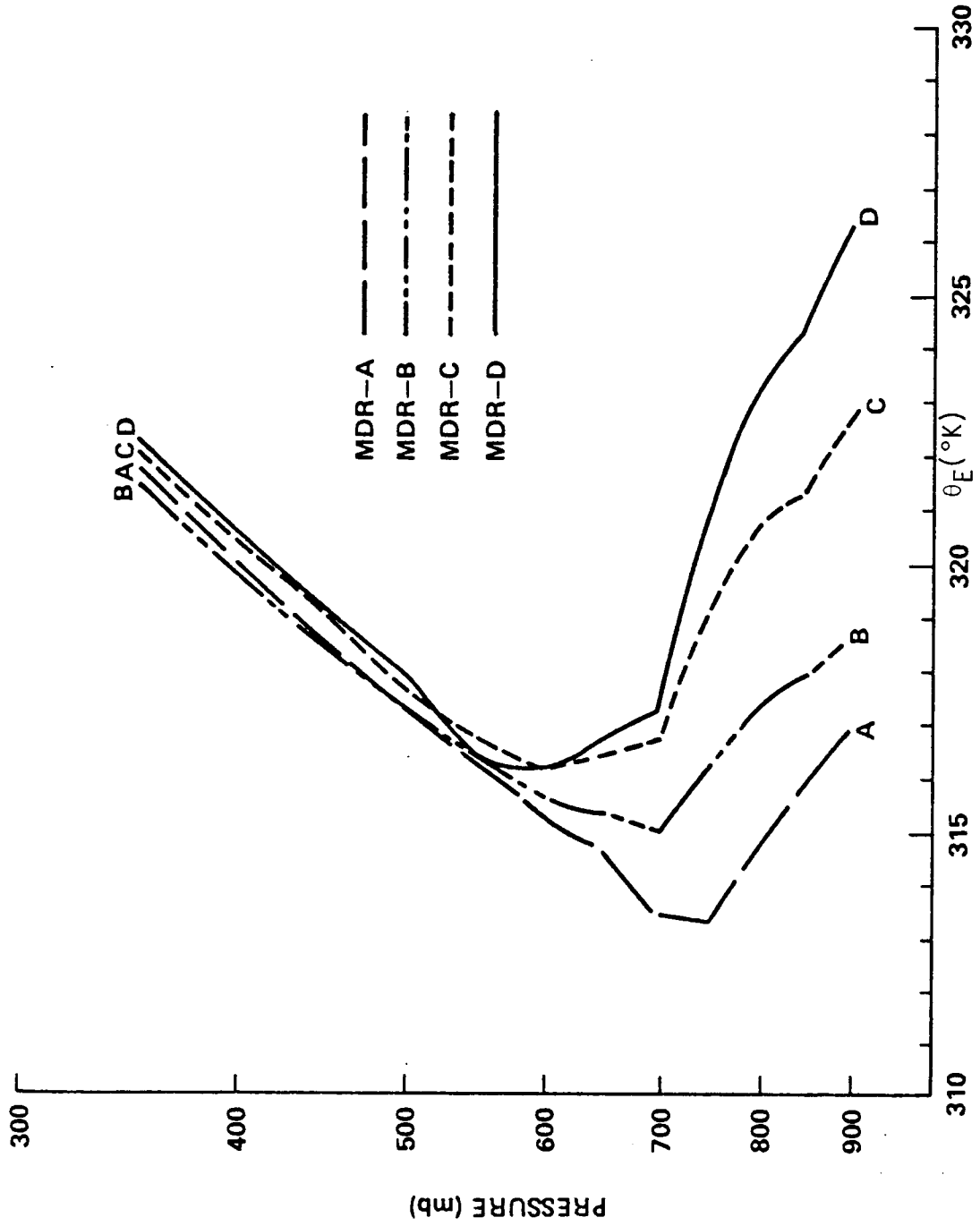


Figure 24. AVG equivalent potential temperature ($\theta_E$) vertical profiles for four MDR categories.

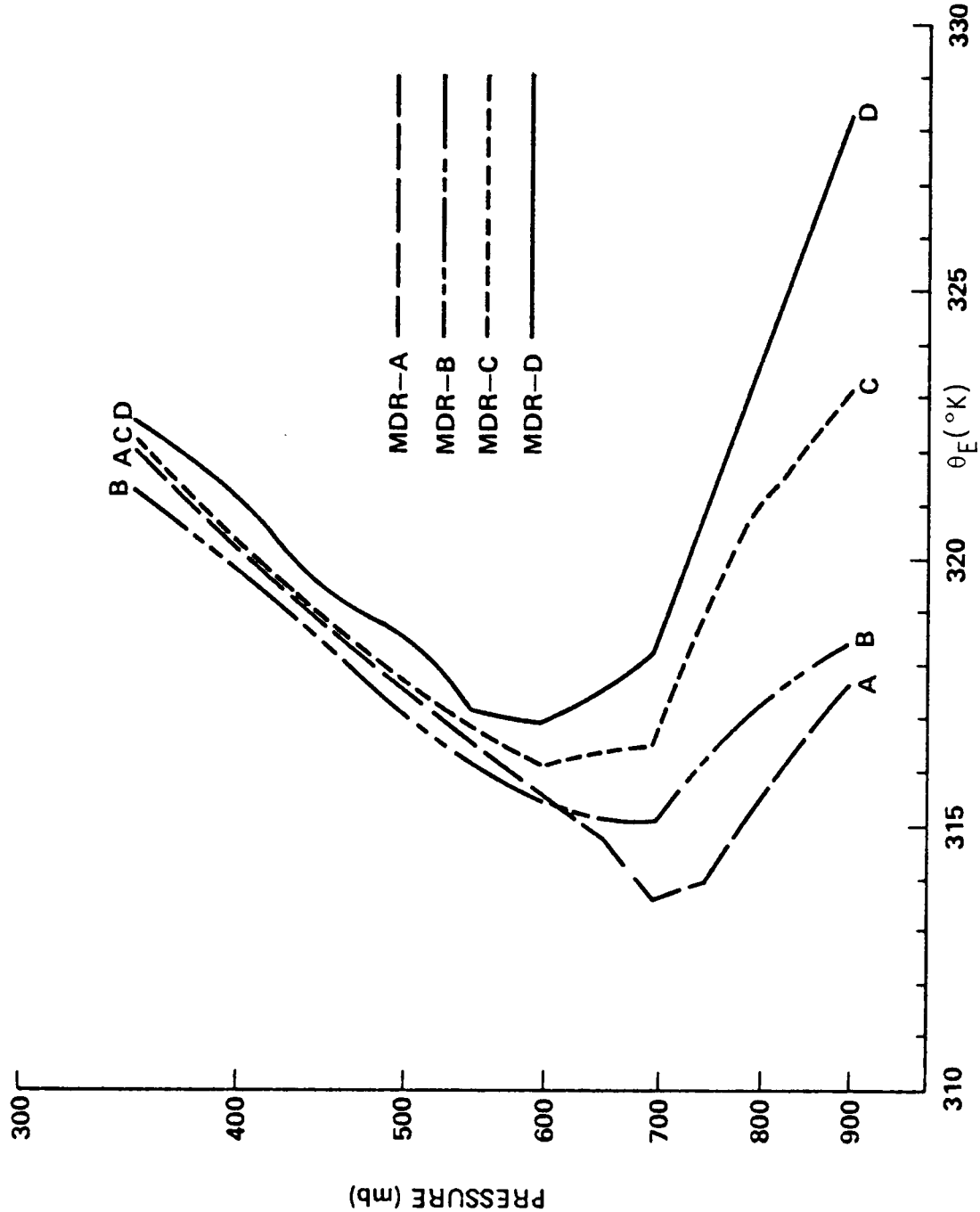


Figure 25. LAG equivalent potential temperature ($\theta_E$) vertical profiles for four MDR categories.

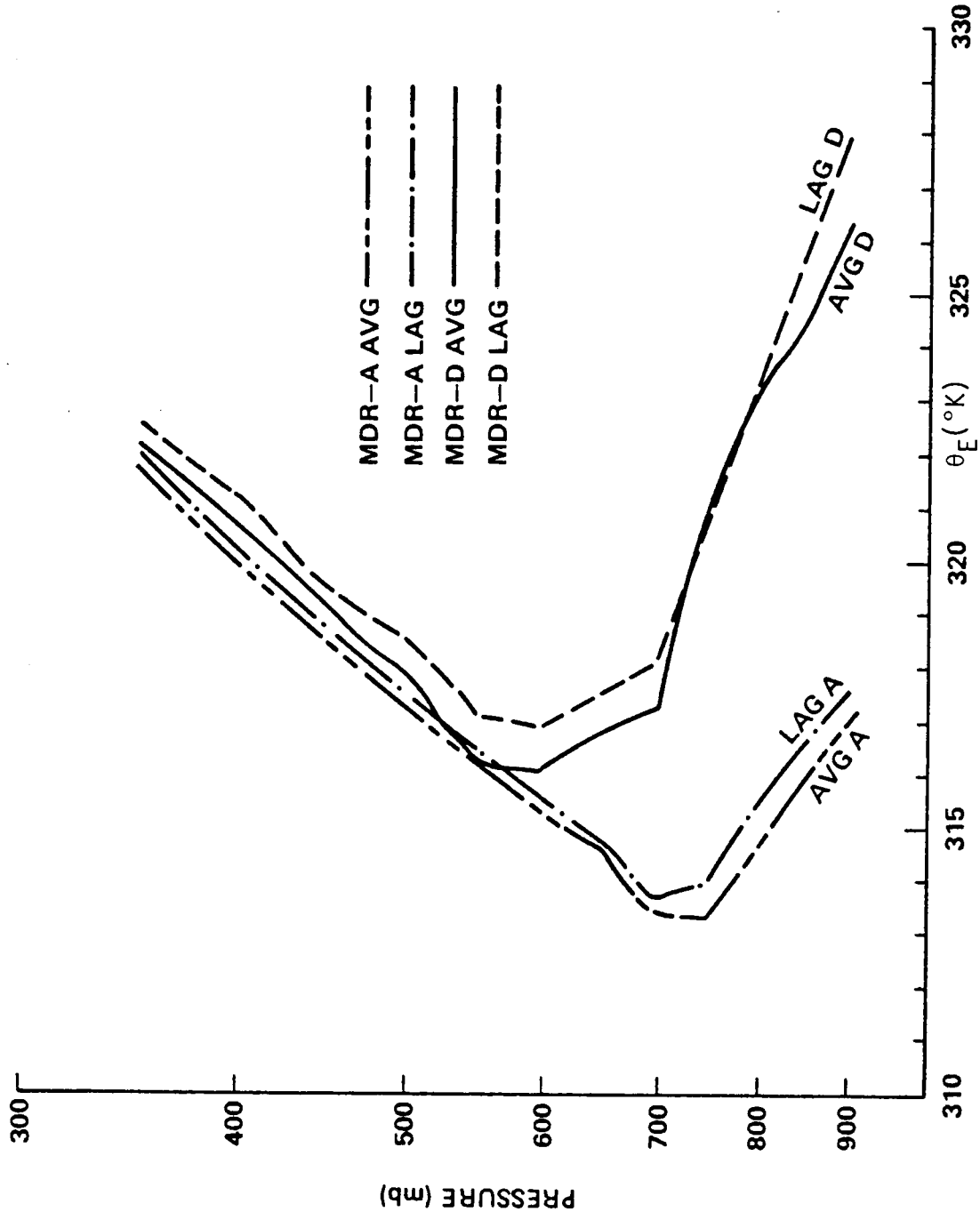


Figure 26. LAG and AVG equivalent potential temperature ($\theta_E$) vertical profiles for type A and D MDR categories.

Table 18. Theta-E Differences ($^{o}K$) Between Given Pressure Levels

| $\theta_E$ Pressure Level Difference Category | LAG MDR Conditions | | | | AVG MDR Conditions | | | | Percent Difference Between AVG-D and LAG-D |
|---|---|---|---|---|---|---|---|---|---|
| | A | B | C | D | A | B | C | D | |
| 1. Alaka $\theta_E^*$ (700 to surf.) | -3.47 | -3.17 | -6.02 | -8.73 | -2.95 | -3.36 | -5.31 | -8.12 | -7 |
| 2. $\Delta\theta_E$ (800 to 850) | -1.15 | -0.85 | -1.05 | -2.35 | -1.30 | -0.60 | -0.55 | -1.10 | -53 |
| 3. $\Delta\theta_E$ (800 to 900) | -2.25 | -1.34 | -2.14 | -4.77 | -2.25 | -1.28 | -1.92 | -2.98 | -38 |
| 4. $\Delta\theta_E$ (700 to 750) | -0.36 | -1.17 | -2.57 | -2.66 | +0.14 | -1.32 | -2.67 | -3.97 | +49 |

individual soundings, it is not when applied to averaged soundings, as shown in Table 18. The layer between the surface and 700 mb appears to be too large to note meaningful differences (only 7%) between LAG-D and AVG-D conditions.

Values of $\Delta\theta_E$ over narrower layers are presented in Table 18, using two lower atmospheric levels (items 2 and 3 of Table 18) and one upper atmospheric level (item 4). The significant point to notice is that pre-storm conditions (LAG-D) have a stronger $\theta_E$ lapse rate between 800 mb and below, as compared to storm conditions (AVG-D); the AVG being 38 and 53% lower than LAG conditions. The opposite is true when the 700 to 750-mb $\theta_E$ gradients, for both D MDR conditions, are compared. Here, AVG-D gradients are 49% higher than LAG-D conditions.

The results presented in Table 18 do indicate that possibly a stability index could be arrived at by using one or two $\Delta\theta_E$ parameters in its computation. This would make the index a function of both a temperature and moisture input over a 50- to 100-mb spacing in the atmosphere.

## F. AVG/LAG Conclusions

A few general conclusions can be made regarding the atmospheric environment three hours prior to severe storm development and during the occurrence of the severe storm. They are as follows:

1. The LAG profile exhibits a more unstable temperature gradient ($15.4^{o}C$/150 mb) in the upper atmosphere between 650 and 500 mb three hours before severe storm activity.

By the time of severe storm occurrence, this unstable layer has fallen 150 mb and is located between 650 and 800 mb with a 12.0°C/150 mb gradient.

2. Dew-point temperatures are warmer (more humid) from 900 to 850 mb by 1°C three hours prior to severe weather.
3. Scalar wind and zonal wind speeds are stronger by ~2 m $sec^{-1}$ three hours prior to storms. At storm occurrence time the 2 m $sec^{-1}$ stronger, southerly, AVG meridional wind component, located between 8 and 12 km altitude (400 to 200 mb), results in producing a more southerly direction (248 deg) than three hours prior (253 deg).
4. Equivalent potential temperature ($\theta_E$) differences between 800 and 850 mb are the most unstable three hours prior to convective weather; whereas, $\theta_E$ differences between 700 and 750 mb are more unstable at the time of severe weather occurrence.

The results obtained here could be used in the construction of a type of three-hour lead time severe storm index. However, these changes noticed in the atmospheric structure are, indeed, all very small changes. It should be noted that they are small due to the fact that they are based on the average of many pre-storm soundings taken during only one independent major storm system development/movement. It may also turn out that these AVE-IV conclusions may or may not apply to a different storm sounding history

for a station. One purpose of the present study is to test this theory, thereby affecting current understanding of the severe storm environment.

## G. Possible Stability Index

At this point, a stability-type of index could be constructed consisting of a temperature difference ($\Delta T$), or an equivalent potential temperature difference ($\Delta\theta_E$), between two levels. A low-level dew-point indicator ($\Delta T_d$), and possibly a wind magnitude term ($\Delta W$) and directional term ($\Delta WD$) could be included. The combination of these terms, with the appropriate multiplication weighting factors (M), could result in a meaningful severe storms lag index (SSL). A possible form of the equation is:

$$SSL = M_1(\Delta T) + M_2(\Delta T_d) + M_3(\Delta W) + M_4(\Delta WD) + M_5(\Delta\theta_E) \ . \qquad (24)$$

All or only a couple of the terms expressed in Eq. (24) may prove useful as an index parameter when compared to its respective severe storm threshold value. Considering the broad scale in which these five terms were expressed, only general inferences may prove useful. Terms from this type of equation will be used and tested in Chapter VI.

# CHAPTER VI

# AVE-IV STABILITY ANALYSES

## A. Introduction

This chapter will deal with the AVG and LAG AVE-IV profiles as they are applicable to the current standard stability indices of thunderstorms and severe weather reported in Chapter IV. The profile indices will be compared and the ability of each to forecast/measure severe convective weather will be determined. Temperature-dependency for each index will also be included, as well as the introduction of a new lag index.

## B. Temperature-Dependence

It is generally desirable to know if a stability index changes with the changing temperature of an air column. The index is said to be temperature-dependent if this is the case. An index with a very large temperature-dependency is undesirable for use in representing the stability over a large geographical area in which differing air masses may reside. The changing air characteristics would affect the threshold value of an index, as reported by McPherson [29].

McPherson [29] suggested a method to determine the temperature-dependency of an index. His method is the approximate procedure used in the present investigation. A range of stability conditions for each index is determined first. The selection of two

hypothetical vertical temperature profiles, which represent (a) near normal stability and (b) less stable conditions, is accomplished by assuming moist-adiabatic and dry-adiabatic vertical temperature lapse rate conditions, respectively. These two conditions are chosen because they separate the area for conditional stability, and also give index values on either side of the threshold values (Chapter IV) which are representative of thunderstorm/severe thunderstorm conditions as used in this study. For both adiabatic conditions, the temperature at 700 mb was assumed fixed at $0^{o}C$, and the dew-point depression at all levels was assumed to be $10^{o}C$. The resulting range for all indices is presented in Table 19.

Index values were next obtained given five different cases of moist-adiabatic lapse rate conditions from 900 to 500 mb, with $\theta_W$ values of 0, 6, 12, 18, and $24^{o}C$, assuming saturation at all levels. These index results are presented in Table 20, which now gives a relationship between index value and temperature changes. The range of index values obtained from the five different temperature ($\theta_W$) cases is presented in the next-to-last column of Table 20. The right-most column of Table 20 presents a percentage change of the range of each index with respect to the index's total range, as given in Table 19 for the five temperature categories.

From these calculations it is shown that the Showalter and Bradbury indices have small or no temperature-dependence since they involve conservative moist-adiabatic procedures ($\theta_W$) in their computation. The Jefferson, Modified-Jefferson, $\theta_E^*$, Energy, and Modified-Martin indices are only moderately (~1 to 10%) temperature-dependent.

Table 19. Stability Index Range Determined by Moist and Dry Adiabatic Lapse Rates

| Index | Normal Stability Moist-Adiabatic | Lesser Stability Dry-Adiabatic | Range of Values |
|---|---|---|---|
| SWEAT | 8 | 549 | 541 |
| Vertical Totals | 26 | 41 | 15 |
| Cross Totals | 16 | 31 | 15 |
| Total Totals | 41 | 72 | 31 |
| $\theta_E^*$ | -14 | 3 | 17 |
| Showalter | 7 | -10 | 17 |
| Rackcliff | 28 | 44 | 16 |
| Jefferson | 34 | 55 | 21 |
| Mod. Jefferson | 21 | 42 | 21 |
| Boyden | 2.5 | 2.5 | 0[a] |
| Bradbury | 3 | -7 | 10 |
| K-Index | 14 | 37 | 23 |
| Energy | 2 | -4 | 6 |
| Mod. Martin | 10 | -20 | 30 |

[a]In defining the 700-mb temperature as a constant here for both adiabatic processes, the Boyden index will result in a constant value. McPherson [29] concludes that the Boyden index is very temperature-dependent.

Table 20. Stability Index Dependency as a Function of Temperature Change

| Index | $\theta_w$ 0°C | $\theta_w$ 6°C | $\theta_w$ 12°C | $\theta_w$ 18°C | $\theta_w$ 24°C | $\theta_w$ Range of Values | $\theta_w$ Range[a] as Percent of Table 19 Range | |
|---|---|---|---|---|---|---|---|---|
| SWEAT | -76.6 | -71.0 | -36.2 | 44.2 | 123.4 | 200 | 37% | ## |
| Vertical Totals | 32.6 | 30.7 | 26.2 | 23.9 | 20.6 | 12 | 80% | ## |
| Cross Totals | 22.6 | 20.7 | 16.2 | 13.9 | 10.6 | 12 | 80% | ## |
| Total Totals | 55.2 | 51.4 | 42.4 | 37.8 | 31.2 | 24 | 77% | ## |
| $\theta_E^*$ | 2.8 | 3.0 | 2.7 | 3.2 | 3.6 | 0.9 | 5% | # |
| Showalter | 0 | 0 | 0 | 0 | 0 | 0 | 0% | * |
| Rackcliff | 41.4 | 38.7 | 33.3 | 30.3 | 26.4 | 15 | 94% | ## |
| Jefferson | 41.4 | 42.3 | 40.5 | 41.1 | 40.8 | 1.8 | 9% | # |
| Mod. Jefferson | 28.4 | 29.3 | 27.5 | 28.1 | 27.8 | 1.8 | 9% | # |
| Boyden[b] | 22.7 | 14.9 | 6.9 | -1.0 | -8.6 | 31 | --- | ## |
| Bradbury | 0 | 0 | 0 | 0 | 0 | 0 | 0% | * |
| K-Index | 3.8 | 8.7 | 11.1 | 15.5 | 18.8 | 15 | 65% | ## |
| Energy | 1.21 | 1.28 | 1.80 | 1.60 | 1.55 | 0.59 | 10% | # |
| Mod. Martin | -1.2 | -1.6 | -2.0 | -2.4 | -2.6 | 1.4 | 5% | # |

[a] Temperature-dependency code: * = None or small; # = Moderate; ## = High.

[b] McPherson [29] concludes that the Boyden index is very temperature-dependent.

Finally, the SWEAT, K, three Totals, Boyden, and Rackcliff indices are all highly dependent upon temperature changes. Since $\theta_E^*$ was derived by using the $\theta_{GE}$ approximate equation for $\theta_E$, the resulting moderate temperature-dependency actually would have been less had this equation not been used.

Temperature-dependency on an averaged profile, as compared to an individual provile, may appear unimportant since only averaged (AVG or LAG) severe storm thermodynamic profiles and indices are developed. However, when other individual vertical soundings (and their computed stability indices) are compared to those of the averaged profile, temperature-dependent indices may give unrealistic results. Also, the results of the AVE-IV soundings being averaged springtime soundings, over two independent days for the east/central United States, may not apply accurately for a different season (temperature regime) or location, if temperature-dependent indices are used. Therefore, in the evaluation of index performance, it is well to know in advance which indices are temperature-dependent and which are not.

## C. Stability Index Results

This section presents the stability index results, based on the LAG and AVG profiles. The 14 stability indices described in Chapter IV were used in conjunction with the MDR LAG and AVG averaged atmospheric profiles. These results are presented in Table 21.

Table 21. Stability Index Values for LAG and AVG MDR Profiles

| Index | MDR-LAG A | B | C | D[a] | MDR-AVG A | B | C | D[a] | Approximate Threshold Index Value |
|---|---|---|---|---|---|---|---|---|---|
| SWEAT | 194 | 237 | 271 | (331[b]) | 186 | 233 | 249 | 290 | 250 to 350 |
| Vertical Totals | 26.6 | 26.1 | 27.3 | 29.4 | 26.6 | 26.0 | 27.6 | (29.5) | 26 |
| Cross Totals | 17.7 | 20.9 | 22.0 | (22.5) | 17.1 | 21.1 | 22.0 | 22.1 | 18 |
| Total Totals | 44.3 | 47.0 | 49.3 | (51.9) | 43.7 | 47.1 | 49.6 | 51.6 | 44 to 50 |
| $\theta_E^*$[c] | -3.5 | -3.2 | -6.0 | (-8.7) | -2.9 | -3.4 | -5.3 | -8.1 | --- |
| Showalter[c] | 4.1 | 1.9 | 0.0 | -1.2 | 3.6 | 1.7 | -0.6 | (-2.4) | -3 to -6 |
| Rackcliff | 29.1 | 30.4 | 31.3 | (32.5) | 28.8 | 30.2 | 31.3 | 32.0 | 30 to 35 |
| Jefferson | 38.1 | 39.8 | 41.7 | (43.8) | 37.6 | 39.5 | 41.5 | 42.9 | 30 |
| Mod. Jefferson | 20.8 | 26.2 | 27.1 | (29.0) | 19.6 | 26.2 | 27.8 | 28.6 | 28 to 29 |
| Boyden[c] | 6.8 | 6.4 | 5.8 | 5.2 | 6.7 | 6.5 | 5.2 | (5.3) | --- |
| Bradbury[c] | 0.8 | -0.1 | -2.0 | (-2.7) | 0.7 | -0.4 | -1.5 | -2.4 | --- |
| K-Index | 11.5 | 21.1 | 22.2 | 24.7 | 9.6 | 21.8 | 23.9 | (25.1) | 30 to 35 |
| Energy[c] | 0.20 | -0.27 | -1.08 | (-1.78) | 0.26 | -0.18 | -0.94 | -1.61 | <-2 |
| Mod. Martin[c] | 2.2 | 0.7 | -3.4 | (-7.3[b]) | 2.6 | 0.3 | -3.8 | -4.8 | --- |

[a]Circled "D" category values indicate the largest unstable index value.

[b]Potential Lag index. [c]Indices in which instability is negative (-).

As can be seen from Table 21, the category D profiles produced the largest instability index values, as one would expect. Since category D conditions are the main items of interest in the present investigation, emphasis will be placed on them. The circled category D LAG and AVG stability indices indicate the index with the largest D-category index value. Two indices, in particular, show a much greater LAG instability than their AVG counterpart index value. The SWEAT and modified-Martin indices both indicate a LAG-REG difference greater than 7%, as a function of the index range. These two indices would be potential LAG stability index forecast indicators when used prior to the occurrence of severe weather.

To establish concrete threshold values for all the indices used here is difficult, since each index may offer a threshold index value for only a selected type of thunderstorm condition (i.e., scattered thunderstorms rather than numerous severe thunderstorms). However, an attempt has been made to include approximate threshold index values for severe-type thunderstorms (see last column of Table 21).

Note that most indices equal or exceed the threshold values indicated, with the exception of perhaps the K-index. However, the K-index has been designed for routine, non-severe thunderstorm prediction.

Therefore, all indices presented in Table 21 appear to be potentially equal by this analytical comparison between prior and actual severe storm averaged conditions. This supposition will have to be considered in Chapter VII, when an actual, independent set of

severe storm soundings is presented and analyzed with respect to atmospheric stability.

## D. Johnson Lag Index

As contemplated in Chapter V, Section G, it is believed that the development of a forecast-type procedure or index should be attempted that is based entirely upon the differences noted in the averaged AVG and LAG profiles. If the environment three to six hours prior to severe weather shows any type of parametric structure difference from that at the time of severe weather, a stability index/procedure should be developed to model this phenomenon. Since wind differences are small between LAG and AVG profiles, and the individual wind profiles are so variable, it was felt that for the initial attempt, winds should not be used--only the use of significant thermodynamic parameter changes versus altitude to keep the index simple.

As explained earlier, the major differences observed in the temperature structure between LAG and AVG profiles occur throughout the 800- to 650-mb and 650- to 500-mb levels. The main $\theta_E$ differences noted occur between the 900- to 800-mb and 750- to 700-mb levels. The LAG and AVG temperature and equivalent potential temperature lapse rates that exist between these pressure levels were then calculated. A gradient halfway between the LAG and AVG gradients was selected as being a most representative standard of atmospheric conditions between three hours prior to storms and storm occurrence itself. Lapse rates on one side of this standard gradient

would represent conditions of the LAG, while gradients observed on the other side of this standard would represent AVG conditions.

The four thermodynamic terms mentioned earlier were therefore selected as potential forecast terms: Two terms to represent temperature gradients in lower and upper atmospheric areas, and two $\theta_E$ gradient terms to represent the low- and middle-atmosphere temperature and moisture structure. The four terms were then combined so as to maximize the negative value of the index in representing extreme instability only during LAG-D time (three to six hours before storms). Since this gradient procedure, or index, is maximized a few hours before storm occurrence, the application of the index during periods of severe weather (AVG-D conditions) should result in a positive value. This new Johnson Lag Index (JLI) is expressed as:

$$JLI = (-11.5 - \Delta T_{650-800}) + 2(\Delta T_{500-650} + 14.9) + 2(\Delta\theta_{E\ 800-900} + 3.5) - 1/3(3.0 + \Delta\theta_{E\ 700-750}) , \quad (25)$$

where,

$$T_{650-800} = T_{650} - T_{800} ,$$

$$T_{500-650} = T_{500} - T_{650} ,$$

$$\theta_{E\ 800-900} = \theta_{E\ 800} - \theta_{E\ 900} ,$$

$$\theta_{E\ 700-750} = \theta_{E\ 700} - \theta_{E\ 750} ,$$

(T and $\theta_E$ units in $^oC$ or $^oK$) .

The four terms of Eq. (25) were weighted by applying multiplication factors of 1, 2, 2, and 1/3, respectively. This was done to offset the effect of the category A (non-precipitation) small temperature and potential temperature gradients, which tended to allow the unweighted JLI equation to produce an unstable negative JLI value close in magnitude to LAG-D JLI conditions. Thus, this weighting will help eliminate the occurrence of false alarms whenever category A, non-precipitation areas are encountered. The weighting factors were determined from a subjective, trial-and-error procedure involving different combinations of weighting, in order to arrive at a large JLI difference between A and D precipitation conditions.

The JLI values calculated for LAG-D conditions equaled -4.35. Likewise, JLI values computed for AVG-D conditions resulted in a value of +2.76. The theory, then, is that if atmospheric conditions from an individual sounding produce a negative JLI of similar or greater magnitude, one should expect severe weather to occur within the next three to six hours. This conclusion has yet to be proven, and is only stated at this time. In Chapter VII the theory will be tested as to its performance along with the other stability indices. The complete JLI values versus MDR categories of LAG and AVG profiles are given in Table 22.

Again, it should be realized that the very small parametric differences noted in these averaged profiles have been used in the construction of the JLI; whereas, in reality, individual atmospheric

Table 22. JLI versus MDR Categories for LAG and AVG Conditions

| MDR Category | LAG JLI | AVG JLI |
|---|---|---|
| A | 0.52 | -0.15 |
| B | 4.11 | 4.78 |
| C | 1.78 | 3.45 |
| D | -4.35 | 2.76 |

soundings do, indeed, have a much greater range of variability in the vertical. The question is, how well will the JLI model the real atmosphere?

# CHAPTER VII

# STABILITY CRITERIA APPLIED TO AVE-SESAME-I

## A. Introduction

This chapter will present an analysis which will use the stability indices defined in the previous chapters. These are applied to a different and independent set of individual data soundings taken during severe weather situations. The AVE-SESAME-I [2] data case of April 10-11, 1979 was selected for the present study as the comparison data set against which to run all of the indices.

The synoptic situation for AVE-SESAME-I will be presented along with the individual soundings. Stability indices will be computed for all soundings prior to, during, and after severe storm occurrence. The computed indices will be compared in helping determine how each index varies throughout this data set, and how each index might be used as a short-term predictor of severe weather.

## B. Synoptic Situation

The AVE-SESAME-I time period was chosen for the stability index evaluation case because the AVE-IV and AVE-SESAME-I projects involved April storm cases in which similar synoptic weather situations developed.

A low-pressure system located north of western Texas with associated frontal positions existed, allowing a moist Gulf flow to

persist over the southeastern and southern/middle plains areas of the United States. This situation, coupled with the advancing cold front, caused extensive convective and severe weather to form, with the development of two pre-frontal squall lines, during both AVE cases. The destructive Wichita Falls, Texas, tornado that occurred during AVE-SESAME-I was only one of more than 40 tornado occurrences.

Abilene, Texas, was the sounding station chosen to analyze during AVE-SESAME-I because it was the closest station during most of the tornado and severe weather occurrences in the north-Texas and southern-Oklahoma areas. A preliminary weather summary for AVE-SESAME-I has been published by Williams [68], and the individual upper-air sounding data are available in the Gerhard et al. [2] document.

Since the Abilene sounding data were selected for analysis in this study, the time and location of the severe weather/tornado occurrence around Abilene during April 10-11, 1979 will be discussed at this time. Generally speaking, there were three separate severe weather patterns which occurred near Abilene during the afternoon of April 10, 1979 and extended through the early morning hours of April 11, 1979.

The first severe weather event consisted of hail damage between 125 and 150 miles north and northeast of Abilene, between 1730-1800 GMT on April 10. The second very severe weather outbreak occurred between 2050-0100 GMT, with tornado and hail occurrence from 75 to 150 miles north and then north-northeast of Abilene. This included the Wichita Falls tornado. Finally, a squall line

developed around 0245 GMT (April 11) from Abilene and extended ~75 miles south-southwest to San Angelo, Texas. For the next six hours (until 0817 GMT), this squall line moved eastward producing hail and some tornadoes from 35 to beyond 125 miles of Abilene. The severe weather occurred at Abilene and then moved south of, southeast of, east of, and finally, northeast of the city. Figure 27 indicates the severe weather pattern which occurred around Abilene (ABI) from 1200 GMT on April 10 to 1200 GMT on April 11, 1979.

## C. Sounding Analyses

For the Abilene site, eight atmospheric soundings were taken between 1200 GMT on April 10, 1979 and 1200 GMT on April 11, 1979. Only the 0600 GMT sounding of April 11 was missing due to tracking problems, with no second release as backup.

Five of the eight critical Abilene severe weather soundings are presented in Skew-T form in Figures 28 and 29. Given are the April 10, 1979 soundings for 1442, 1740, 2034, and 2333 GMT, together with the one for 0226 GMT on April 11, 1979. The progression of these soundings in time indicates that low-level moisture was confined by a capping inversion to levels under 800 mb prior to 1442 GMT. From these profiles, extremely dry air can be seen above this level. After 1500 GMT, the capping inversion lifted and, with storm development, allowed moist air to penetrate upward to beyond 600 mb by 2034 GMT. The April 11, 1979 Abilene sounding for 2333 GMT shows that during this time period, while severe weather was currently affecting the Wichita Falls area, the dry-line behind this system

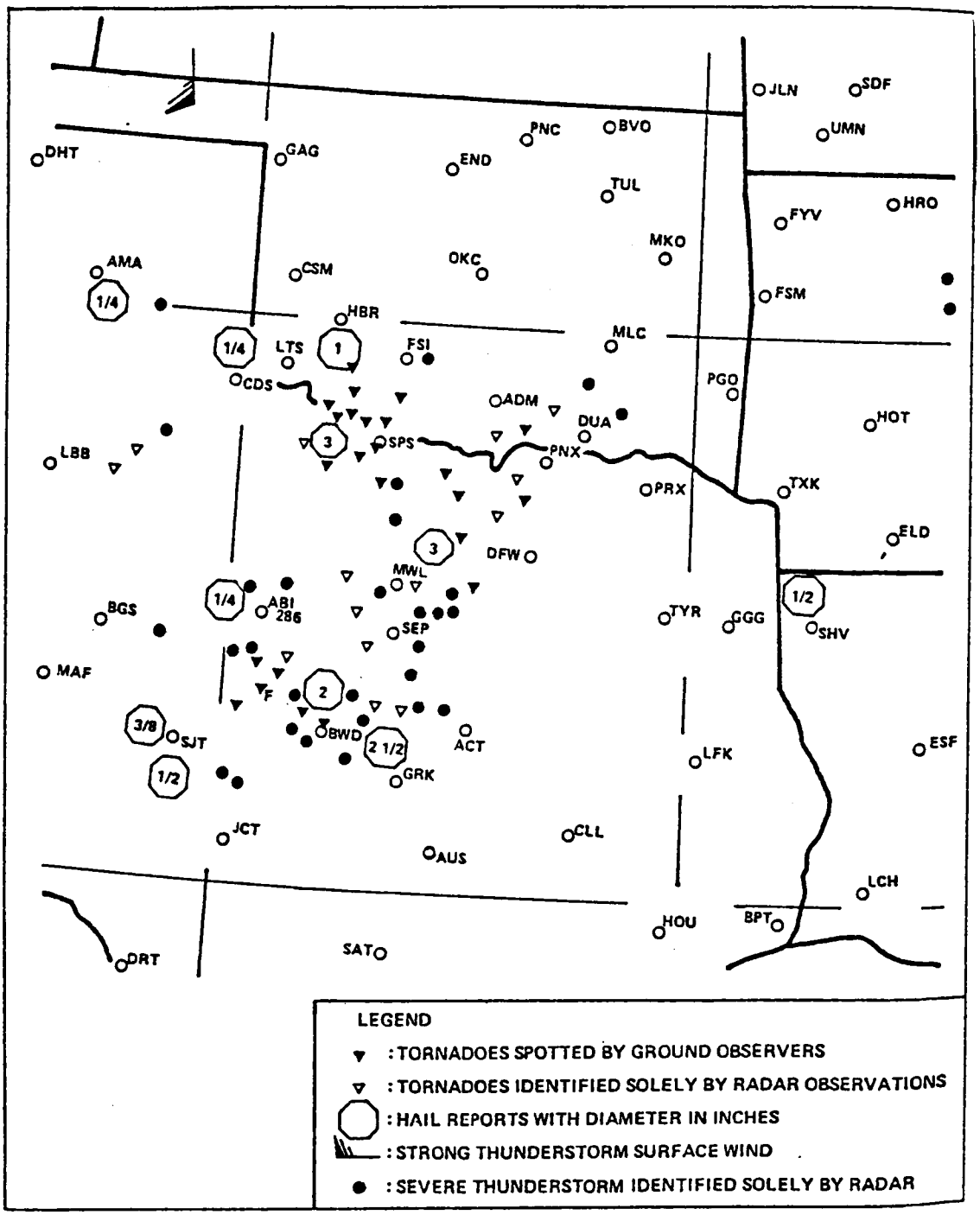


Figure 27. Severe weather occurences between 1200 GMT on April 10, and 1200 GMT on April 11, 1979 in the south central United States [68].

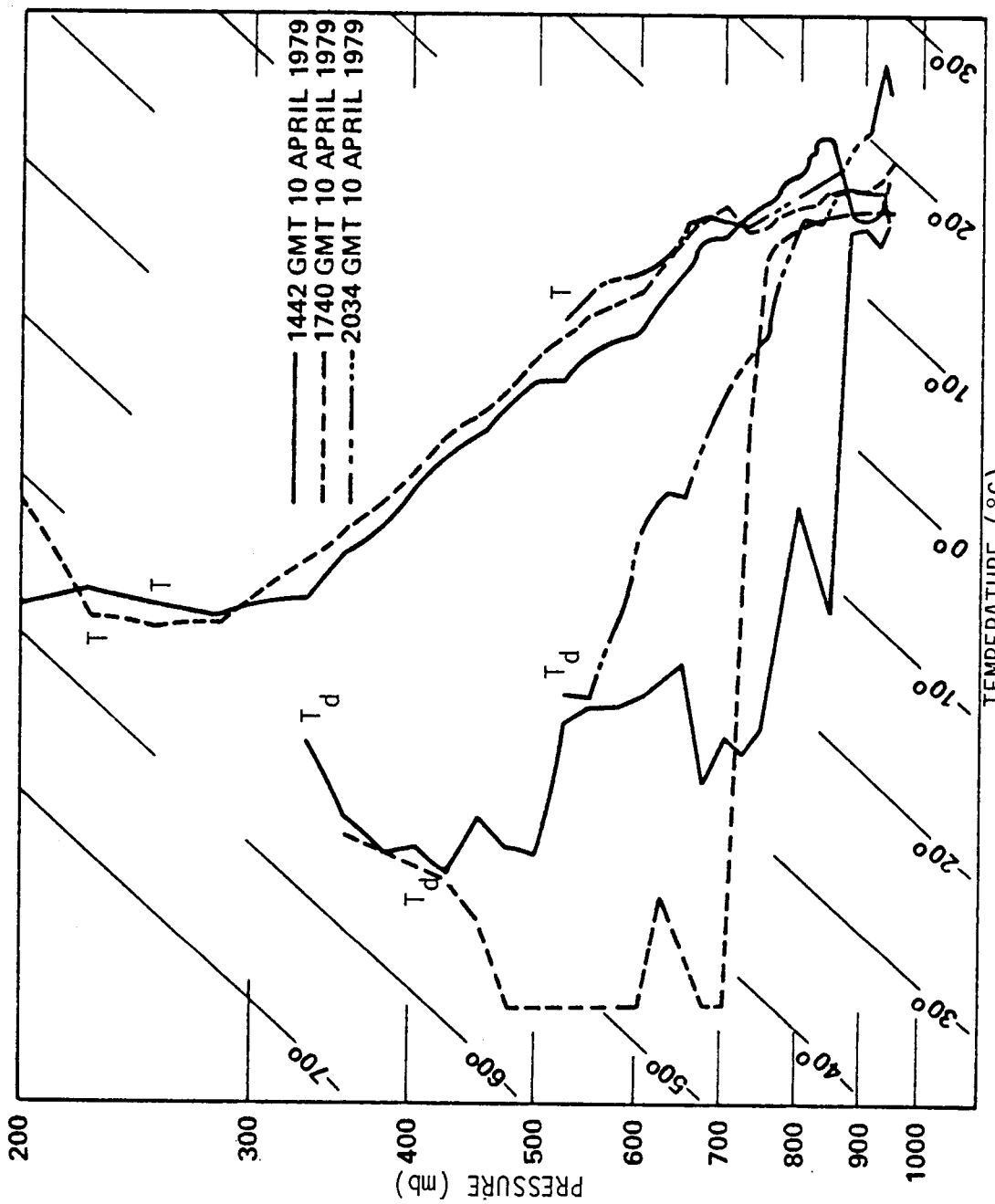
1442 GMT 10 APRIL 1979
1740 GMT 10 APRIL 1979
2034 GMT 10 APRIL 1979
T
T
T

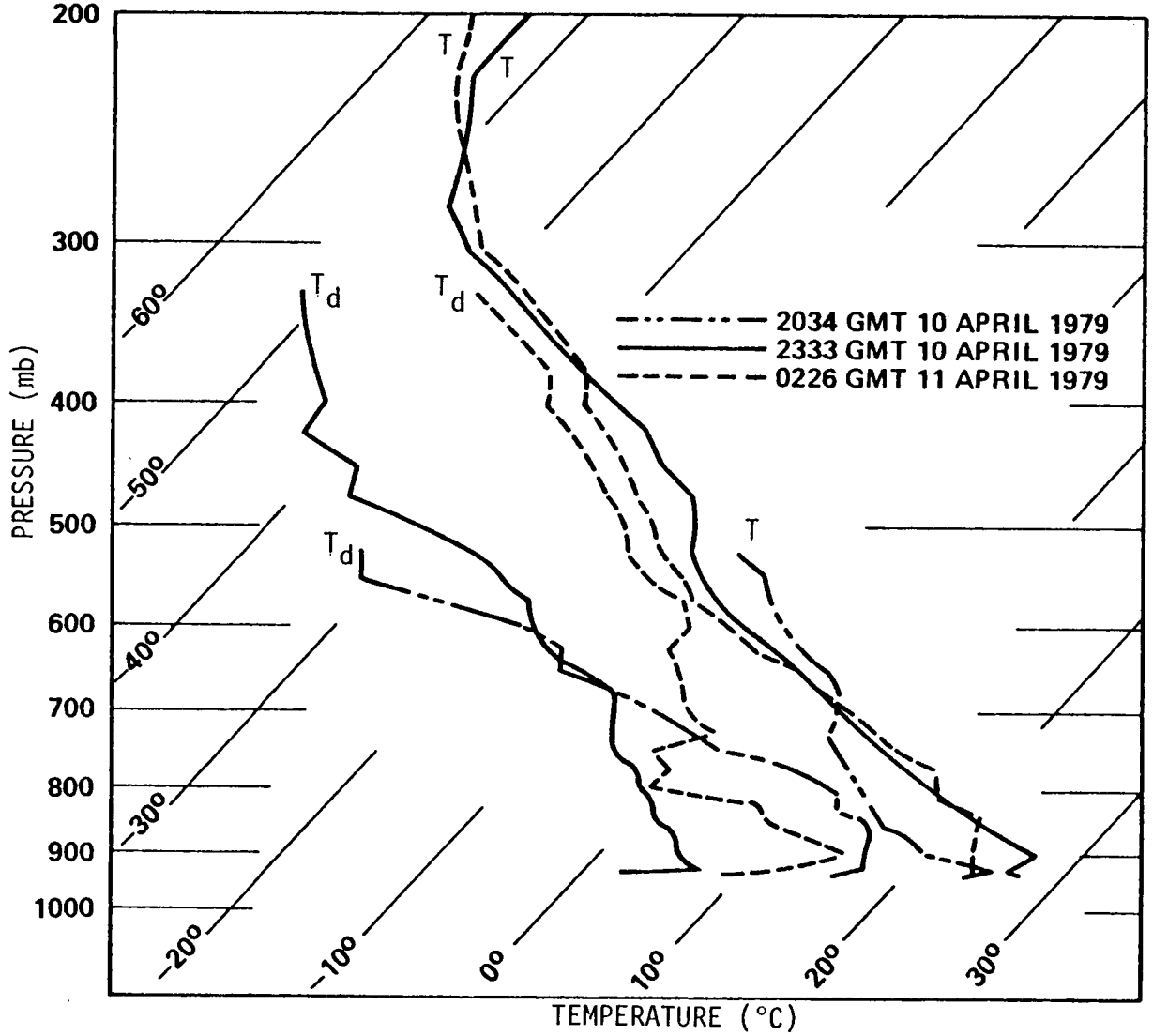


Figure 29. Abilene, Texas, severe weather soundings for April 10-11, 1979.

had now moved into the Abilene area. This condition was relatively short-lived because a second squall line was forming near Abilene and started inflicting severe weather there and eastward by 0245 GMT. The 0226 GMT sounding of Figure 29 shows an abrupt increase in moisture up to 350 mb, where the data terminate. Sometime after 0600 GMT on April 11, 1979, the cold front began entering the Abilene area, bringing dry air close to the surface while still leaving a pocket of moisture above the front between 550 and 750 mb.

Since stability is the item of interest in the present investigation, the 15 stability indices used earlier were computed for each Abilene sounding. These stability index results are presented in Table 23, together with the exact time of radiosonde release. Listed below the index values in this table is a severe weather timeline applicable to the north-central Texas area, within 150 miles of Abilene. This separation of sounding site and area of severe weather occurrence is, indeed, too large to be completely applicable to the Abilene data. Therefore, one should keep in mind that the Abilene timeline needs to be shortened somewhat. Also on Table 23, the highest three unstable index values for each index have been circled for easy reference. The most unstable value has also been marked with a superscript "a."

As can be seen in Table 23, there seems to be good general agreement that most all indices appear to perform adequately in the evaluation of atmospheric instability during the passage of the two squall systems near Abilene. Profiles 4 and 6 were the two soundings taken at Abilene just prior to the severe weather which occurred

Table 23. Abilene, Texas, AVE-SESAME-I Sounding Stability Index Values

| Sounding No. / Time (GMT) / Index | April 10, 1979 | | | | | April 11, 1979 | | | |
|---|---|---|---|---|---|---|---|---|---|
| | 1<br>1121[a] | 2<br>1442[a] | 3<br>1740[a] | 4<br>2034[a] | 5<br>2333[a] | 6<br>0226[a] | 0600 | 7<br>0806 | 8<br>1105 |
| SWEAT | 221 | 69 | (472) | (557) | 292 | (621[b]) | --- | -33 | -37 |
| Vertical Totals | 28.5 | (32.9) | 27.8 | 27.9 | (35.0) | (37.8[b]) | --- | 26.6 | 26.3 |
| Cross Totals | 16.1 | 3.1 | (26.1) | (26.9[b]) | 15.0 | (24.7) | --- | 9.3 | 6.3 |
| Total Totals | 44.6 | 36.0 | (53.9) | (54.8) | 50.0 | (62.5[b]) | --- | 35.9 | 32.6 |
| $\theta_E^*$[c] | -11.3 | -8.1 | (-25.9[b]) | (-16.1) | -6.0 | (-12.0) | --- | 11.2 | 14.0 |
| Showalter[c] | -1.1 | 7.0 | (-3.9) | (-5.0) | 0.8 | (-6.5[b]) | --- | 8.9 | 10.3 |
| Rackcliff | 32.2 | (33.3) | 32.6 | (33.6) | 31.4 | (37.5[b]) | --- | 26.0 | 26.1 |
| Jefferson | 43.0 | 44.3 | (44.4) | (46.6) | 42.4 | (50.6[b]) | --- | 33.1 | 32.6 |
| Mod. Jefferson | 19.9 | 20.8 | 10.5 | (33.4) | (27.1) | (37.5[b]) | --- | 21.9 | 22.9 |
| Boyden[c] | -3.2 | -3.9 | -7.3 | (-8.9) | (-9.2) | (-10.4[b]) | --- | -7.1 | -6.9 |
| Bradbury[c] | -0.7 | 1.7 | (-4.9) | (-5.6[b]) | -1.8 | (-4.1) | --- | 2.8 | 3.8 |
| K-Index | 0.2 | -10.0 | -10.8 | (32.4) | (22.4) | (36.6[b]) | --- | 15.3 | 13.9 |
| Energy[c] | -0.2 | 1.0 | (-3.6) | (-4.0[b]) | -1.1 | (-2.8) | --- | 1.9 | 2.3 |
| Mod. Martin[c] | -7.3 | (-13.3) | -9.4 | (-10.7) | -1.2 | (-20.8[b]) | --- | 13.5 | 13.8 |
| JLI[c] | (-29[b]) | (-18) | -7 | -10 | 1 | (-28) | --- | 6 | 12 |
| Abilene Area Severe Weather Timeline GMT: | | | 1730-1800 | 2050 | 0100 | 0245 | | 0817 | |
| Description: | (No Convective Activity) | | (Hail) | | (Tornadoes and Hail) | | (Hail and Tornadoes) | | (Storms Move Eastward) |

[a]Circled values indicate the highest three unstable index values for each index.

[b]Most unstable stability index value. [c]Indices in which instability is negative (-).

near and around the city. Stability index values from Table 23 indicate that most indices peak (with instability) using soundings 4 and 6 data; 10 of the 15 indices peak using sounding 6, while three peak using sounding 4. This means that 13 of the 15 peaked during the occurrence of upper-level moisture buildup, just prior to the onset of the Abilene storms. Only two indices ($\theta_E^*$ and JLI) peaked at times prior to this. Sounding 6 is more unstable than sounding 4 because the storms developed very close to the sounding site, and the moisture aloft had developed more extensively than during sounding 4. The dry-line passage at Abilene between 2200-0000 GMT can readily be seen by the sudden increase in stability in most all of the indices during sounding 5 (2333 GMT). While weather activity existed eastward of Abilene during sounding 8 (0806 GMT, April 11), all indices show a general increase in stability as the cold front arrives.

Table 23 also hints that soundings taken when storms are not in progress in the general area result in slightly greater instability than when storms have formed in the area during the radiosonde release. This may seem to indicate that the instablity (stored potential energy) which can build up prior to storm occurrence can be relieved (made more stable) through the release of thunderstorm kinetic energy activity.

## D. Exceptions to the Norm

There are a few stability indices which peak at an earlier sounding than the rest. It was decided to look at each index that fell into this category.

Since the $\theta_E^*$ index peaked out during sounding 3, the cause was sought. The index is based on a $\theta_E$ difference between 700 mb and the surface level. Since sounding 3 indicated that the atmosphere dried out very quickly between 750 and 700 mb, this would also produce a very dramatic $\theta_E$ drop between the same two levels, resulting in a very unstable $\theta_E^*$ index value.

The modified Martin index indicated a slight instability peak using sounding 2. This index uses the 850-mb level as the comparison altitude. At this time interval there existed a large capping temperature inversion top located at 850 mb. This large temperature value would produce a higher index value than if this cap inversion top were located at a different level.

The Energy index peaking during soundings 3 and 4 is believed to be due to the ample abundance of moisture at 850 mb during these two sampling times, which would strengthen the 850-mb $E_T$ value. Sine the JLI was designed to peak out during time periods prior to storm development, this early peaking of the JLI index during soundings 1 and 2 is expected and desirable.

## E. Lag Testing

In Chapter VI it was indicated that, based on the AVE-IV LAG profile as it related to the AVG profile, three indices appeared to be potential lag indices. These three indices were: SWEAT, modified Martin, and the JLI. According to the AVE-SESAME-I sounding data (Table 23, page 111), all of these indices, with the exception of the JLI, fail to qualify as a lag index, since the peak index outliers which occur before storm development have been explained away.

The JLI does give large negative values (-29 and -18) during the non-storm time period represented by soundings 1 and 2. When distant storms occur, Abilene sounding 3 records a JLI = -7. Just prior to the first major outbreak of storms closer to Abilene, sounding 4 gives a JLI = -10. The dry-line passage, during sounding 5, produces a JLI = +1. Sounding 6, released 19 minutes prior to hail occurrence near Abilene (51 minutes prior to first tornado report) gave a JLI = -28. This large negative index value was surprising, since the sounding represents squall line-produced activity. However, the JLI could still be sensing the intense, unstable, pre-squall line environment which appears not to have passed the release site at this time. Overall, the JLI has functioned well and it gives large positive values (+6 and +12) when the cold front moved into the area. This indicates that no more storms were due to follow.

Based on only one severe storm case, it appears that of 15 stability indices tested as a pre-storm lag index, only the JLI appears to give satisfactory results thus far. However, since the JLI is a new index, representing low- and middle-level temperature and moisture, it will have to be tested further, and possibly be adjusted, before it can quality as a lag/forecast index for severe storms.

# CHAPTER VIII

## CONCLUSIONS

The following project goals and conclusions were accomplished and presented in this study:

1. Averaged AVE-IV environmental thermodynamic/wind profiles have been presented for different MDR severe storm periods (AVG), and for periods three to six hours prior to severe storm occurrence (LAG).
2. The AVE-IV AVG and LAG profiles were analyzed parametrically and with 14 common atmospheric stability indices to determine if a severe storm forecast index or procedure could be developed based on these averaged severe storm profiles.
3. A thermodynamic lag index, called the Johnson Lag Index (JLI), was developed, based upon low- and middle-tropospheric level temperature and moisture structure using the AVE-IV averaged profiles. The JLI was designed to have short-termed forecasting ability.
4. Based on the averaged AVE-IV profiles, two other stability indices (SWEAT and modified Martin) had some potential as forecast lag indices.
5. All 14 stability indices and the Johnson Lag Index were tested by employing an independent severe storm case study using the AVE-SESAME-I individual data soundings from one station.

6. All AVE-SESAME-I stability indices tested appeared to recognize the severe weather environment with unstable values, as well as presenting stable values when severe weather had passed.
7. All AVE-SESAME-I stability indices tested as a pre-storm, three-hour lag forecast index performed unsatisfactorily. Only the JLI appeared to show promise in terms of forecasting severe weather three to six hours prior to occurrence. However, more testing of this index with case study data is needed.

# BIBLIOGRAPHY

# BIBLIOGRAPHY

1. Fucik, Nancy F., and Robert E. Turner. "Data for NASA's AVE-IV Experiment: 25-mb Sounding Data and Synoptic Charts," National Aeronautics and Space Administration TMX-64952, George C. Marshall Space Flight Center, Marshall Space Flight Center, Alabama, August, 1975.

2. Gerhard, Myron L., Henry E. Fuelberg, Steven F. Williams, and Robert E. Turner. "AVE-SESAME I: 25-mb Sounding Data," National Aeronautics and Space Administration TM-78256, George C. Marshall Space Flight Center, Marshall Space Flight Center, Alabama, December, 1979.

3. Use of the Skew-T, Log P Diagram in Analysis and Forecasting. AWSM 105-124. Scott Air Force Base, Illinois: United States Air Force, Air Weather Service, Headquarters Air Weather Service (MAC), July, 1969 (reprint October 1971).

4. Scoggins, James R., and James E. Wood. "Factors in the Formation and Prediction of Convective Clouds and Thunderstorms." Paper presented at American Meteorological Society Seventh Severe Local Storms Conference, Kansas City, Missouri, October 5-7, 1971.

5. Showalter, A. K. "A Stability Index for Thunderstorm Forecasting," Bulletin of the American Meteorological Society, 34:250-252, June, 1953.

6. Huschke, Ralph E. Glossary of Meteorology. Boston: American Meteorological Society, 1959.

7. Connell, James R., and Lillian Ey. "Wind Shear and Wet and Dry Thermodynamic Indices as Predictors of Thunderstorm Motion and Severity and Applications to the AVE-IV Experimental Data," National Aeronautics and Space Administration CR-150220, George C. Marshall Space Flight Center, Marshall Space Flight Center, Alabama, March, 1977.

8. Scott, Robert W., and James R. Scoggins. "The Moisture Budget in Relation to Convection," National Aeronautics and Space Administration CR-2817, George C. Marshall Space Flight Center, Marshall Space Flight Center, Alabama, March, 1977.

9. Read, William L., and James R. Scoggins. "Vorticity Imbalance and Stability in Relation to Convection," National Aeronautics and Space Administration CR-2819, George C. Marshall Space Flight Center, Marshall Space Flight Center, Alabama, March, 1977.

10. Fuelberg, Henry E. "Atmospheric Energetics in Regions of Intense Convective Activity," National Aeronautics and Space Administration CR-2826, George C. Marshall Space Flight Center, Marshall Space Flight Center, Alabama, March, 1977.

11. Dupuis, Leonard R., and James R. Scoggins. "Differences Between Measured and Linearly Interpolated Synoptic Variables Over a 12-h Period During AVE-IV," National Aeronautics and Space Administration CR-3150, George C. Marshall Space Flight Center, Marshall Space Flight Center, Alabama, June, 1979.

12. Turner, Robert E. "The Mechanics of Atmospheric Systems Derived Through Vertical and Horizontal Analysis of Parametric Data," National Aeronautics and Space Administration TP-1072, George C. Marshall Space Flight Center, Marshall Space Flight Center, Alabama, November, 1977.

13. Fuelberg, Henry E., and James R. Scoggins. "Relationship Between the Kinetic Energy Budget and Intensity of Convection." Paper presented at the American Meteorological Society Tenth Conference on Severe Local Storms, Omaha, Nebraska, October 18-21, 1977.

14. Turner, Robert E., and Kelly Hill. "Skew-T, Log P Diagrams for NASA's AVE-IV Experiment," National Aeronautics and Space Administration NASA/MSFC-ES-84-1, George C. Marshall Space Flight Center, Marshall Space Flight Center, Alabama, March, 1977.

15. Maddox, R. A. "The Evolution of Middle and Upper Tropospheric Features During a Period of Intense Convective Storms." Paper presented at the American Meteorological Society Eleventh Conference on Severe Local Storms, Kansas City, Missouri, October 2-5, 1979.

16. Wilson, Gregory S. "Relationships Between Convective Storms and Their Environment in AVE-IV Determined from a Three-Dimensional Subsynoptic-scale, Trajectory Model." Paper presented at the American Meteorological Society Tenth Conference on Severe Local Storms, Omaha, Nebraska, October 18-21, 1977.

17. Wilson, Gregory S. "Large-scale Vertical Motion Calculations in the AVE-IV Experiment--of Atmospheric Wind Velocity," Geophysical Research Letters, 3(No. 12):735-738, December, 1976.

18. Davis, James G., and James R. Scoggins. "The Development of Convective Instability, Wind Shear, and Vertical Motion in Relation to Convective Activity and Synoptic Systems in AVE-IV," National Aeronautics and Space Administration CR-3386, George C. Marshall Space Flight Center, Marshall Space Flight Center, Alabama, February, 1981.

19. Fucik, Nancy F., and Robert E. Turner. "Data for NASA's AVE-IV Experiment: 25-mb Sounding Data and Synoptic Charts," National Aeronautics and Space Administration TND-8161, George C. Marshall Space Flight Center, Marshall Space Flight Center, Alabama, March, 1976.

20. Wilson, Gregory S., and James R. Scoggins. "Environmental Conditions Associated with the Development of Severe Thunderstorms as Determined from 3-h AVE Data." Paper presented at the Americal Meteorological Society/American Institute of Aeronautics and Astronautics Conference on Atmospheric Environment of Aerospace Systems and Applied Meteorology, New York, New York, November 14-16, 1978.

21. Wilson, Gregory S. "Thunderstorm-Environment Interactions Determined with Three-Dimensional Trajectories," National Aeronautics and Space Administration RP-1054, George C. Marshall Space Flight Center, Marshall Space Flight Center, Alabama, January, 1980.

22. McCown, Milton S., and James R. Scoggins. "Gradients of Meteorological Parameters in Convective and Non-convective Areas," National Aeronautics and Space Administration CR-2818, George C. Marshall Space Flight Center, Marshall Space Flight Center, Alabama, March, 1977.

23. Foster, D. S., and R. M. Reap. "Archiving of Manually-Digitized Radar Data," Techniques Development Laboratory Office Note 73-6, National Weather Service, Silver Springs, Maryland, 1973.

24. Reap, R. M. "Thunderstorm and Severe Weather Probabilities Based on Model Output Statistics--No. 3," Technical Procedures Bulletin No. 138, National Weather Service, Silver Springs, Maryland, 1975.

25. Barr, S., W. K. Widger, I. A. Miller, and R. Stanton. "Objective Subsynoptic Upper Level Analysis," Journal of Applied Meteorology, 10:410-417, June, 1971.

26. Wilson, Gregory S., and James R. Scoggins. "Atmospheric Structure and Variability in Areas of Convective Storms Determined from 3-h Rawinsonde Data," National Aeronautics and Space Administration CR-2678, George C. Marshall Space Flight Center, Alabama, April, 1976.

27. Booth, David M. "A Study of Stability Indices and Vertical Motion in Relation to Convective Clouds Over Texas." Unpublished Master's thesis, Texas A&M University Graduate College, College Station, Texas, January, 1970.

28. Whitehead, Darell R. "A Comparison of Objective Convective Activity Indices," University of Oklahoma Research Institute Report OURI-1828-71-1, Atmospheric Research Laboratory, Department of Meteorology, Norman, Oklahoma, November, 1971.

29. McPherson, G. A. "A Survey of Stability Indices," Department of Transport, Meteorological Branch Technical Memoranda TEC-739, Ontario, Canada, August, 1970.

30. Saunders, W. E. "Tests of Thunderstorm Forecasting Techniques," Meteorlogical Magazine, 95:204-210, 1966.

31. Alaka, M. A., W. D. Bonner, J. P. Charba, R. L. Crisci, R. C. Elvander, and R. M. Reap. "Objective Techniques for Forecasting Thunderstorms and Severe Weather--Final Report," Federal Aviation Administration Report FAA-RD-73-117, Systems Research and Development Service, Washington, D. C., July, 1973.

32. Miller, R. C., and A. Bidner. "The Use of Computer Products in Severe-Weather Forecasting," Automated Weather Support Proceedings of the Sixth AWS Technical Exchange Conference, U. S. Naval Academy, 21-24 September, 1970. Technical Report 242. [n.p.]: Air Weather Service (MAC), United States Air Force, April, 1971. Pp. 224-228.

33. Bidner, A. "The Air Force Global Weather Central Severe Weather Threat (SWEAT) Index (A Preliminary Report)," Automated Weather Support Proceedings of the Sixth AWS Technical Exchange Conference, U. S. Naval Academy, 21-24 September, 1970. Technical Report 242. [n.p.]: Air Weather Service (MAC), United States Air Force, April, 1971. Pp. 229-231.

34. Bidner, A. "The Air Force Global Weather Central Severe Weather Threat (SWEAT) Index--A Preliminary Report," Air Weather Service Aerospace Sciences Review, AWS RP 105-2, No. 70-3. [n.p.]: USAF Environmental Technical Applications Center, December, 1970. Pp. 2-5.

35. Miller, R. C., and R. A. Maddox. "Use of the SWEAT and SPOT Indices in Operational Severe Storm Forecasting." Paper presented at the Ninth Conference on Severe Local Storms, Norman, Oklahoma, October 21-23, 1975.

36. "Surface Potential Thunderstorm Index (SPOT)," Air Weather Service Technique Development Annual Summary. Scott Air Force Base, Illinois: Headquarters Air Weather Service (MAC), United States Air Force, May, 1975. P. 11.

37. Maddox, R. A. "A Severe Thunderstorm Surface Potential Index (SPOT)." Paper presented at the American Meteorological Society Eighth Conference on Severe Local Storms, Denver, Colorado, October 15-17, 1973.

38. Miller, R. C. "Notes on Analysis and Severe-Storm Forecasting Procedures of the Military Weather Warning Center," Air Weather Service TR-200, Air Weather Service (MAC), United States Air Force, [n.p.], July, 1967.

39. Jones, J. J. "Equivalent Potential Temperature as a Measure of Atmospheric Stability," 2143d Air Weather Wing Technical Bulletin No. 8, Tokyo Weather Central, January, 1952.

40. Nolte, G. G. "Theta-E Analysis," Second Weather Wing Detachment 40, 28th Weather Squadron, [n.p.], January, 1961.

41. Petterssen, Sverre. Weather Analysis and Forecasting. Vol. II, second edition. New York: McGraw-Hill Company, 1956.

42. Berry, F., E. Bolay, and N. Beers. Handbook of Meteorology. New York: McGraw-Hill Company, 1945.

43. "Theta-E Charts and Thunderstorm Forecasting," Air Weather Service Bulletin No. 3. Washington, D. C.: Headquarters, Air Weather Service, 1950. Pp. 25-27.

44. Instability Chart Evaluation. Technical Bulletin. [n.p.]: Second Weather Wing, April, 1954.

45. Fawbush, E. J., and R. C. Miller. "A Method for Forecasting Hailstone Size at the Earth's Surface," Bulletin of the American Meteorological Society, 34(No. 6):235-244, June, 1953.

46. Severe Weather Forecasting. Air Weather Service Manual AWSM 105-37. Washington, D. C.: Headquarters, Air Weather Service, United States Air Force, May, 1956.

47. Cox, Myron K. "The Distribution and Variability of Cold-Front Precipitation," Bulletin of the American Meteorological Society, 40:477-480, September, 1959.

48. Schuetz, John. "The Relationship Between Maximum Echo Top and Stability," Proceedings, Sixth Weather Radar Conference, Cambridge, Massachusetts. [n.p.]: [n.n.], March, 1957. Pp. 215-220.

49. Granitzny, Peter. "Dependence of the Maximum Number of Convective Radar Echoes on Various Parameters and Stability Indices," Institut Fur Meteorologie und Geophysik, Meteorologische Abhandlungen No. 91(3), Berlin, Germany, 1969.

50. Rackcliff, P. G. "Application of an Instability Index to Regional Forecasting," Meteorological Magazine, 91(No. 1078): 113-120, May, 1962.

51. Galway, J. G. "The Lifted Index as a Predictor of Latent Instability," American Meteorological Society Bulletin, 37(No. 10):528-529, December, 1956.

52. Jefferson, G. J. "A Modified Instability Index," Meteorological Magazine, 92(No. 1088):92-96, March, 1963.

53. Jefferson, G. J. "A Further Development of the Instability Index," Meteorological Magazine, 92(No. 1095):313-316, October, 1963.

54. Boyden, C. J. "A Simple Instability Index for Use as a Synoptic Parameter," Meteorological Magazine, 92(No. 1092):198-210, July, 1963.

55. George, J. J. Weather Forecasting for Aeronautics. New York: Academic Press, 1960. Pp. 409-415.

56. Bryan, K. E. "The Relationship of K-Values to Probability of Showers in the Mid-South," Environmental Science Services Administration (ESSA) Technical Memorandum WBTM SR-37, Weather Bureau Southern Region, Fort Worth, Texas, October, 1967.

57. Hambridge, R. E. "'K' Chart Application to Thunderstorm Forecasts Over the Western United States," Western Region Technical Memorandum No. 23, Environmental Science Services Administration, U. S. Weather Bureau, [n.p.], May, 1967.

58. The K Index Chart. Technical Procedures Bulletin No. 61. U. S. Department of Commerce, National Oceanic and Atmospheric Administration, National Weather Service, Silver Spring, Maryland, April 12, 1971.

59. Bradbury, T. A. M. "The Use of Wet-Bulb Potential Temperature Charts," Meteorological Magazine, 106(No. 1261):233-251, August, 1977.

60. Darkow, G. L. "The Total Energy Environment of Severe Storms." Paper presented at the Fifth Conference on Severe Local Storms, American Meteorological Society, St. Louis, Missouri, October 19-20, 1967.

61. Eagleman, J. R., V. U. Muirhead, and N. Willems. "Energy-Shear Index for Forecasting Tornadoes," Thunderstorms, Tornadoes, and Building Damage. Lexington, Massachusetts: Lexington Books, D. C. Heath and Company, 1975. Pp. 169-188.

62. Craiglow, L. H. "A Mesoscale Investigation of Convective Activity." Unpublished Master's thesis, United States Naval Postgraduate School, Monterey, California, 1971.

63. Bencks, E. G. "Thunderstorm Forecasting for the Northeast," Detachment 42, 12th Weather Squadron Report, Topsham Air Force Station, Maine, January, 1969.

64. Renne', D. S., and P. C. Sinclair. "Stability and Synoptic Features of High Plains Hail Storm Formation." Paper presented at the American Meteorological Society Sixth Conference on Severe Local Storms, Chicago, Illinois, April 8-10, 1969.

65. Darkow, G. L., and R. L. Livingston. "Hourly Surface Static Energy Analysis as a Delineator of Thunderstorm Outflow Areas," Monthly Weather Review, 103:817-822, September, 1975.

66. Darkow, G. L., and R. L. Livingston. "The Evolution of the Surface Static Energy Fields on 3 April 1974." Paper presented at the American Meteorological Society Ninth Conference on Severe Local Storms, Norman, Oklahoma, October 21-23, 1975.

67. Terminal Forecast Manual for Wright-Patterson Air Force Base, Ohio. Section IV - Local Forecast Studies. A - Thunderstorms and Rain Showers. Detachment 11, 6th Weather Group, Dayton, Ohio, November, 1956.

68. Williams, Steven F. "A Preliminary Look at AVE-SESAME-I Conducted on April 10-11, 1979," National Aeronautics and Space Administration TM-78262, George C. Marshall Space Flight Center, Marshall Space Flight Center, Alabama, February, 1980.

# VITA

Dale Leroy Johnson was born in Flint, Michigan, on June 1, 1943. He is the son of Verner Helge Johnson and the former Pearl Maria Lescelius. He has two brothers, Rodney Vern Johnson and Kenneth Wayne Johnson. He received his high school education at Flint Central High School in Flint, graduating in June, 1961. In 1961 he entered Flint Community Junior College and received his Associates degree in the Science of Engineering in June, 1963. In the fall of 1963 he transferred to the University of Michigan's School of Engineering in Ann Arbor, Michigan. He completed his requirements for a B.S.E. (Meteorology) degree at the University of Michigan in the spring of 1966. He did post-graduate work at the University of Alabama in Huntsville from 1971 to 1974. In the fall of 1975 he entered the graduate school at The University of Tennessee Space Institute and was awarded the Master of Science degree in Engineering Science in June, 1982.

After graduation from the University of Michigan in 1966, he has been employed by the National Aeronautics and Space Administration Marshall Space Flight Center, Huntsville, Alabama, as an Aerospace Engineer.

Mr. Johnson is married to the former Shirley Ann Dabbs. They have two daughters, Natalie Lynn, and Freda Marie, along with two sons, Stanley Dale, and Kevin Vern. They all reside in Madison, Alabama.